



Title	Chemical and Physical Synthesis of Cationically Charged Photoluminescent Noble Metal Nanoclusters
Author(s)	Corpuz, Ryan Dula
Citation	北海道大学. 博士(工学) 甲第12899号
Issue Date	2017-09-25
DOI	10.14943/doctoral.k12899
Doc URL	http://hdl.handle.net/2115/71514
Type	theses (doctoral)
File Information	Ryan_Dula_Corpuz.pdf



[Instructions for use](#)

**CHEMICAL AND PHYSICAL SYNTHESIS OF
CATIONICALLY CHARGED
PHOTOLUMINESCENT NOBLE METAL
NANOCLUSTERS**



Ryan D. Corpuz

Graduate School of Engineering

Hokkaido University

September 2017

**CHEMICAL AND PHYSICAL SYNTHESIS OF
CATIONICALLY CHARGED
PHOTOLUMINESCENT NOBLE METAL
NANOCLUSTERS**



Ryan D. Corpuz

Laboratory of Novel Materials Hybrid Engineering

Division of Materials Science and Engineering

Faculty of Engineering

Hokkaido University

A dissertation submitted to the Graduate School of Engineering of Hokkaido University in
partial fulfillment of the requirements for the degree of
Doctor of Philosophy in Materials Science and Engineering

to Lyn Marie, Aura Vanya, my family, and country...

ABSTRACT

Metal Nanoclusters had received increasing popularity for the past decades due to its important role in both experimental and theoretical studies. It is considered as the missing link to understand the behavior of individual atoms as it forms to a more ordered nanoparticles and thus controlling the number of atoms as the cluster increases or decreases in size had been a challenge and priority among nanocluster organic chemist, physical chemist and materials scientists. To do so, several chemical and physical approaches had been developed which could be broadly classified as top down or bottom up approaches.

In most chemical synthetic methods, metal precursors are usually reduced with the use of reducing reagents like NaBH_4 and then capped or stabilized with ligand such as proteins, DNA, polymers, dendrimers and monomers which have functional groups that have strong affinity to coordinate with the metal atoms. Among of these ligands, phosphines and thiols are the most popular and intensively studied. In this work, the researcher focused on the latter, which is commonly referred to as thiolated metal nanoclusters.

Thiol ligands which had been popularized by Brust for the synthesis of nanoparticles and had been extended by Murray and Whetten for the synthesis of metal nanoclusters could be broadly classified in to neutral, anionic and cationic. However, among of these thiols, the cationic one is the less popular and rarely found in literatures especially for the synthesis of photoluminescent noble metal nanoclusters. Thus, this study aims to synthesize a cationically charged photoluminescent noble metal nanoclusters.

Cationically charged photoluminescent metal nanoclusters had important application particularly in the field of biomedicine. In a lot of studies, it was found that cationic species has high affinity to interact with proteins than the neutral and anionic ones and thus if a cationic photoluminescent metal nanoclusters is used to investigate cellular activities, it could easily enter the cell and could potentially be used as luminescent probe and biosensor which is important for biotherapy and selective drug delivery.

The first topic of this dissertation pertains to chemical synthesis of positively charged photoluminescent gold nanoclusters. Specifically, thiocholine molecule, a short quaternary ammonium cation which is positively charged in all pH conditions was used as stabilizing and capping ligand coupled with Sodium dodecylsulfate (SDS) to control the electrostatic repulsion of coordinating ligands as it attach to the surface of the particle. Consequently, we are able to observe a correlation between the thiocholine-SDS concentrations with the particle size of the nanoclusters produced. At higher concentrations of thiocholine-SDS combination, we successfully produced blue photoluminescent Au monometallic nanoclusters. However, due to the difficulty of collecting a pure product with this strategy and the inherent toxicity of the reagents used (NaBH_4 , SDS, methanol and NaOH), we resort to physical synthesis by means of sputtering method to make our product useful for biomedical applications.

The second topic of this study is the synthesis of positively charged photoluminescent Au, Ag and Cu nanoclusters by single target sputtering in liquid polymer matrix using 11-mercaptoundecyl-*N,N,N*-trimethylammonium bromide (MUTAB) as stabilizing and capping ligand. Accordingly, photoluminescent Ag and Cu nanoclusters with blue emission and photoluminescent Au nanocluster with orange emission in both solution and solid states were generically produced in this green strategy.

The final topic of this work is the most ambitious and novel one. For the first time, we demonstrated the correlation of composition with the observed emission of a positively charged photoluminescent bimetallic Au-Ag nanoclusters synthesized by means of double target sputtering on a biocompatible polymer matrix using MUTAB as ligand. We made this possible by controlling the applied current of the metal targets. As a result, we are able to tune the emission color of the bimetallic nanoclusters from blue to Near Infrared regions.

ACKNOWLEDGMENT

Thanks to my mentor, Assistant Professor Yohei Ishida and
to my kind and supportive Supervisor, Professor Tetsu Yonezawa
who shared their expertise and knowledge for the completion of this work.
Thanks also to all my labmates and staffs in Laboratory of Novel Materials Hybrid
Engineering who cried, laughed, and celebrated the challenges of life with me.

Thanks to JICA for the financial support
for the whole duration of my stay here in Sapporo.

ありがとうございました

TABLE OF CONTENTS

1. General Introduction	1
1.1 Photoluminescent metal nanocluster- A new class of sub 2 nanometer material which shows interesting molecule-like behavior.....	2
1.2 Chemical Synthesis of Photoluminescent Noble metal nanoclusters.....	4
1.3 Purification and PAGE isolation- a major breakthrough in understanding the photophysical property of metal nanoclusters.....	7
1.4 Scalable and precise synthesis of glutathione protected photoluminescent nanoclusters- pivotal to the realization of its practical applications.....	9
1.5 Generic Synthesis of photoluminescent metal nanoclusters.....	10
1.6 ESI-MS spectroscopy- the indispensable tool to characterize photoluminescent metal nanoclusters.....	13
1.7 Photoluminescent metal nanoclusters for biomedical applications.....	14
1.8 Physical Synthesis - A “greener” alternative for the synthesis of photoluminescent metal nanoclusters.....	17
1.9 Fundamentals of the sputtering process- history and preparation of thin films/nanoparticles.....	18
1.10 Sputtering deposition over liquid matrix- preparation of colloidal nanoparticles.....	19
1.11 Size control of nanoparticles via sputtering deposition.....	24
1.12 Matrix Sputtering Method –towards fluorescent nanoclusters.....	26
1.13 Formation mechanism of the fluorescent nanoclusters via Matrix Sputtering Method.....	35
1.14 Summary and perspective.....	39
1.15 References.....	43

2. Photoluminescent Au nanocluster by chemical reduction.....	52
2.1 Introduction.....	53
2.2 Experimental Section.....	55
2.2.1 Materials.....	55
2.2.2 Synthesis of photoluminescent Au nanocluster.....	56
2.2.3 Characterization.....	56
2.3 Results and Discussion.....	57
2.4 Conclusions.....	61
2.5 References.....	62
3. Photoluminescent Au, Ag and Cu nanoclusters by single target sputtering.....	64
3.1 Introduction.....	65
3.2 Experimental Section.....	67
3.2.1 Materials.....	67
3.2.2 Synthesis of Photoluminescent Au, Ag and Cu nanoclusters by sputtering in polymer liquid.....	67
3.2.3 Characterization.....	68
3.3 Results and Discussions.....	68
3.4 Conclusions.....	77
3.5 References.....	78
4. Photoluminescent bimetallic Au-Ag nanoclusters by double target sputtering.....	82
4.1 Introduction.....	83

4.2 Experimental Section.....	84
4.2.1 Materials.....	84
4.2.2 Synthesis of monometallic and bimetallic nanocluster.....	85
4.2.3 Characterization.....	87
4.3 Results and Discussion.....	88
4.4 Conclusions.....	98
4.5 References.....	99
5. General Conclusion	102
Appendix I. Supplementary Information for Chapter 2	105
Appendix II. Supplementary Information for Chapter 3.....	108
Appendix III. Supplementary Information for Chapter 4.....	111
Resume.....	119
List of publications.....	120
List of accomplishments.....	121

LIST OF FIGURES

Figure 1.1 Nanocluster is the missing link between isolated metal atoms and plasmonic metal nanoparticles.....	3
Figure 1.2 Dependence of emission color with respect to number of atoms.....	4
Figure 1.3 Correlation of number of atoms with emission energy.....	5
Figure 1.4 Commonly used template / ligand for the synthesis of photoluminescent metal nanoclusters in chemical reduction method.....	6
Figure 1.5 PAGE isolation of photoluminescent Au nanoclusters.....	8
Figure 1.6 Scalable and precise synthesis of glutathione protected Au ₁₀₋₁₂ , Au ₁₅ , Au ₁₈ and Au ₂₅ Nanoclusters via pH Controlled CO reduction.....	10
Figure 1.7 Generic synthetic scheme to synthesize glutathione protected Au, Ag, Cu and Pt nanoclusters.....	11
Figure 1.8 Aggregation induced emission of bimetallic Au-Ag nanocluster synthesized by glutathione.....	12
Figure 1.9 ESI-MS basic principle.....	13
Figure 1.10 Schematic diagram of typical ESI-MS (TOF).....	14
Figure 1.11 Au ₁₀₋₁₂ (SG) ₁₀₋₁₂ as a potential potential radiosensitizers for cancer radiotherapy.....	15
Figure 1.12 Au ₁₀ (SG) ₁₀ proposed crystal structure and ESI-MS isotopic pattern.....	16
Figure 1.13 Single target sputtering system for thin film production.....	19
Figure 1.14 Typical example of nanoparticles prepared by sputtering process.....	22
Figure 1.15 (a) colloidal bimetallic Au-Ag nanoparticles in Torimoto's bimetallic target system (b) our colloidal bimetallic Au-Ag nanoparticles and (c) schematic diagram of our double-head sputtering system for preparing alloy NPs.....	24

Figure 1.16 Size dependence of Au NPs varied by the viscosity of the liquid matrix by temperature.....	26
Figure 1.17 Molecular structures of the ligands used for matrix sputtering method.....	31
Figure 1.18 Concept of matrix sputtering method, without ligands, with volatile ligands, with non-volatile ligands.....	32
Figure 1.19 Effect of ligand functional groups (–COOH, –NH ₂ , and –SH) on the stabilization of NPs via matrix sputtering method.....	33
Figure 1.20 Absorption spectra, TEM diameter and fluorescence spectra of Au nanoclusters prepared by the sputtering deposition over PEG with varied MUA concentration.....	35
Figure 1.21 Correlation between TEM core diameters and fluorescence spectral change ($\Delta\lambda_{em} / nm$).....	37
Figure 1.22 Plausible mechanism for the formation of fluorescent Au nanoclusters via matrix sputtering method.....	38
Figure 1.23 Schematic illustrations of (a) primary aggregation (coalescence and growth), (b) secondary aggregation, and (c) immobilization of Ag NPs in thiourethane resin after polymerization.....	38
Figure 1.24 cellular imaging and sensing using choline inspired photoluminescent metal nanocluster.....	42
Figure 2.1 UV-Vis extinction spectra of Au nanoparticles and nanoclusters synthesized in the absence or presence of SDS (Au:TC:SDS = 1:5:0 and 1:5:5 (mol/mol/mol) for black and red spectra).....	57
Figure 2.2 TEM images and particle size distributions of Au nanoparticles or nanoclusters synthesized at Au:TC:SDS mol ratios of (a) 1:3:3, (b) 1:5:5, and (c) 1:7:7(mol/mol/mol).....	59
Figure 2.3 Fluorescence emission (blue) and excitation (black) spectra of synthesised gold nanoclusters (excitation wavelength = 300 nm, Au:TC:SDS = 1:7:7 (mol/mol/mol)).....	60
Figure 2.4 STEM-HAADF image of obtained Au nanoclusters.....	61
Figure 3.1 Schematic diagram of experimental sputtering set-up.....	69

Figure 3.2 UV-Vis Extinction spectra of Au, Ag and Cu nanoclusters in PEG dispersions with MUTAB.....	70
Figure 3.3 Photoluminescence spectra of Au, Ag and Cu nanoclusters in PEG dispersions with MUTAB.....	71
Figure 3.4 Transmission Electron Microscopy (TEM) images and size distribution histograms of (a) Au, (b) Ag and (c) Cu nanoclusters.....	73
Figure 3.5 XPS spectra at Au 4f and Ag 3d for photoluminescent Au and Ag nanoclusters respectively.....	75
Figure 3.6 STEM-HAADF image of photoluminescent (a) Au, (b) Ag and (c) Cu nanoclusters.....	76
Figure 4.1 Schematic diagram of experimental double target sputtering set up to produce bimetallic Au-Ag photoluminescent nanoclusters.....	85
Figure 4.2 UV-Vis Extinction spectra of as synthesized samples without and with MUTAB.....	89
Figure 4.3 TEM images and particle size distribution histogram of samples with MUTAB. (5) Ag@34mA, (7) Au@14mA-Ag@46mA, (9) Au@20mA-Ag@34mA, and (11) Au@26mA-Ag@14mA.....	91
Figure 4.4 Emission spectra of obtained photoluminescent monometallic nanoclusters (4 and 5), and bimetallic nanoclusters (6–11).....	92
Figure 4.5 Correlation between the emission energies and the atomic percent of Ag determined by XPS.....	95
Figure 4.6 Representative STEM-HAADF image and EDS mapping of sample 8 (Au@18mA-Ag@38mA).....	98

LIST OF TABLES

Table 4.1 Sputtering conditions for the synthesis of Au-Ag bimetallic nanoclusters.....	86
Table 4.2 Bimetallic composition measured by XPS and ICP-AES with respect to average diameter and emission peak energy.....	94
Table 4.3 Summary of Binding energies at Au 4f and Ag 3d regions.....	96

LIST OF ABBREVIATIONS

TEM	Transmission Electron Microscopy
HR-TEM	High Resolution Transmission Microscopy
UV-Vis	Ultraviolet-Visible spectroscopy
XANES	X-ray Absorption Near Edge Spectroscopy
XAFS	X-ray Absorption Fine Structure Spectroscopy
EXAFS	Extended X-ray absorption fine structure Spectroscopy
EDS	Energy Dispersive X-ray Spectroscopy
STEM	Scanning Transmission Electron Microscopy
HAADF-STEM	High Angle Annular Dark Field- Scanning Transmission Electron Microscopy
XRF	X-ray Fluorescence Spectroscopy
XRD	X-ray Diffraction
FTIR	Fourier Transform Infrared Spectroscopy
XPS	X-ray photoelectron Spectroscopy
EELS	Electron Energy Loss Spectroscopy
AFM	Atomic Force Microscopy
SAXS	Small Angle X-ray Spectroscopy
NMR	Nuclear Magnetic Resonance Spectroscopy
DLS	Dynamic Light Scattering Spectroscopy
AAS	Atomic Absorption Spectroscopy
ICP-AES	Inductive Coupled Plasma Atomic Emission Spectroscopy
ESI-MS	Electrospray Ionization Mass Spectrometry
MALDI	Matrix-Assisted Laser Desorption Ionization
SEC-HPLC	Size Exclusion Chromatography- High- Performance Liquid Chromatography
PL	Photoluminescence
TGA	Thermogravimetric Analysis
MUTAB	11-mercaptoundecyl- <i>N,N,N</i> -trimethylammonium Bromide
MUA	mercaptoundecanoic Acid
SMP	sodium 3-mercaptopropionate
PEEL	pentaerythritol ethoxylate
PEMP	pentaerythritol tetrakis(3-mercaptopropionate)

RTILs	Room Temperature Ionic Liquids
PEG	Polyethylene Glycol
DES	Deep Eutectic Solvents
LCs	Liquid Crystals
DMSO	Dimethylsulfoxide
TC	Thiocholine chloride
SDS	Sodium Dodecylsulfate
PAGE	Polyacrylamide Gel Electrophoresis
DFT	Density Functional Theory

1 GENERAL INTRODUCTION

Abstract

This chapter provides the general introduction for the topics of this dissertation containing the relevant related literature reviews for both chemical and physical approaches to synthesize photoluminescent metal nanoclusters. At the end of the chapter, a summary and research perspective was provided to direct the reader for future direction of this very promising field.

1.1 Photoluminescent metal nanocluster- A new class of sub 2 nanometer material which shows interesting molecule-like behavior.

Photoluminescent noble metal (Au, Ag and Cu) nanoclusters could be defined as a new class of materials with dimension less than 2 nm which typically consist of around 3 to 39 atoms and show absorbance and emission in the blue to Near Infrared (NIR) region of the electromagnetic spectrum.¹⁻⁵ It is considered as the transition between a single noble metal atom which shows distinct optical property and noble metal nanoparticles which shows characteristic plasmon absorbance in the visible region.⁶⁻¹⁰ The photoluminescence property of this material is attributed firstly, to “quantum size effects”^{1-5,11} wherein the clusters behave somewhat like a molecule and show tunable absorbance and emission depending on the number of atoms, secondly, to “surface-ligand effects”¹² for emissive clusters with strong coordinating ligands that deviate from the predictions based on cluster nuclearity, thirdly, to “relativistic effects”¹³ for clusters which exhibit aggregation induced emission due to presence of metal (I) species which has closed shell electronic configuration capable of metallophilic attraction and fourthly, to “synergistic effects”¹⁴ for photoluminescent bimetallic nanoclusters formed by mixing two different types of metal atoms.

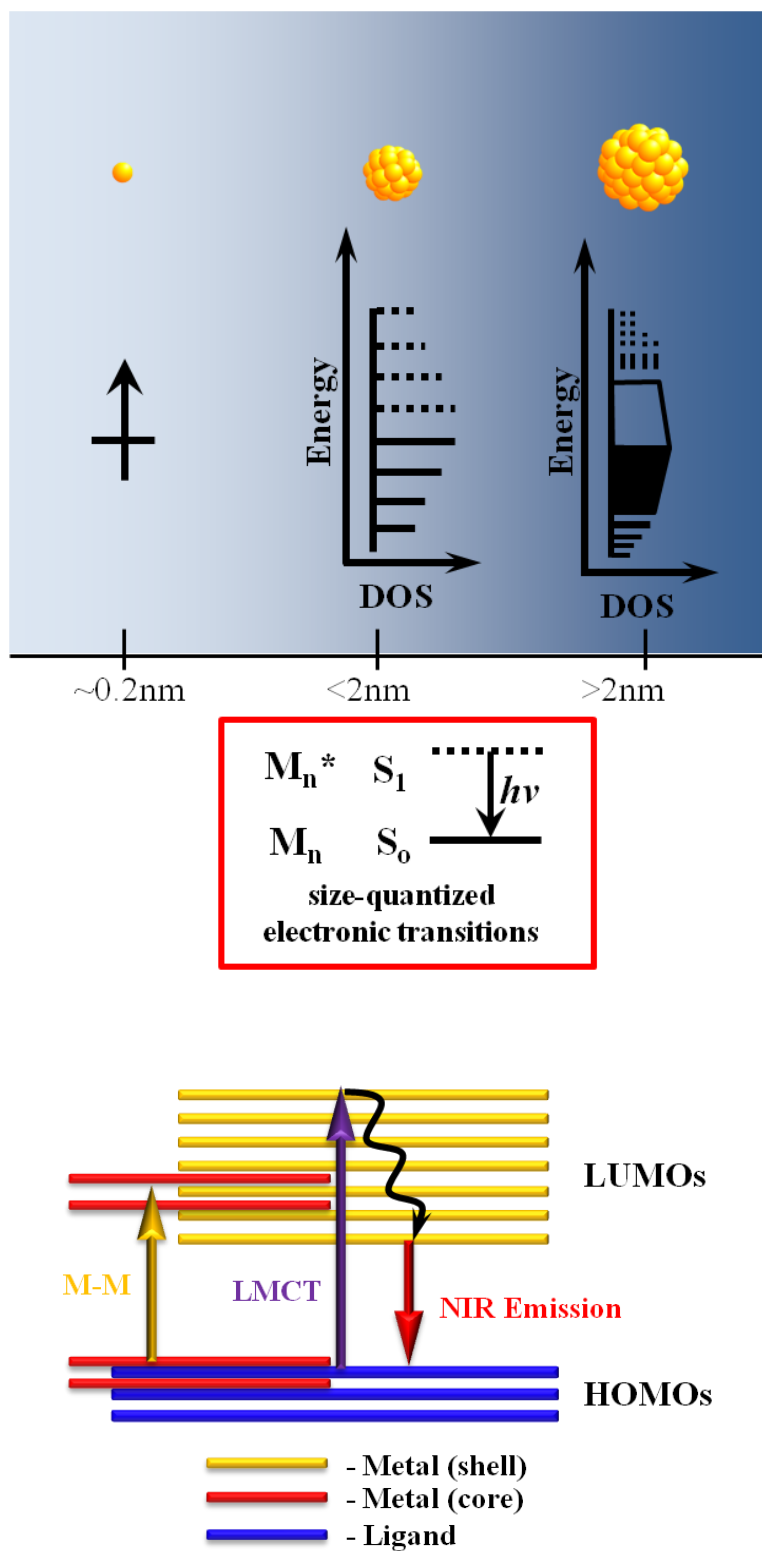


Figure 1.1 Nanocluster is the missing link between isolated metal atoms and plasmonic metal nanoparticles which behave somewhat like a molecule exhibiting absorbance within the UV-Visible region and emission within the Visible-NIR region of the electromagnetic spectrum.

1.2 Chemical Synthesis of Photoluminescent Noble metal nanoclusters.

Tunability of emission colors within the blue to NIR region with respect to number of atoms was first experimentally demonstrated by Dickson et al.⁴ for clusters encapsulated in PAMAM dendrimers. In their study a scaling function, $E_{\text{emission}} = E_{\text{Fermi}} / N^{1/3}$ which relates the emission energy with the nuclearity (N) of the cluster was introduced wherein they hypothesized that there will be no emission in the visible region once the number of atoms exceeds 30 which is in good agreement with the experimentally observed values. Interestingly, the quantum yield of these PAMAM based nanoclusters significantly increased as the number of atoms comprising the cluster decreased. Along with this diminution of number of atoms is the corresponding blue shift of excitation and emission peak energy.

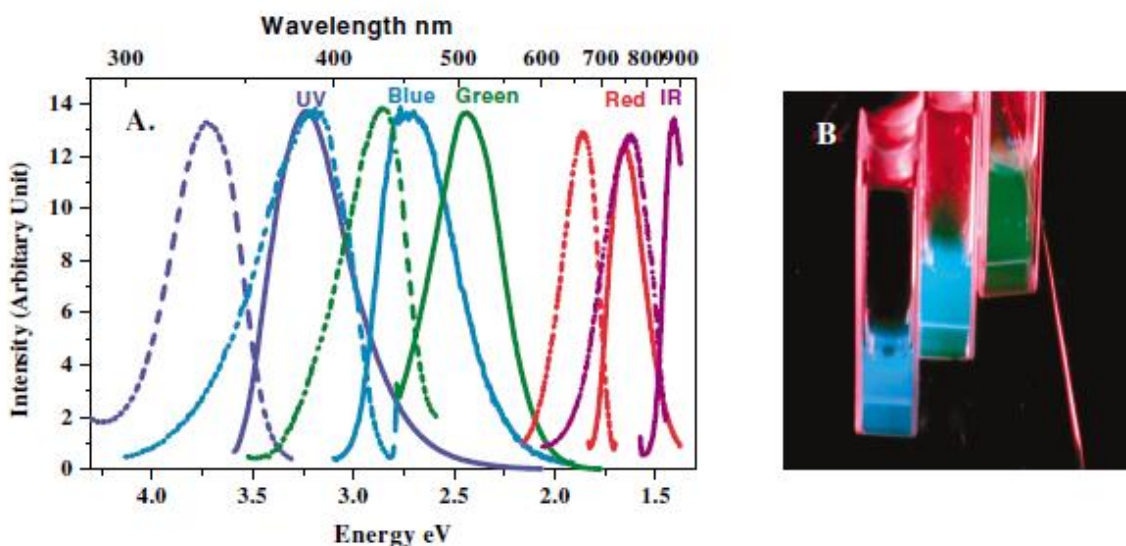


Figure 1.2 Dependence of emission color with respect to number of atoms. Reproduced with permission from ref 4. Copyright 2004 American Physical Society.

Gold cluster	Excitation (FWHM) (eV)	Emission (FWHM) (eV)	Quantum yield (%)	Lifetime (ns)
Au ₅	3.76 (0.42)	3.22 (0.45)	70	3.5
Au ₈	3.22 (0.54)	2.72 (0.55)	42	7.5
Au ₁₃	2.86 (0.38)	2.43 (0.41)	25	5.2
Au ₂₃	1.85 (0.21)	1.65 (0.26)	15	3.6
Au ₃₁	1.62 (0.20)	1.41 (0.10)	10	

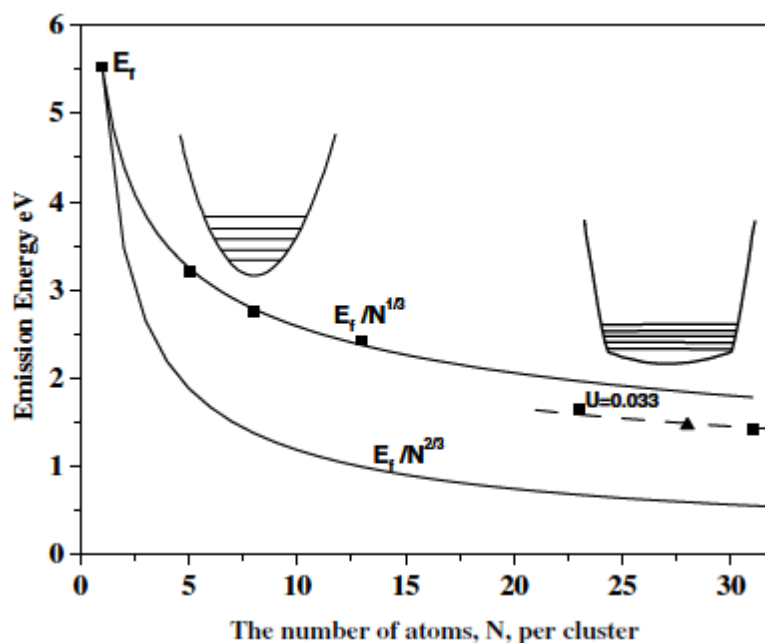


Figure 1.3 Correlation of number of atoms with emission energy. Reproduced with permission from ref 4. Copyright 2004 American Physical Society.

However, this scaling function failed to predict emissions of photoluminescent nanoclusters with stabilizing ligand that contains functional groups that has strong affinity with the metal atoms like thiols and phosphines which trigger the curiosity and imagination among nanocluster chemists, physical scientists and material scientists. This anomalous behavior opens up new avenues of researches especially in theoretical studies with the aid of structural modeling and first principle calculations (DFT) to understand the effect of this strong coordinating ligand on the observed photoluminescence.¹⁵⁻²⁰

Common methods to synthesize photoluminescent monometallic clusters were usually by means of chemical reduction using metal salt precursors and reducing agents like NaBH_4 to reduce a high valence metal ions (M^{+n}) to lower valence or neutral (M^{+1}/M^0) species.²¹⁻²³ Under this scheme, templates/ligands such as DNA, protein, dendrimer, phosphine and thiols are commonly employed to cap, protect, stabilize and control the growth of the cluster.²⁴⁻²⁶

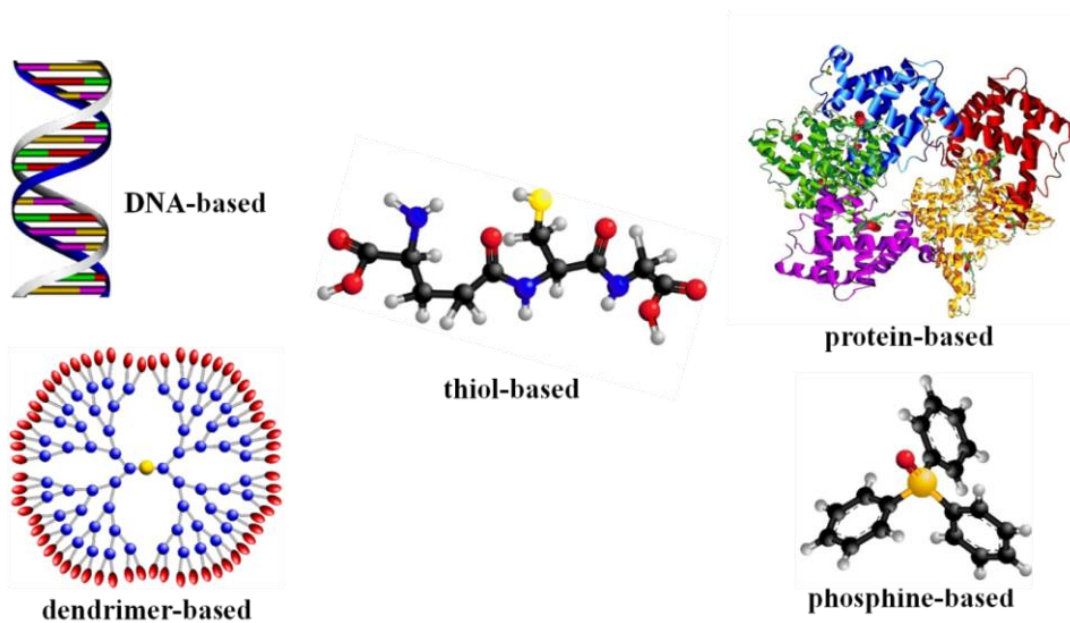


Figure 1.4 Commonly used template / ligand for the synthesis of photoluminescent metal nanoclusters in chemical reduction method.

Among of these strategies, thiol based synthesis pioneered by Brust for the synthesis of plasmonic nanoparticles and extended by Whetten and Murray for the synthesis of photoluminescent metal nanoclusters is becoming popular and is known to produce clusters with atomic precision.^{5,11} In a typical Brust synthesis, AuCl_4^- aqueous solution is transferred to an organic phase (toluene) using a phase transfer reagent, tetraoctylammonium bromide and then reduced with the aqueous solution of sodium borohydride in the presence of thiol molecules such

as dodecanethiol (C₁₂H₂₅SH). Within a few seconds, the yellow color of the organic phase will eventually turn deep brown.

The reaction could be summarized as follows:



In this typical scheme, BH₄⁻ ion is considered as the electron source to facilitate reduction.

Most of the thiol based synthetic scheme nowadays is classified as either one phase or two phase Brust-like scheme and had been modified considerably specially in nanocluster synthesis. Modification are usually done by varying the parameters such as (Metal/SR) ratio, type of thiol ligand used, temperature, reducing reagents, mode of reducing reagents addition, solvents used and the synthesis environment (reducing/oxidizing). For photoluminescent metal nanoclusters, typical technique is to use lower metal to thiol (M/SR) ratio (typically 1:5) and either to control the synthesis kinetically or thermodynamically for systematic control of particle size and its particle size distributions.

Among of the thiols, glutathione which is a natural peptide containing one thiol group in its cysteine residue is the most widely used ligand particularly for the synthesis of photoluminescent Au, Ag, Cu and Pt nanoclusters which are known plasmonic elements.²⁷

1.3 Purification and PAGE isolation-a major breakthrough in understanding the photophysical property of metal nanoclusters.

Successful synthesis and PAGE isolation of glutathione protected nanocluster was done by Negishi et al.⁵ way back in 2004 leading to the discovery of stable photoluminescent nanoclusters with core-shell structure: Au₁₅(SR)₁₃, Au₁₈(SR)₁₄, Au₂₅(SR)₁₈ and Au₃₈(SR)₂₄ and photoluminescent nanoclusters with ring type structure: Au₁₀(SR)₁₀, Au₁₁(SR)₁₁ and Au₁₂(SR)₁₂

which exhibit NIR emission. Spectroscopic measurements of these isolated clusters show their molecular nature and the optical and photophysical properties are highly dependent on the core size/number of atoms as well as the number of coordinating thiolates.

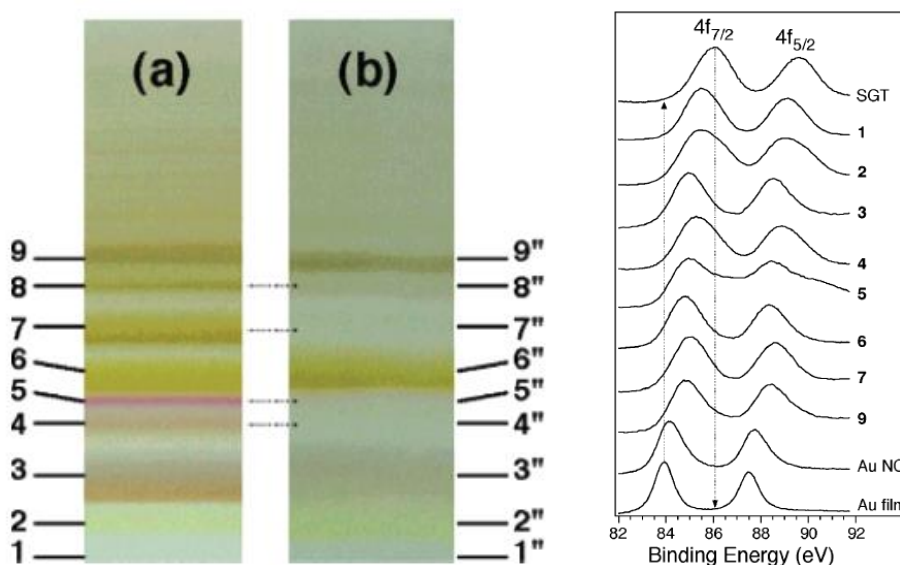


Figure 1.5 PAGE isolation of photoluminescent Au nanoclusters. Reproduced with permission from ref 5. Copyright 2005 American Chemical Society.

The isolated subnanometer photoluminescent nanoclusters convincingly filled up the information pertaining to structural evolution of Au(I)-thiolate complexes to a much larger thiolate protected Au NCs. To understand this structural evolution, the clusters were characterized with TEM, UV-Vis absorption, Photoluminescence (PL) spectroscopy and quantum yield measurements, XPS, NMR, FTIR, LC-MS and ESI-MS. From their result what can be deduced is that the synthetic protocol in this study produced variety of subnanometer nanoclusters separable according to its different m/z and electrophoretic mobilities. What is interesting in this result is that they were able to use XPS analysis and relate the spectra with the ESI-MS, PL and UV-Vis measurements which became pivotal for fundamental understanding of

structure and photophysical properties of these very small nanoclusters. With decreasing nuclearity, they found the position of binding energy of small Au nanoclusters deviated considerably towards higher binding energies with respect to the bulk Au and there is corresponding broadening of spectrum as the number of Au atoms decreased.

The seminal work of Negishi et al.⁵ however, is typically of low yield and may not be practical for large scale synthesis. After almost a decade, Yu et al.¹¹ reported a scalable and precise synthesis of glutathione protected Au₁₀₋₁₂, Au₁₅, Au₁₈ and Au₂₅ nanoclusters via pH controlled CO reduction.

1.4 Scalable and precise synthesis of glutathione protected photoluminescent nanoclusters-pivotal to the realization of its practical applications.

Yu et al.'s¹¹ method is based on using a gaseous reducing reagent such as CO to support a mild reaction environment for a slow and controlled growth of metal nanocluster. The reaction kinetics is then fine-tuned by adjusting the pH of the solution which eventually led to formation of atomically precise nanoclusters. These atomically precise nanoclusters were then characterized by TEM, UV-Vis, ESI-MS, XPS and NMR. This result is interesting for a number of reasons: firstly, the synthetic protocol is quite generic; secondly it is scalable, thirdly, the clusters could simply be produced by pH adjustment without further isolation. This achievement is more or less a step forward for the realization of potential application of photoluminescent Au nanocluster especially in biomedical fields.

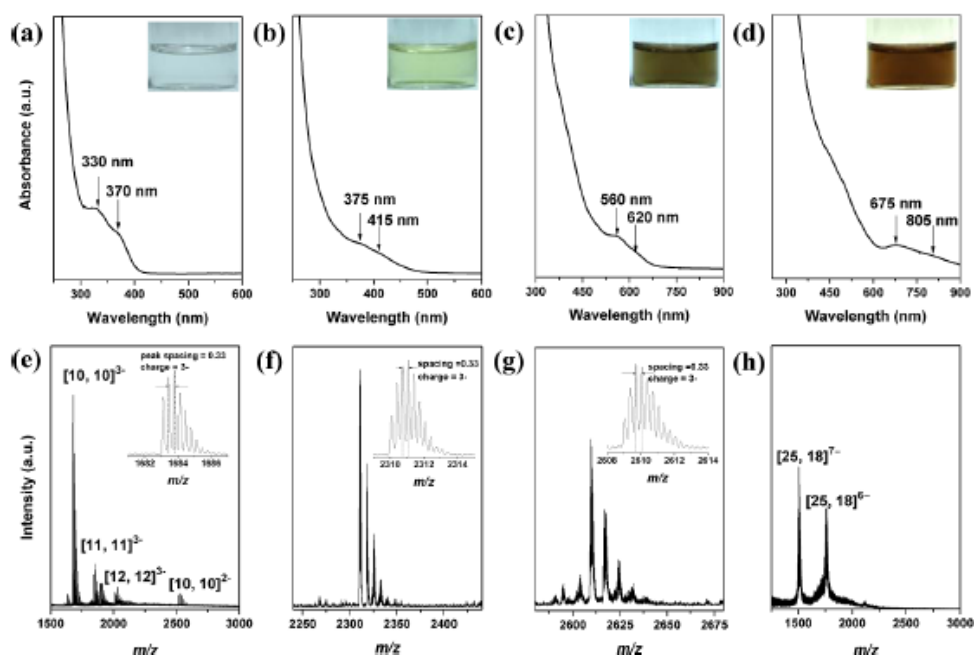


Figure 1.6 Scalable and precise synthesis of glutathione protected Au_{10-12} , Au_{15} , Au_{18} and Au_{25} Nanoclusters via pH Controlled CO reduction. Reproduced with permission from ref 11. Copyright 2013 American Chemical Society.

1.5 Generic Synthesis of photoluminescent metal nanoclusters

Yuan et al.²⁷ on the other hand, introduced a high yield general chemical reduction scheme using the glutathione ligand to synthesize a highly photoluminescent Au, Ag, Cu and Pt nanoclusters. Their scheme is based on electrostatically induced reversible phase transfer of a

non-fluorescent polydispersed nanoclusters protected by glutathione. This strategy involves interaction with glutathione protected nanoclusters with Cetyltrimethylammonium bromide (CTAB) which electrostatically interact with the carboxyl group of the ligand and facilitates the transfer from aqueous to organic phase (toluene). In the organic phase, the polydispersed non-fluorescent clusters experienced mild etching upon incubation until it becomes fluorescent. The clusters in organic phase were then transferred in aqueous phase by adding hydrophobic salt tetramethylammonium decanoate TMAD (in chloroform). In the process, the carboxyl group of the glutathione is freed which made the transfer from organic phase back to aqueous phase possible. The clusters were characterized using UV-Vis, PL and fluorescence lifetime measurement, EDS analysis, TEM, XPS, FTIR, ICP-MS and TGA. Although this result is practically interesting, the structure of the produced nanoclusters were not determined which is fundamentally needed particularly in theoretical studies to better understand the photophysical properties of these photoluminescent nanoclusters. Further study is needed in this area.

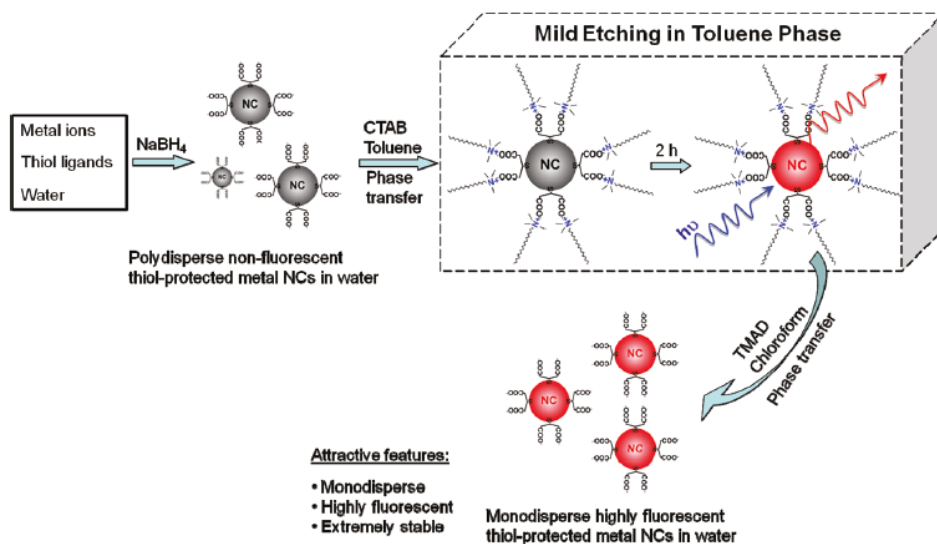


Figure 1.7 Generic synthetic scheme to synthesize glutathione protected Au, Ag, Cu and Pt nanoclusters. Reproduced with permission from ref 27. Copyright 2011 American Chemical Society.

Other than monometallic photoluminescent nanoclusters, glutathione was also successfully used to synthesize photoluminescent bimetallic Au-Ag nanoclusters. To date, there are three common methods to synthesize Au-Ag bimetallic nanoclusters: co-reduction, galvanic replacement and anti-galvanic replacement methods. However, using these techniques only weak photoluminescence is achieved, thus to enhance the luminescence, Dou et al²⁸, proposed a simple strategy by using Ag(I) ions to bridge small Au(I)-thiolate motifs on the weakly luminescent glutathione protected Au NCs. With this scheme, large Au(I)/Ag(I)-thiolate motifs were formed on the surface of the nanocluster which consequently enhanced the luminescence via aggregation induced emission (AIE). The method is quite facile, fast, scalable and generic. The bimetallic Au-Ag nanoclusters were characterized using UV-Vis, Photoluminescence and fluorescence lifetime measurements, XPS, MALDI-TOF and ICP-MS. This result shows a new strategy to enhance the quantum yield of weakly photoluminescent monometallic nanoclusters but offers no direct evidence as to how the silver ions selectively adhere to the surface of the Au nanocluster. Structural information needs further clarification to understand clearly the proposed aggregation induced emission mechanism.

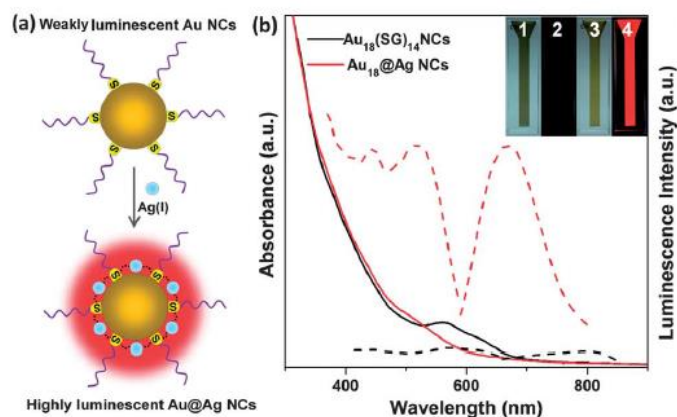


Figure 1.8 Aggregation induced emission of bimetallic Au-Ag nanocluster synthesized by glutathione. Reproduced with permission from ref 28. Copyright 2013 Royal Society of Chemistry.

1.6 ESI-MS spectroscopy- the indispensable tool to characterize photoluminescent metal nanoclusters.

Characterization of thiol protected photoluminescent nanoclusters is quite challenging. Whetten et al.²⁹ introduced ESI-MS characterization technique to determine the composition, charge states, isotope patterns and purity of the clusters produced. However, in their pioneering work they mistakenly identified $\text{Au}_{25}(\text{SG})_{18}$ with $\text{Au}_{28}(\text{SG})_{16}$ which was later corrected by Negishi et al's⁵ report. This correction becomes pivotal in understanding the property of the said nanocluster since even an extra atom at this size regime will already introduced significant misinformation particularly in theoretical studies.

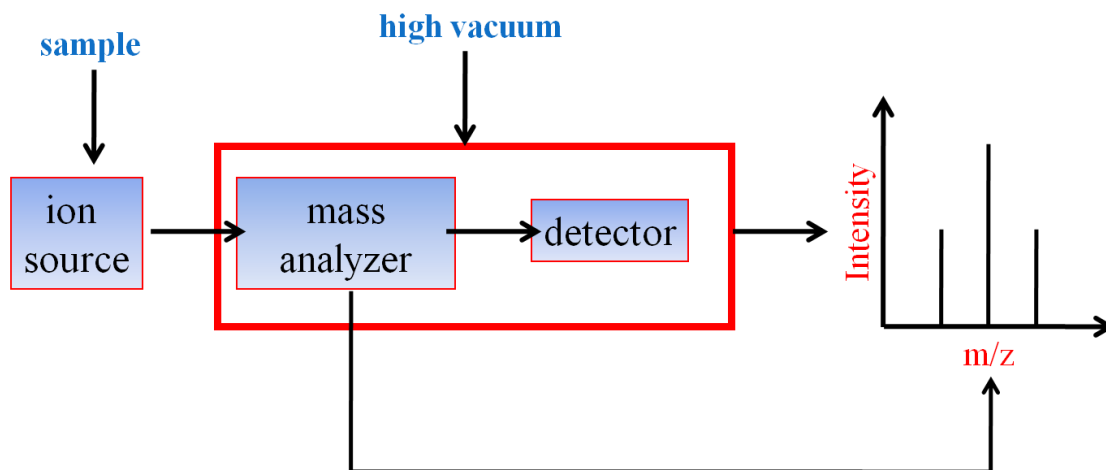


Figure 1.9 ESI-MS basic principle

ESI-MS basically consists of an ion source, mass analyzer and detector operated under high vacuum. Once the sample is introduced to the ionization chamber; it will obtain charge depending on the mode of ionization used: (+) / (-). Species with opposite charge with respect to the applied bias enter the desolvation assembly and freed from solvent. The desolvated charge species then enter to series of skimmers which act like a funnel before it enters to the mass analyzer (ex. TOF assembly) where it will be segregated according to its m/z .³⁰

Since the seminal work of Whetten et. al,²⁹ ESI-MS became an indispensable tool among nanocluster scientists to evaluate nanoclusters synthesized by other strongly coordinating ligand other than the glutathione such as anionic thiol³¹ and the infamous cationic thiol^{22,23} ligand, which we initiated for the synthesis of metal nanoclusters. Other than ESI-MS, characterization techniques like: MALDI, XPS Analysis, UV-Vis spectroscopy, and Photoluminescence spectroscopy, NMR, FTIR and Thermogravimetry (TGA) were also utilized to understand the chemistry of glutathione protected nanoclusters synthesized by chemical reduction.^{5, 27-32}

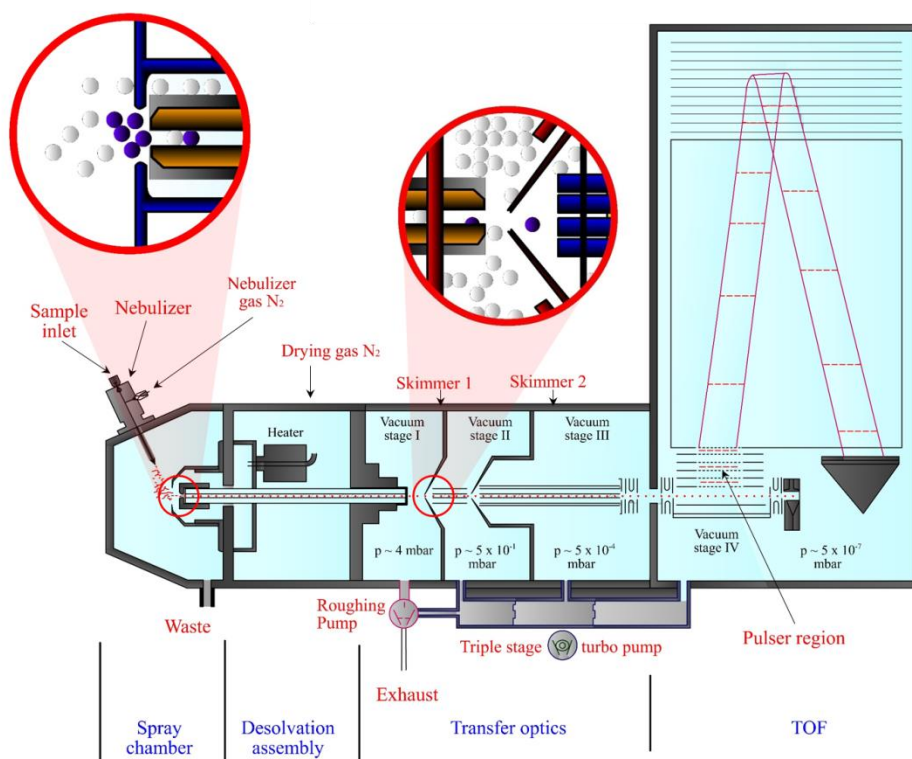


Figure 1.10 Schematic diagram of typical ESI-MS (TOF)

1.7 Photoluminescent metal nanoclusters for biomedical applications.

Potential application of chemically synthesized photoluminescent metal nanoclusters includes biomedical applications and is hypothesized to someday replace organic dye and

quantum dots particularly for sensing, imaging, therapy and targeted drug delivery.^{24-26,32} Relevant literature reviews for this topic had recently been reported by Zheng et al.²⁴, Zhang et al.²⁵ and Sun et al.²⁶

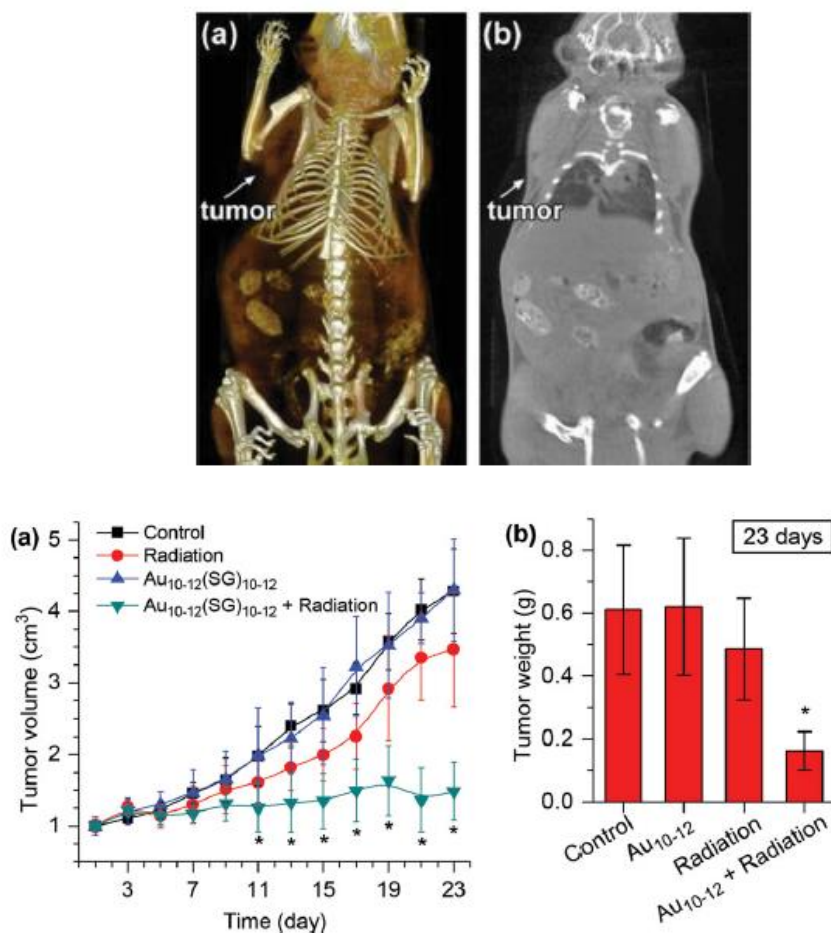


Figure 1.11 Au₁₀₋₁₂(SG)₁₀₋₁₂ as a potential potential radiosensitizers for cancer radiotherapy. Reproduced with permission from ref 32. Copyright 2014 WILEY-VCH Verlag GmbH & Co. KGaA, Weinheim.

Zhang et al.³² for instance demonstrated that the glutathione protected Au₁₀₋₁₂(SG)₁₀₋₁₂ is a potential radiosensitizers for cancer radiotherapy. These ultras small nanoclusters showed high tumor uptake, selectivity, efficient renal clearance and insignificant damage to normal tissues. This result offers a new hope for cancer research and may in the future be applied in vitro and in vivo not only for mice specimen but to actual human patients particularly for biomedical cancer

therapy. To understand the optical property of this promising ultrasmall glutathione protected Au nanoclusters, Bertorelle et al.¹⁷ recently performed synthesis, isolation and first principles theoretical analysis. They proposed that the cluster has no metallic core and may have a homoleptic catenane centrosymmetric-broken structure with two $\text{Au}_5(\text{SG})_5$ interconnected rings which enhanced the second harmonic circular dichroism signals in the spectral region: 250-400 nm.

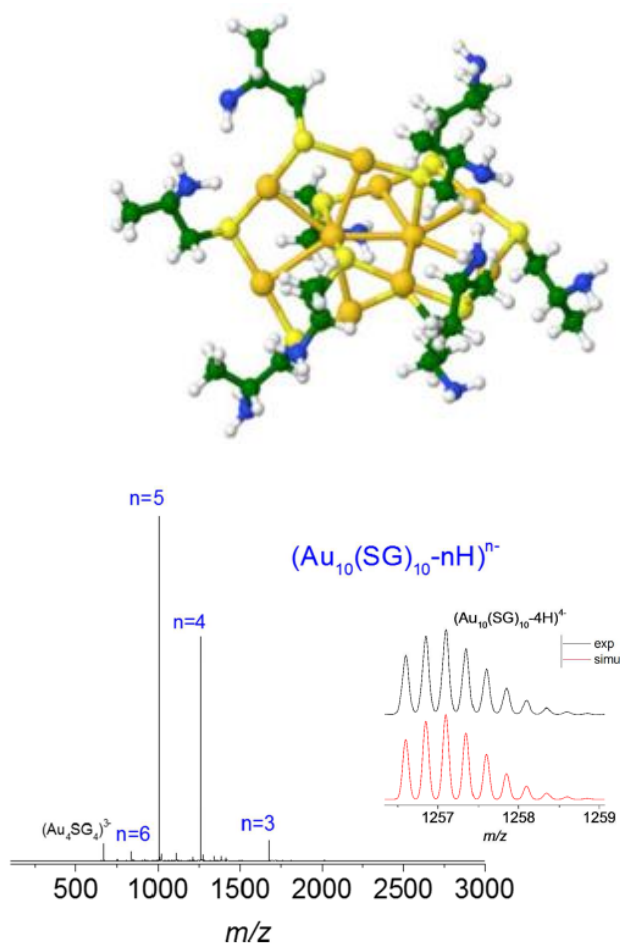


Figure 1.12 $\text{Au}_{10}(\text{SG})_{10}$ proposed crystal structure and ESI-MS isotopic pattern. Reproduced with permission from ref 17. Copyright 2017 American Chemical Society.

To date, exact crystal structure of these ultrasmall glutathione protected nanocluster have not been successfully obtained due to the difficulty of obtaining a single crystal in this type of

ligand. Ligand exchange with other thiol, such phenylethylthiolate (PET) which is dispersible in organic solvents are usually employed to obtain the single crystal and determine the structure. This is an opportunity to explore thiol ligands other than the commonly used glutathione. In fact, research in this direction is currently in progress especially the utilization of cationic thiol molecules like thiocholine and 11-mercaptoundecyl-*N,N,N*-trimethylammonium bromide.

Promising as it may sounds, photoluminescent metal nanoclusters however, is still in its infancy to date and still need to deal with intensive investigations especially for in vitro and in vivo biomedical applications due to purity and toxicity related issues arising from these chemically synthesized thiolated photoluminescent nanoclusters.²⁴ A “green synthetic” approach will be a better alternative in this regard, leading some scientists (including us) to strategies developed in physical synthesis such as laser ablation techniques³³⁻³⁵ and sputtering techniques³⁶⁻³⁹ which is a new emerging field for the synthesis of “greener” metal nanoclusters.

1.8 Physical Synthesis - A “greener” alternative for the synthesis of photoluminescent metal nanoclusters.

Noble metal nanoclusters synthesized by physical means are quite rare except for few reports which use sputtering techniques.⁴⁰⁻⁵⁰ As far as our knowledge is concern, this method which is originally designed for the production of thin films under high vacuum and dry state condition is now applicable even for liquid substrate for as long as the liquid has low vapor pressure.³⁶⁻³⁹ Because of this advancement, liquids with low vapor pressure are now exploited not only for the production of thin films but even for the synthesis of nanoparticles in wet conditions. Common example for this is the use of Castor oil, vegetable oil and Ionic liquids for the synthesis of plasmonic metal nanoparticles. Iimori et al.⁵¹ exploited ionic liquids for the

synthesis of photoluminescent Au nanocluster by means of sputtering and our group using liquid polymer matrix³⁴⁻⁴² like Polyethylene Glycol (PEG). Our liquid polymer matrix strategy was not only successful for the synthesis of plasmonic nanoparticles with controllable particle size and particle size distribution but most importantly for the synthesis of photoluminescent Au, Ag and Cu nanocluster as well as its corresponding bimetallic nanoclusters using variety of neutral, negative and positive charge, short and long carbon chain thiol molecules.

The succeeding subsections summarized the recent progress on the preparation of metal nanoparticles and photoluminescent noble metal nanoclusters using sputtering deposition over liquid matrix.

1.9 Fundamentals of the sputtering process –history and preparation of thin films

Historically discovered by Grove⁵² in 1852, sputtering is a technique employed for the fabrication of thin films⁵³⁻⁵⁷ and is commonly executed at high vacuum and dry conditions. Typically, there are three ways in which it could be performed: DC-diode, RF-diode and magnetron sputtering wherein the basic idea is the physical ejection of surface atoms through collision of ionized gas on a metal target and deposition of these ejected atoms / clusters on a solid substrate to obtain the thin film.³⁶⁻³⁹ To control the structure of the deposited film, sputtering, parameters such as discharge voltage, discharge current, distance between the target and substrate and working pressure are usually manipulated.³⁶ With the advancement of understanding however, sputtering system which is historically employed in solid substrates and dry conditions are now available even in liquid substrates and wet conditions which in the past is unimaginable.³⁶⁻³⁹ Examples of effective substrates employed are Ionic Liquids (ILs), Deep Eutectic Solvents (DES), Liquid Crystals (LCs), silicone oils, pentaerythritol tetrakis(3-

mercaptopropionate (PEMP), pentaerythritol ethoxylate (PEEL), Castor Oil, Canola Oil, Caprylic/Capric triglyceride, propane-1,2,3-triol, glycerol, diglycerol and Polyethylene Glycol (PEG).³⁶⁻⁵⁰ Fundamentally, common feature of these liquids is its low vapor pressure which is prerequisite to prevent vaporization under vacuum conditions.

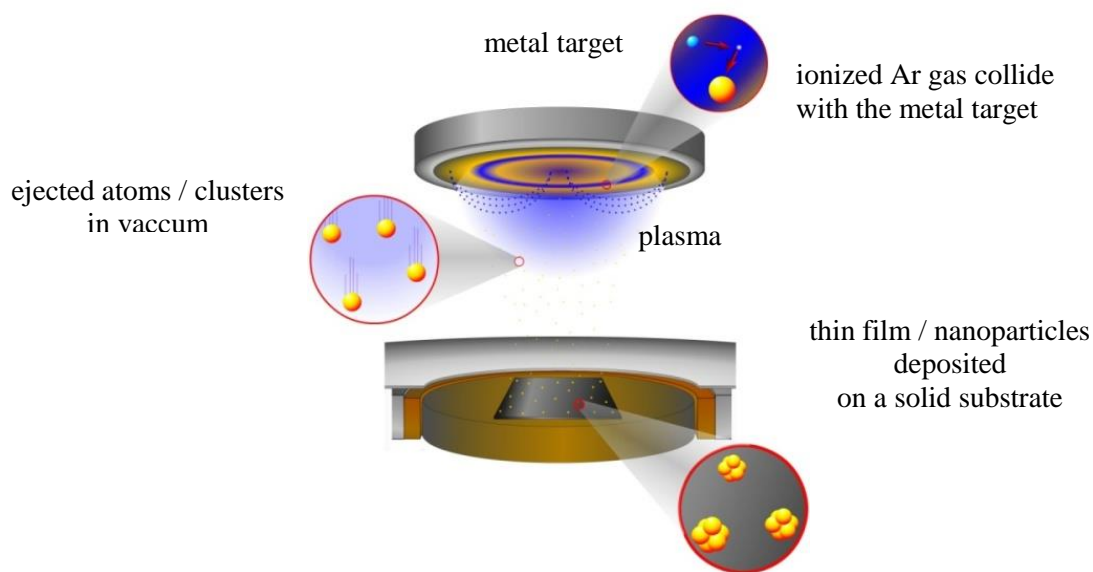


Figure 1.13 Single target sputtering system for thin film/nanoparticles production

1.10 Sputtering deposition over liquid matrix –preparation of (colloidal) nanoparticles

Nowadays, it is a common knowledge that any liquid which has low vapor pressure is in principle could be utilized as substrate in a sputtering system. This revolutionary concept widens the application of sputtering technique which is a very promising means to synthesize high purity materials at a high yield and opens new avenues of researches particularly in the synthesis of nanoparticles and nanoclusters in liquid form. Torimoto et al.⁵⁸ for instance, pioneered the utilization of Room Temperature Ionic Liquids (RTILs) in sputtering system for the synthesis of metal nanoparticles with dimension less than 10 nm in an environment-friendly way without the necessity of using toxic reducing reagents. RTILs became popular first, because of its high thermal and chemical stability, second, it has low surface energy, third, it is nonvolatile, fourth, it

has high conductivity, fifth, it has extended hydrogen bond systems, and sixth, it has the ability to dissolve many kinds of nanomaterials. Following Torimoto's seminal report, RTILs became a well exploited substrate not only for the synthesis of Au, Ag and Cu plasmonic nanoparticles⁵⁸⁻⁷⁸ but also for other metal nanoparticles⁷⁹⁻⁸⁹ and semiconducting nanoparticles. The popularity of RTILs had expanded not only for the synthesis of monometallic nanoparticles but also for the synthesis of bimetallic nanoparticles which is usually produced by sequential sputtering⁹¹⁻⁹³ using two different kind of metal targets, by sputtering using metal alloy⁹⁴⁻¹⁰⁰ targets and by simultaneous sputtering using two different metal targets in a double-head¹⁰¹⁻¹⁰⁴ sputtering system. Among of the monometallic nanoparticles produced using RTILs in sputtering systems are Au, Ag, Cu, Pd, Pt, Rh, Ir, Ru, W, Mo, Nb, Ti, In, Sn, Zr and bimetallic nanoparticles: AuAg, AuCu, AuPt, and AuPd as well as nanoparticles of metal oxides: Titanium oxide, Copper oxide and Tantalum oxide. Common techniques employed to characterize these nanoparticles include: Transmission Electron Microscopy (TEM), High Resolution-Transmission Electron Microscopy (HR-TEM), Ultraviolet-Visible (UV) spectroscopy, X-ray Absorption Near Edge Spectroscopy (XANES), X-ray Absorption Fine Structure Spectroscopy (XAFS), Extended X-ray Absorption Fine Structure Spectroscopy (EXAFS), Energy Dispersive X-ray Spectroscopy (EDS), Scanning Transmission Electron Microscopy (STEM), X-ray Fluorescence Spectroscopy (XRF), X-ray Diffraction (XRD), Fourier Transform Infrared Spectroscopy (FTIR), X-ray Photoelectron Spectroscopy (XPS), Electron Energy Loss Spectroscopy (EELS), Atomic Force Microscopy (AFM), Small Angle X-ray Spectroscopy (SAXS), Neutron Molecular Resonance Spectroscopy (NMR), Dynamic Light Scattering (DLS) and Atomic Absorption Spectroscopy (AAS).⁵⁸⁻¹⁰⁴

In the current research trends, RTILs is now reaching the realm of noble metal nanoclusters, especially the photoluminescent ones. For instance, Iimori et al.⁵¹ is able to

synthesized photoluminescent Au nanoclusters using ionic liquids in sputtering system. However, their synthesized Au nanoclusters showed emission peak shifts which are highly dependent on the excitation wavelengths used. This phenomenon most probably arose due to polydispersity of the nanoclusters produced in Ionic liquids which is typically stabilized “electrostatically”. Other than photoluminescent Au nanocluster, no other known reports which exploited the idea of using sputtering technique for the synthesis of photoluminescent metal nanoclusters stabilized in low vapor pressure liquid matrix other than RTILs except the reports of our group⁴⁰⁻⁵⁰ which are the first documented reports utilizing molten matrix and liquid polymer like (PEG) for the synthesis of photoluminescent metal nanoclusters.

Similar with Ionic Liquids, PEG is biocompatible, environment friendly, has low vapor pressure and commonly used. In contrast however, PEG is much cheaper than most RTILs and thus it is a much economical alternative for the synthesis of high purity nanomaterials in sputtering system. Hatakeyama et al.¹⁰⁵ demonstrated the first documented report in using PEG as a substrate, however, the concern is not on photoluminescent metal nanoclusters but on plasmonic metal nanoparticles. Among of the nanoparticles synthesized in PEG are Au, Ag, Cu and Ag-Au bimetallic nanoparticles which in comparison with the ones synthesized in RTIL are much larger and more polydispersed since there is no effective coordinating group in PEG unlike that of RTIL to prevent coalescence and growth. To address this issue, thiol molecule was introduced together with PEG and improvement in particle size and particle distribution was achieved also by the same researchers.¹⁰⁶ Our group however extended the concept of using PEG-thiol tandem in sputtering system for the synthesis of photoluminescent nanoclusters of Au, Ag, Cu and bimetallic Au-Ag using variety of thiol molecules with anionic, cationic and neutral charge states with either long or short carbon chain.

Unlike the nanoparticles with defined crystal structures, characterization of photoluminescent nanoclusters produced in PEG system is somewhat a challenge and limited only to some spectroscopic techniques like UV-Vis, Photoluminescence and quantum yield measurement, XPS Analysis, TEM, Thermogravimetric Analysis (TGA), Size Exclusion Chromatography-High Performance Liquid Chromatography (SEC-HPLC), High Angle Annular Dark Field-Scanning Transmission Electron Microscopy (HAADF-STEM) and Inductive Coupled Plasma-Atomic Emission Spectroscopy (ICP-AES).⁴⁰⁻⁵⁰ Currently, our focus is on controlling the particle size and particle size distribution and isolation of these nanoclusters to understand the origin of photoluminescence and its formation mechanism.

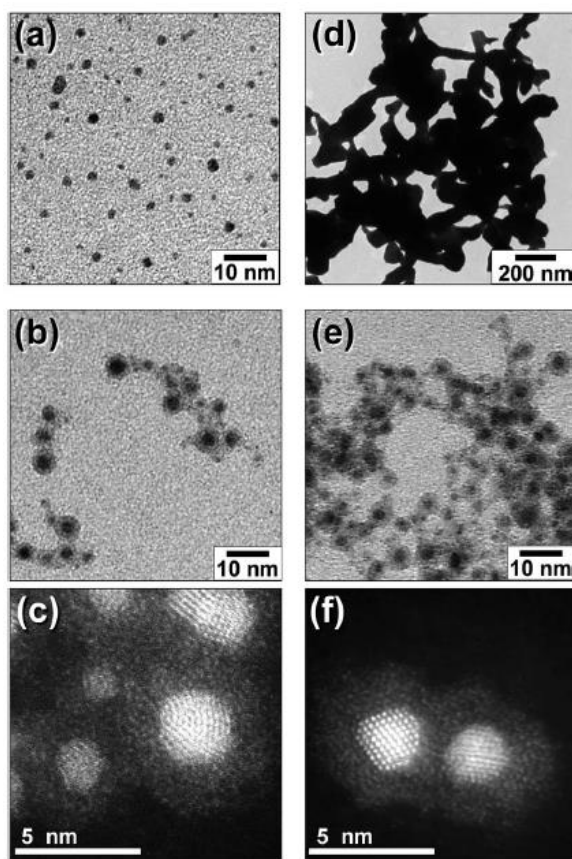
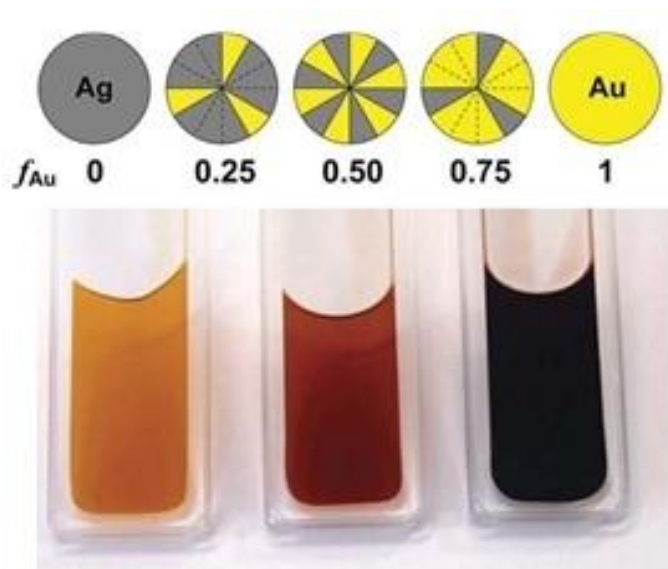
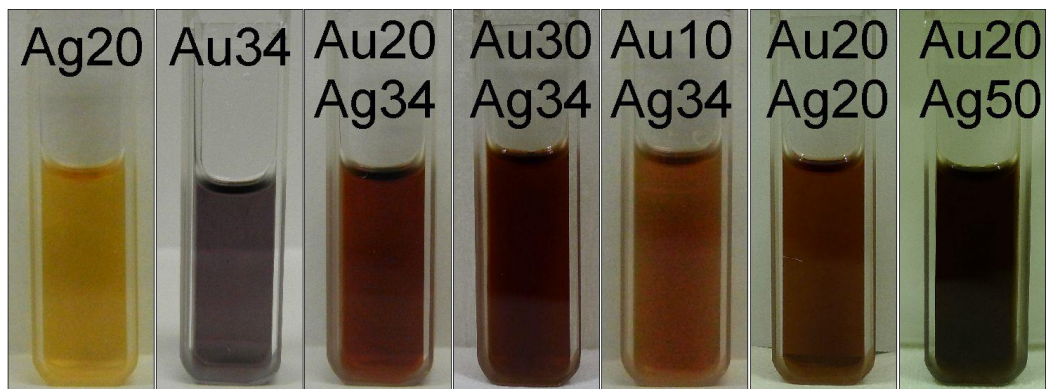


Figure 1.14 Typical example of nanoparticles prepared by sputtering process. Reproduced with permission from ref 93. Published by the Royal Society of Chemistry.

(a)



(b)



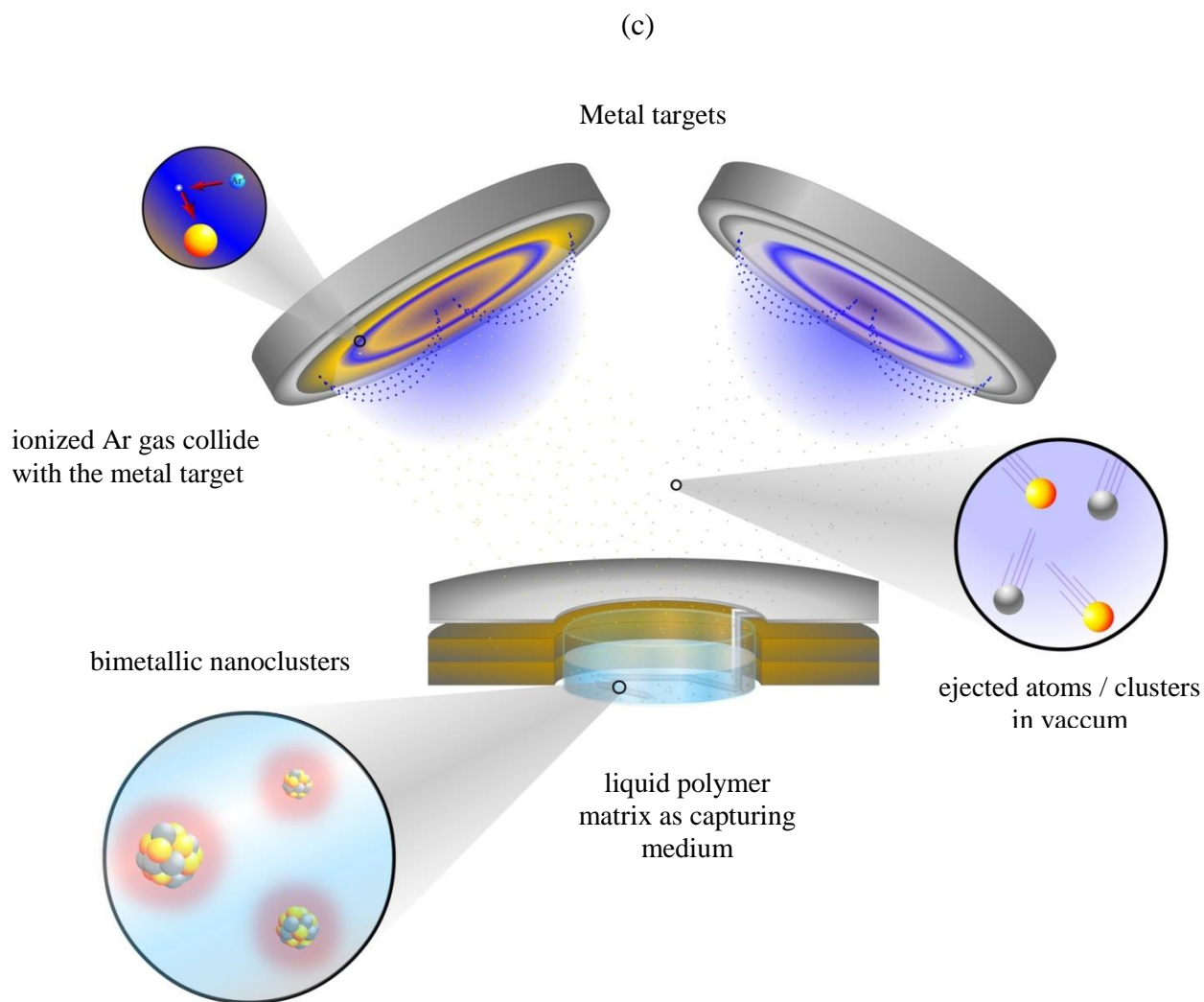


Figure 1.15 (a) colloidal bimetallic Au-Ag nanoparticles in Torimoto’s bimetallic target system. Reproduced with permission from ref 99. Copyright 2007 Royal Society of Chemistry. (b) our colloidal bimetallic Au-Ag nanoparticles. Reproduced with permission from ref 101. Copyright 2016 Elsevier B.V. All rights reserved. and (c) schematic diagram of our double-head sputtering system for preparing alloy NPs.

1.11 Size control of nanoparticles via sputtering deposition

Controlling the particle size and particle size distribution is the primary aim in the synthesis of metal nanoparticle in both chemical and physical means. In sputtering technique, this control could be done in two ways: either manipulating the parameters related to process or manipulating the parameters related to the solution.³⁶

For controlling the parameters which is related to process, parameters such applied current, voltage, distance between the target and substrate, chamber pressure, temperature and sputtering time are the ones being adjusted to control the particle size and distribution.^{36,40,107-110} In the case of Ionic liquids (ILs) sputtering system, Wender et al.¹⁰⁷ reported that sputtering current had significant effect on particle size and independent of sputtering time, whereas Sugioka et al.¹⁰⁸ reported that both sputtering time and sputtering current had significant effect on the particle size and distribution. Recently however, Hatakeyama et al.¹⁰⁹ reported that the temperature of metal target and applied voltage are the ones that had significant effect on the particle size and particle size distribution and only little or no significant effect on other process related parameters.

For controlling the parameters related to solution, parameters such as type, structure, composition, surface tension and viscosity of capturing medium used are usually manipulated.^{36,40,107-109} In ILs, it was found that the type and surface composition of the capturing medium used have significant effect on particle size and distribution whereas viscosity and surface tension have little or no effect at all.¹⁰⁹ In PEG system however, other than the process parameters commonly considered in ILs system: voltage, current, working distance, temperature and chamber pressure, we added additional process parameter such as stirring speed⁴⁰ which we found to be a significant factor for controlling the particle size and its distribution. Other than this, we introduced another parameter related to solution such as concentration⁴⁰ of thiol ligand, which we found to strongly affect the particle size of the nanoparticles produced and could effectively be controlled to produce photoluminescent nanoclusters.

To this end, recently we developed novel methodology to precisely control the size as well as photophysical property of metal NPs by sputtering process. While previous approaches

have relied on the surface composition and viscosity of liquid matrix for controlling particle diameters, our new approach introduced mercaptans as a stabilizer, inspired from chemical methods. In the chemical synthesis of metal NPs, controlling the concentration ratio between metal ions and stabilizing reagents is a possible means of systematic size control, with this regard, will this be applicable in sputtering system as well? Our results show that YES, it is!

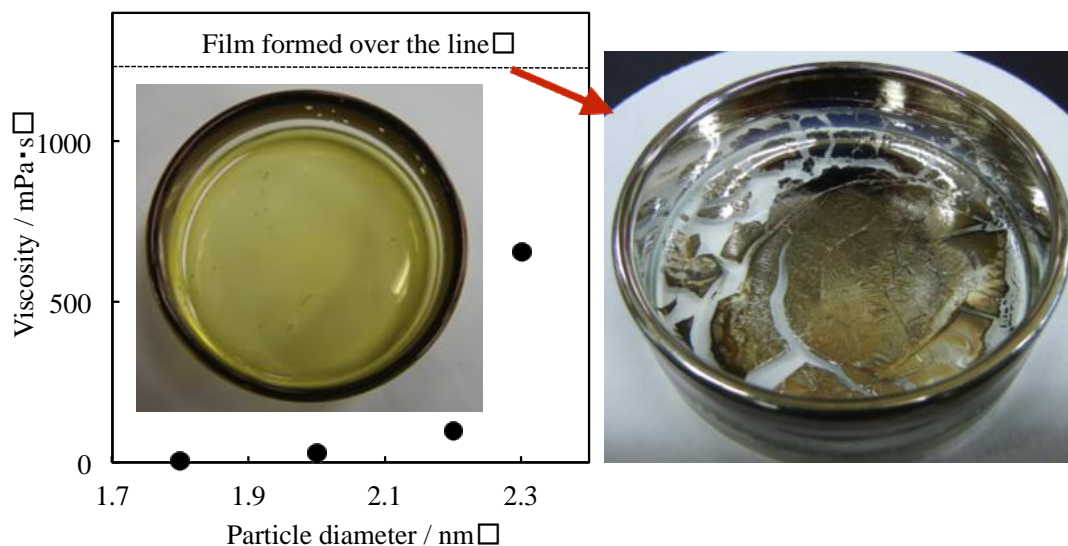


Figure 1.16 Size dependence of Au NPs varied by the viscosity of the liquid matrix by temperature. Reproduced with permission from ref 47. Copyright 2016 Elsevier B.V. All rights reserved.

1.12 Matrix Sputtering Method –towards fluorescent nanoclusters

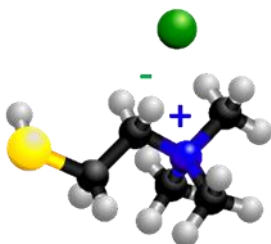
Way back in 2010, we developed a simple matrix sputtering technique using 6-MTAB as ligand for the first synthesis of NIR photoluminescent Au NP / Au nanocluster with large stoke shifts using a sputtering system.⁴¹ The particle size of this synthesized cluster is around 1.3 ± 0.3 nm which is quite monodispersed and is water soluble due to the inherent cationic charged of the ligand used. In the succeeding report, we utilized PEEL and PEMP as matrix for the synthesis of AuNPs/urethane and AuNPs/thiourethane hybrid resins respectively wherein we found non-photoluminescent material in the former, but an NIR photoluminescent hybrid material for the

latter due to strong coordinating thiol group in PEMP with gold atoms (compared with hydroxy group in PEEL) which effectively prevented the coalescence and growth of particles.⁴² We then explored α -TG, a volatile stabilizer to synthesize a novel NIR photoluminescent Au nanocluster wherein we found a red-shift in emission as the particle size increased.⁴³ At optimum condition, the synthesized photoluminescent Au nanocluster has 16.1 % quantum yield which is higher than reported quantum yield for thiolated Au nanoclusters synthesized by chemical reduction. Other than this, we also tried to synthesize Au nanocluster in silicone oil as matrix using octadecanethiol as capping ligand which is the first photoluminescent Au nanoclusters produced in this type of matrix.⁴⁴ We then proceed with systematic investigation of the effect of stabilizing ligand which contains thiol, amine and carboxy groups using diglycerol (DG)⁴⁵ matrix for the synthesis of photoluminescent Au nanoclusters wherein we again verified that photoluminescent Au nanoclusters could readily be produced using ligand with thiol group compared with the ones that contain amine and carboxy groups. Using the same DG matrix, we utilized thiocholine molecule, the shortest quaternary ammonium cation and investigated the effect of thiol concentration to the UV-Vis extinction, Photoluminescence spectra and particle size of Au nanoclusters wherein we found a correlation between thiol concentration and particle size.⁴⁶ At high thiol concentration, the UV extinction profile became featureless and the synthesized clusters exhibited NIR emission as well. With this earlier studies however, we have not employed any attempt to isolate the clusters to systematically understand the photoluminescence behavior of this NIR emitting photoluminescent Au nanocluster. Our first attempt to understand the mechanism by purifying and isolating the clusters according to size was only done recently, using polyethylene glycol (PEG) as the capturing medium and 11-mercaptoundecanoic acid (MUA) as stabilizing ligand.⁴⁰ Likewise, in this study we further verified that with increasing

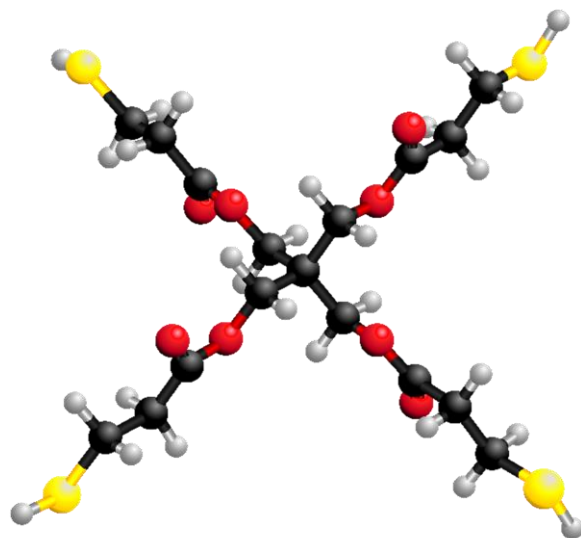
thiol concentration, the UV-Vis extinction profile became featureless and the Au nanoclusters started to exhibit NIR photoluminescence. Moreover, we systematically observed the size dependence of emission which shows a red shift as the clusters became large in sizes with decreasing thiol concentration as verified by TEM. However, when we tried to isolate the very small clusters, we found no significant shift in emission peaks as the particle size increased which led us to conclude that the clusters as seen in TEM are not single crystals but aggregates of these very small clusters or polynuclear complexes. Other than Au nanoclusters, we also tried the PEG-MUA sputtering system for the synthesis of Ag nanoclusters, wherein we likewise found that at higher concentration of ligand, particle size becomes small and the plasmon absorbance of Ag disappeared which is a similar phenomenon with that of photoluminescent gold nanocluster.⁴⁷ This is also the first study wherein we used HAADF-STEM and EDX mapping technique to characterize the Ag nanocluster other than the usual TEM imaging. In another report, again using PEG as matrix, we are able to produce a water dispersible NIR emitting nanoclusters using high concentration of sodium 3-mercaptopropionate (SMP) a very short anionic thiol ligand.¹¹⁰ Only recently, we are able to synthesize a blue emitting Ag nanoclusters using the same PEG matrix but this time we used a long carbon chain cationic thiol, 11-mercaptoundecyl-*N,N,N*-trimethylammonium bromide (MUTAB) as ligand which shows photoluminescence in both solution and solid states.¹¹¹ Other than PEG, we used another matrix with thiol moiety, PEMP to synthesize photoluminescent Ag nanocluster and investigated the time dependence of both extinction and photoluminescence spectra.⁴⁸ In this study we proposed two possible aggregation mechanisms: primary and secondary aggregation to explain the photoluminescence mechanism observed in Ag nanoclusters. Furthermore, we are able to immobilize these photoluminescent Ag nanoclusters in thiourethane resin; however, we observed

degradation of photoluminescence with time for this nanocluster. In addition to Ag nanoclusters, we are able to extend the PEMP sputtering system to synthesize photoluminescent Cu nanocluster which is much challenging since Cu is much prone to oxidation than Ag and Au.⁴⁹ With this technique however, we successfully synthesized blue emitting copper nanocluster with small particle sizes and narrow particle size distribution (1.1 ± 0.2 nm) that could transform into red emitting Cu₂S nanoclusters either by storage for several days or immediately with the aid of UV-light irradiation. Furthermore, a stable blue photoluminescent Cu nanocluster was achieved using 11-mercaptoundecanoic acid (MUA) as ligand in PEG matrix which shows increased in intensity as the amount of ligand increased.⁵⁰ Only recently, using the same PEG matrix and cationic MUTAB as ligand, we finally obtained a much stable blue photoluminescent Cu nanoclusters which show similar blue photoluminescence in both solution and solid states.¹¹¹

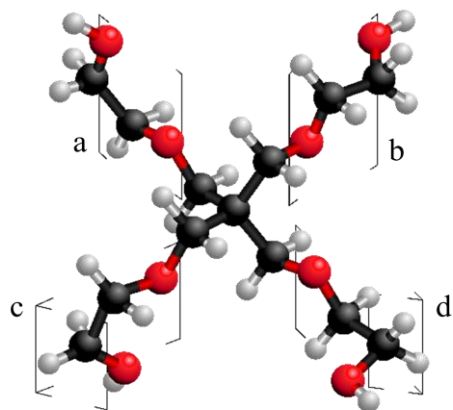
To summarize this section, most of our publications to produce photoluminescent metal nanoclusters on a liquid polymer matrix focused on thiol-based synthesis using varieties of neutral, anionic and cationic charge states with either short or long carbon chain thiol molecules. Particle size and particle size distribution control in this system could be done simply by controlling the concentration of thiol molecule in the liquid matrix while maintaining the process parameters such as working distance, temperature, voltage, current, stirring speed and chamber pressure constant at a fixed amount of time.



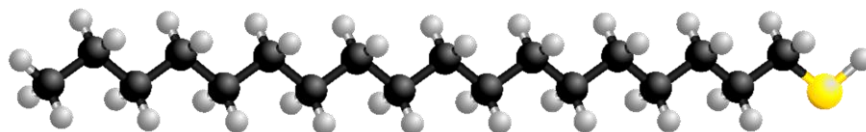
thiocholine chloride



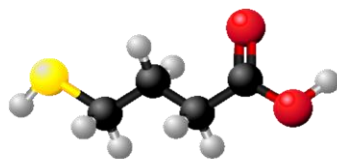
pentaerythritol tetrakis
(3-mercaptopropionate)



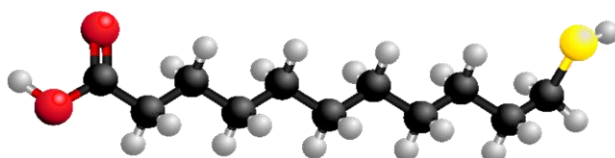
pentaerythritol ethoxylate



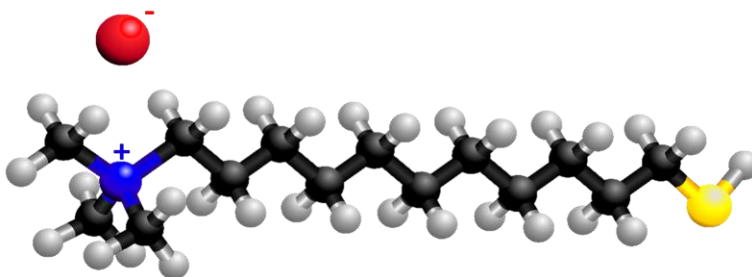
octadecanethiol



3-mercaptopropionic acid



11-mercaptoundecanoic acid



11-mercaptoundecyl-*N,N,N*-trimethylammonium bromide

Figure 1.17 Molecular structures of the ligands used for matrix sputtering method.

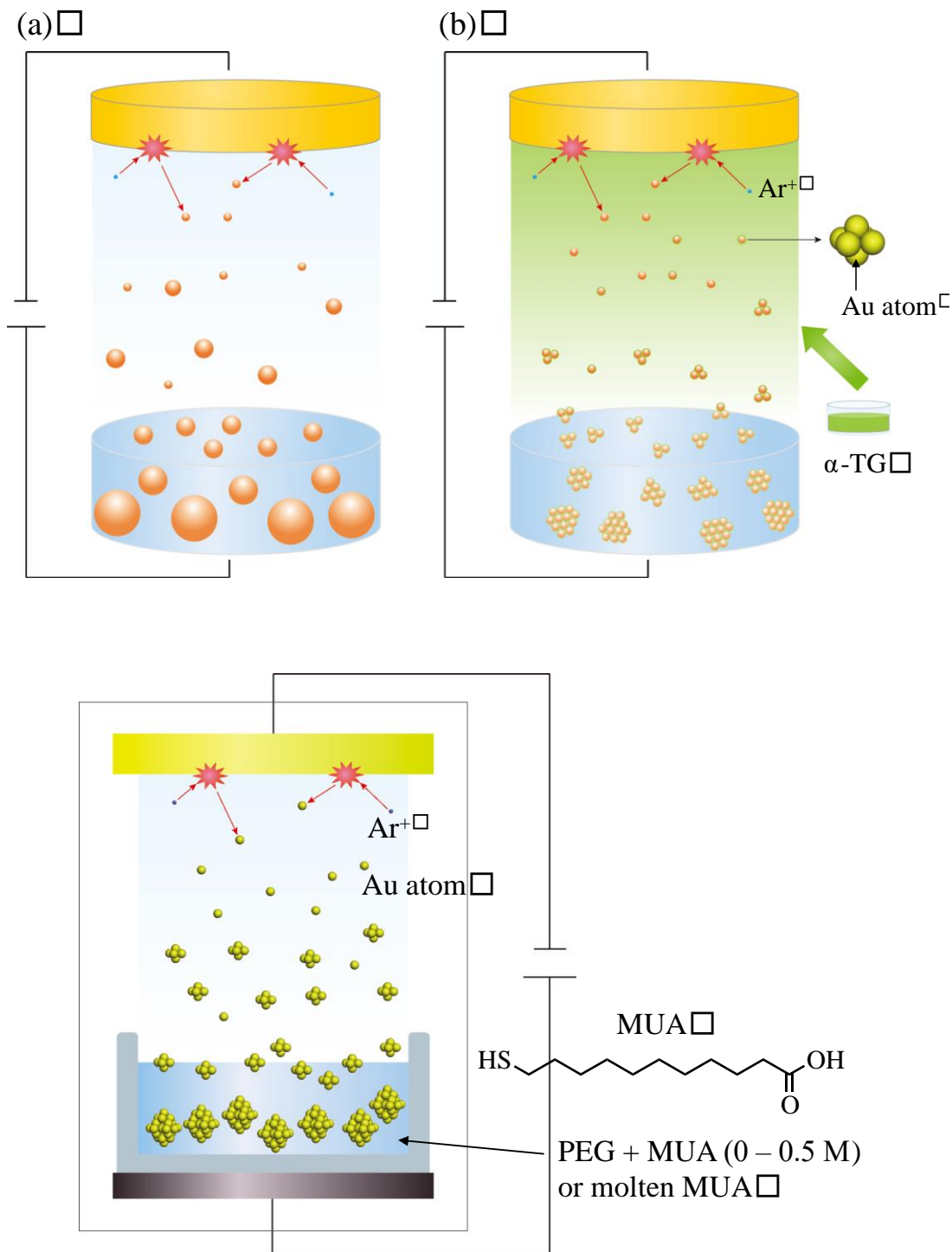


Figure 1.18 Concept of matrix sputtering method. without ligands, with volatile ligands, Reproduced with permission from ref 43. Copyright 2015 American Chemical Society and with non-volatile ligands. Reproduced with permission from ref 40. Copyright 2016 Rights managed by Nature Publishing Group.

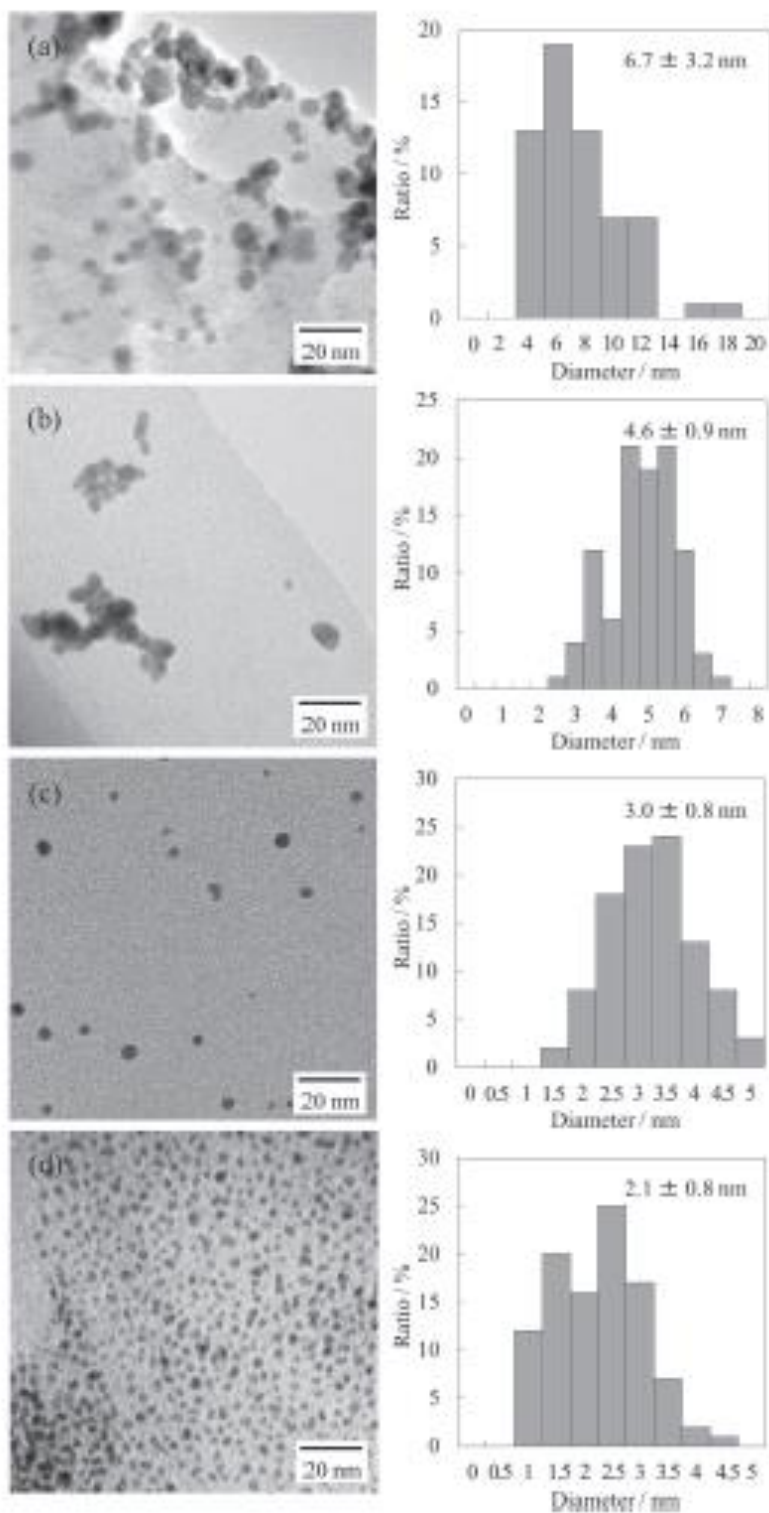
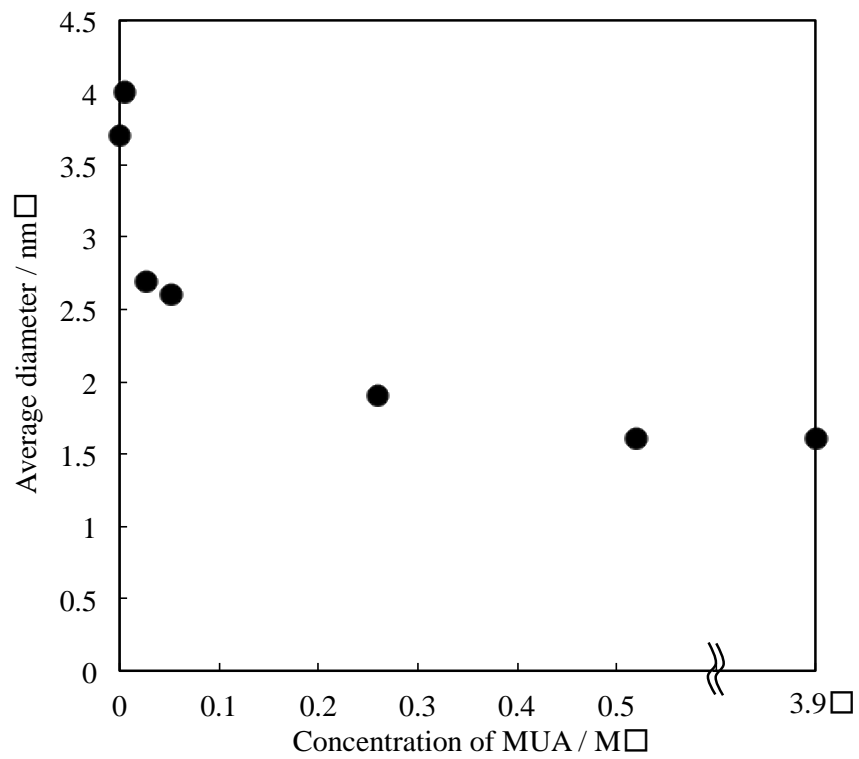
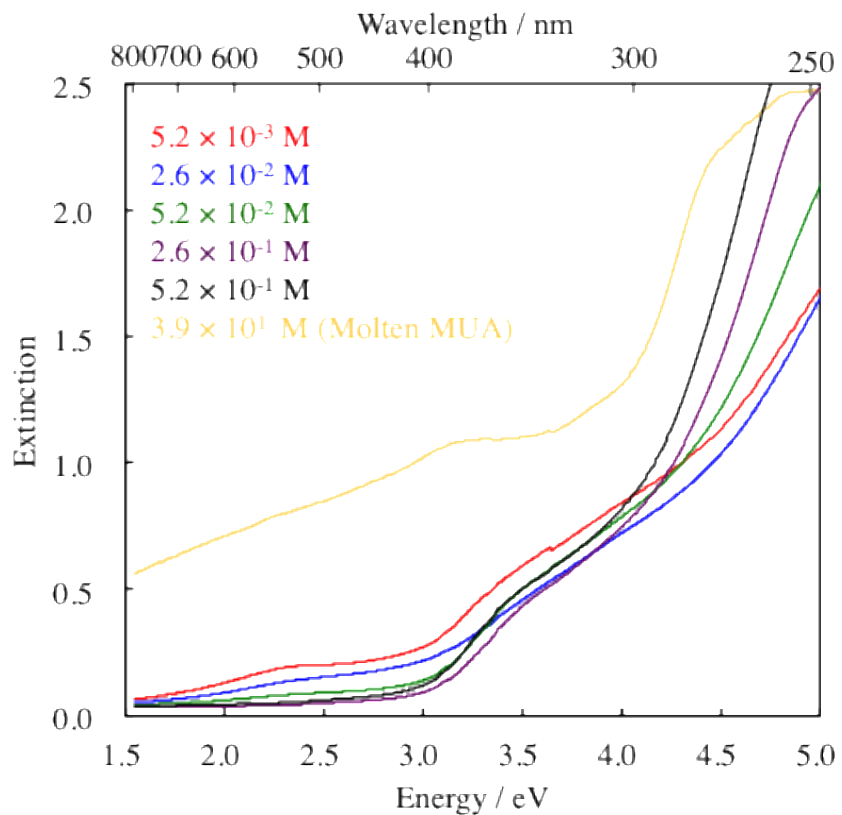


Figure 1.19 Effect of ligand functional groups ($-\text{COOH}$, $-\text{NH}_2$, and $-\text{SH}$) on the stabilization of NPs via matrix sputtering method. Reproduced with permission from ref 45. Copyright 2016 The Chemical Society of Japan.



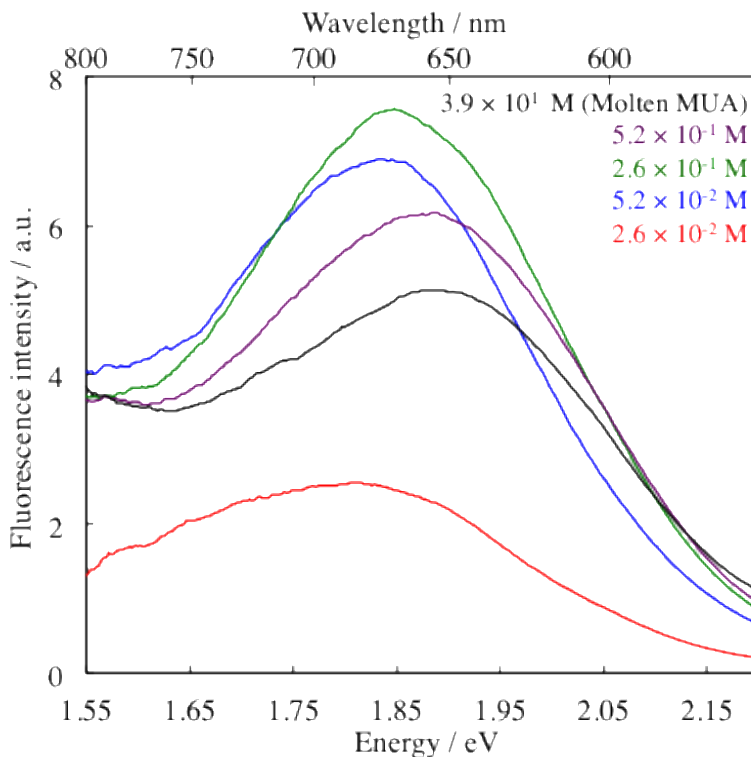


Figure 1.20 Absorption spectra, TEM diameter and fluorescence spectra of Au nanoclusters prepared by the sputtering deposition over PEG with varied MUA concentration. Reproduced with permission from ref 40. Copyright 2016 Rights managed by Nature Publishing Group.

1.13 Formation mechanism of the fluorescent nanoclusters via Matrix Sputtering Method

Understanding the formation mechanism and the origin of photoluminescence of the physically synthesized nanoclusters require isolation of high purity nanocluster, thus we developed purification and isolation protocol.⁴⁰ Our purification process involved re-precipitation of the nanocluster in chloroform and ethanol after dissolving it in DMSO; this is to ensure removal of excess PEG and ligand. The purified sample was then to be analyzed with XPS wherein we found in the case of Au nanoclusters synthesized in our PEG-thiol single target sputtering system that the maximum peaks are shifted at high binding energies with respect to the binding energy of the bulk gold at Au 4f region and coincided with the binding energies of Au nanoclusters with $\text{Au}_{10}(\text{SR})_{10}$, $\text{Au}_{11}(\text{SR})_{11}$, $\text{Au}_{12}(\text{SR})_{12}$ and $\text{Au}_{15}(\text{SR})_{13}$ structures which are

known NIR photoluminescent Au nanocluster. The composition ratio (Au/SR) of the cluster was then to be determined using TG Analysis wherein we found that in the case of Au nanocluster, the Au/SR ratio is around 0.96 which is close to the Au/SR ratio of nanoclusters with $Au_n(SR)_n$ structures with 1:1 (metal atom: thiol) correspondence and strongly verified the hypothesized structure determined by XPS. The particle sizes of the purified nanoclusters were then to be determined using TEM wherein we found that the Au nanoclusters we produced have particle sizes around 1.6 nm which is in good agreement with the particle size of $Au_{144}(SR)_{60}$. However we found this result somewhat contradictory to the results of UV-Vis extinction and Photoluminescence measurement since nanoclusters of this size and structure is typically non-photoluminescent, these findings led us to hypothesize that the nanoclusters most probably contain mixture of very small nanoclusters or multinuclear complexes in its aggregated form and not as single crystals. To further clarify this issue we isolated the clusters by means of SEC-HPLC system wherein we found much smaller nanoclusters around 1.2 ± 0.6 nm which strongly supports the structure assignment. As for the formation mechanism, without the addition of thiol ligand, what we can produced in direct sputtering in PEG are plasmonic nanoparticles which were probably formed by aggregation of atoms / small clusters and coalescence on the vacuum-liquid interface and in the liquid matrix since there is no effective coordinating group in PEG that could suppress this spontaneous coalescence and growth. The introduction of thiol ligand especially at high concentrations on the other hand, effectively prevented this immediate aggregation, coalescence and growth due to strong affinity of thiol molecule with metal atoms. However, these produced nanoclusters have the tendency to form aggregates in PEG matrix which may seem big particles when viewed using TEM due to its limited resolution. Similar observations were also exhibited by both Ag and Cu nanoclusters. To understand the effect of

this aggregation to the photoluminescence phenomena and UV-Vis absorbance, we tried to immobilize the clusters in thiourethane resin and applied polymerization technique, after polymerization we found that the aggregation could effectively be suppressed although degradation of photoluminescence do occur with time in this process.⁴⁸ Thus we continually search for ligands that could effectively avoid this photoluminescence degradation without any polymerization as possible. Only recently, we are able to synthesize extremely stable photoluminescent Cu nanocluster using MUA as ligand which shows increasing photoluminescence intensity as a function of thiol concentration. In our present endeavor, we are pursuing a generic synthetic scheme that could synthesize stable photoluminescent coinage metal nanoclusters and bimetallic nanoclusters of these elements in both solution and solid states using MUTAB as stabilizing ligand. So far, we are gathering good results in this direction and we are positive that this effort is beneficial to the science of this new emerging sputtering technique.

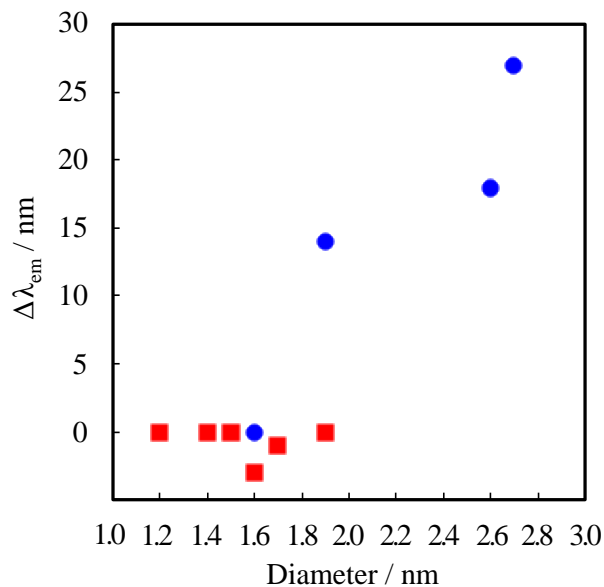


Figure 1.21 Correlation between TEM core diameters and fluorescence spectral change ($\Delta\lambda_{em} / \text{nm}$). Red squares denote the size-fractionated Au nanoclusters by SEC-HPLC, and blue circles denote the different sized fluorescent Au nanoclusters synthesized by varying the concentration of thiolate ligand (MUA) during the sputtering deposition. Reproduced with permission from ref 40. Copyright 2016 Rights managed by Nature Publishing Group.

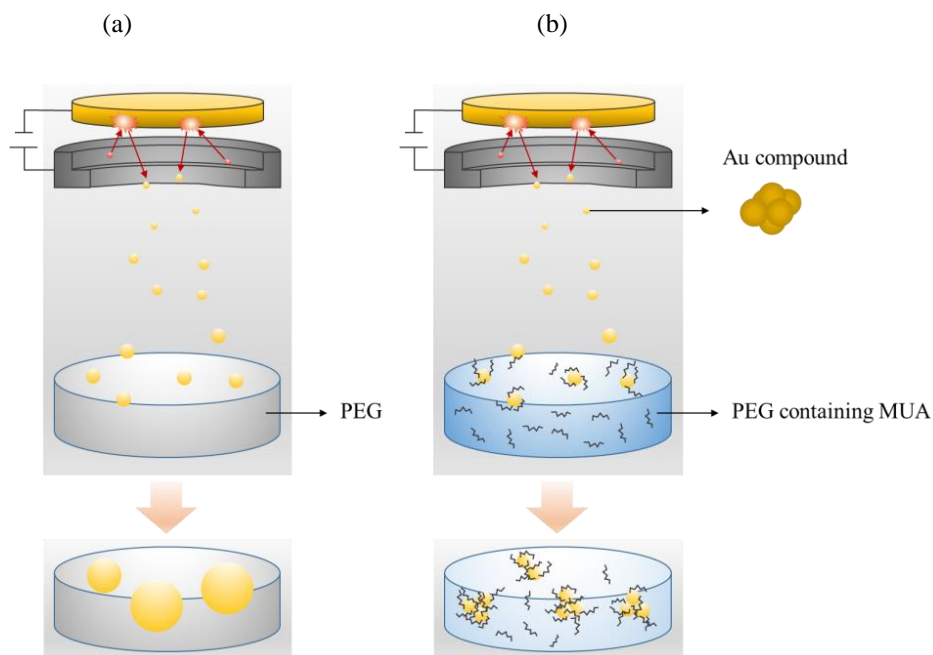


Figure 1.22 Plausible mechanism for the formation of fluorescent Au nanoclusters via matrix sputtering method; (a) plasmonic Au NPs under the absence of MUA, (b) fluorescent Au nanoclusters under the presence of thiols in PEG. Reproduced with permission from ref 40. Copyright 2016 Rights managed by Nature Publishing Group.

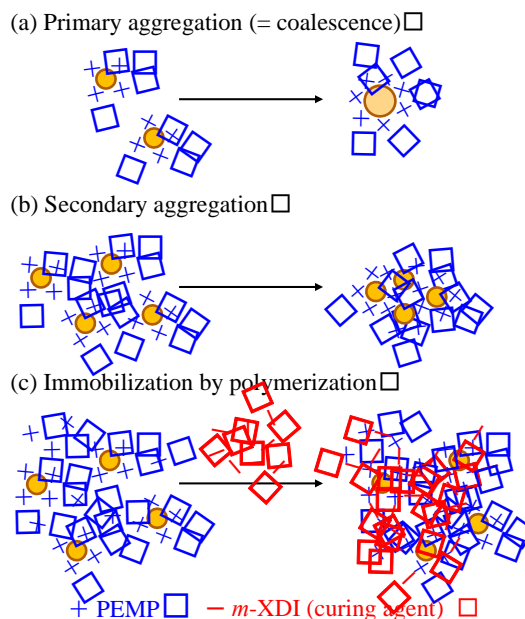


Figure 1.23 Schematic illustrations of (a) primary aggregation (coalescence and growth), (b) secondary aggregation, and (c) immobilization of Ag NPs in thiourethane resin after polymerization. Reproduced with permission from ref 47. Copyright 2016 Elsevier B.V. All rights reserved.

1.14 Summary and perspective

Photoluminescent metal nanocluster is one of the hottest topics in research community today. It is believed to be the link between a single metal atom which shows distinct optical property and metal nanoparticle which shows surface plasmon absorbance. The interesting property of this material arises when the particle size is well below 2 nm wherein the nanoclusters started to behave somewhat like a molecule and shows emission within the UV to NIR region once excited with light. It is hypothesized that if we could understand the mechanism in which these nanoclusters are formed, we will be able to improve its property, the property of nanoparticle and the property of the bulk material as well. Currently, photoluminescence property in metal nanocluster is not well understood primarily because of inefficient synthetic strategy that could synthesize a nanocluster with atomic precision and at high purity which is prerequisite for accurate measurement and analysis. Thus to address this issue, several synthetic strategies were developed particularly in chemical reduction schemes wherein metal ion precursors are reduced using reducing agents in the presence of capping or stabilizing ligand. Commonly used ligands/capping agent in this field include DNA, protein, dendrimer, phosphine and thiol. Another approach for the synthesis of photoluminescent nanoclusters which is recently investigated is physical synthesis which offers greener alternative to produce the nanoclusters. This scheme is a greener strategy in comparison with the chemical reduction for it does not need any reducing reagents or tedious purification processes. One of the green strategies which had been employed for the synthesis of photoluminescent nanoclusters is sputtering technique which historically is applicable only to solid substrates for production of thin films but is now utilized even in liquid substrates for the synthesis of nanomaterials for as long the liquid used had low

vapor pressure. This process involves the ionization of Ar gas under high vacuum which led to physical ejection of surface atoms as the ionized gas collides with a metal target. The most common liquid substrate used in sputtering for nanoparticle synthesis is Ionic Liquids (ILs) which was also successfully employed for the synthesis of photoluminescent metal nanocluster.

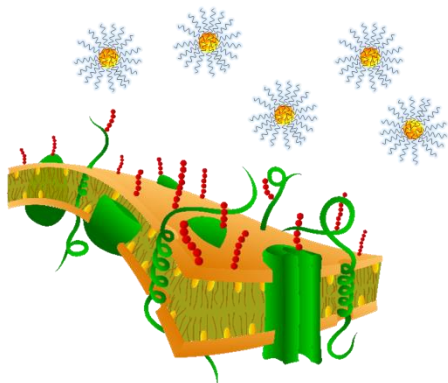
Nowadays, it is a common knowledge that not only ionic liquids but also other liquids such as castor oil, conola oil, and vegetable oil could be introduced in vacuum system and could be used as substrate for as long as these liquids have low or negligible vapor pressure which led our group to exploit varieties of low vapor pressure liquids such as PEEL, PEMP, glycerol, diglycerol, silicone oil and polyethylene glycol (PEG) for the synthesis of monodispersed metal nanoparticles and photoluminescent metal nanoclusters.

Although characterization techniques such as TEM, HR-TEM, UV-Vis, XANES, XAFS, EXAFS, EDS, STEM, XRF, XRD, FTIR, XPS, EELS, AFM, SAXS, NMR, DLS and AAS were successfully used in nanoparticles, in the nanoclusters regime only a few of these could be employed and this is currently a challenge in this area to better understand the nanocluster properties other than the photoluminescence which we initiated. For instance, using TEM as a tool to describe the morphology and particle size of the nanoclusters could overestimate the actual size especially for photosensitive materials that easily coalesce when directly exposed with electron beam. XRD could not provide meaningful data since the clusters do not have enough translation symmetry to describe its crystal structure if they do exist. SAXS and other X-ray related techniques require single crystal specimens which is a challenge since most of the clusters do not readily formed single crystals. The good news however, is that these nanoclusters could be characterized meaningfully! For instance, with our seminal effort, SEC-HPLC separation technique was successfully employed to isolate very small nanoclusters, STEM-

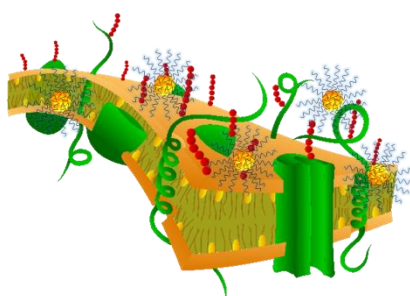
HAADF in tandem with STEM-EDS elemental mapping technique was used to directly view the nanocluster and measure its size, XPS Analysis was utilized to investigate the charge states of the clusters and estimate the nanocluster structure and TG analysis to indirectly estimate the composition ratio of metal atoms with respect to the attached ligand.

Sputtering technique in liquid matrix to synthesize high purity photoluminescent metal nanoclusters is quite a new field of endeavor and opens up possibilities for future explorations and experimentations. Interesting topics in this area include synthesis of photoluminescent bimetallic nanoclusters such as AuAg, AuCu, AuPt, CuPt and etc. and even trimetallic nanoclusters and investigation of its properties like catalytic, electrical, magnetic and optical. With this research direction, characterization techniques such as XPS, HAADF-STEM, EDS Analysis and ICP-AES could be utilized to have meaningful assessment of its structure-property relationship. Synthesizing a single crystal of these physically synthesized nanoclusters is also an interesting avenue. In doing so, characterization using small angle x-ray crystallography could be utilized to investigate the structure of the cluster. Another characterization technique such as ESI-MS could also be exploited specially for the characterization of bimetallic and trimetallic nanoclusters which had been successfully employed in chemical reduction.

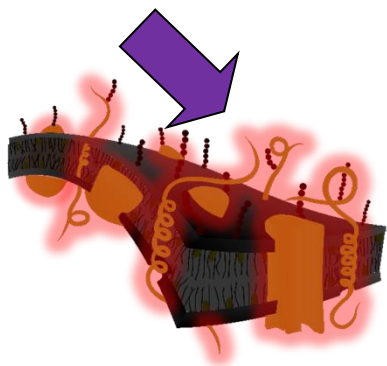
Another interesting research that could be pursued in this area is the development of “choline like” photoluminescent metal nanoclusters which could be used for bioimaging, biosensing, biotherapy and selective drug delivery. Choline is one of the quaternary ammonium cation which is known for its very important biological functions particularly in liver, brain, nerve and muscle. Making an analog of this molecule will provide the society a bio-friendly molecular sensing and imaging probe for both in vivo and in vitro biomedical applications which is important for cancer research today.



proteins inside the cell has high affinity for cationic species like choline molecules.



cationically charged choline like photoluminescent nanoclusters could easily adhere and enter the cell



under UV light irradiation the photoluminescent choline like nanoclusters could potentially be used for imaging and sensing application.

Figure 1.24 cellular imaging and sensing using choline inspired photoluminescent metal nanocluster.

1.15 References

1. G. Schmid, *Adv. Eng. Mater.*, 2001, **10**, 737-743.
2. R. Murray, *Chem. Rev.* 2008, **108**, 2688-2720.
3. M. Daniel and D. Astruc, *Chem. Rev.* 2004, **104**, 293-346.
4. J. Zheng, C. W. Zhang and R. M. Dickson, *Phys. Rev. Lett.*, 2004, **93**, 0077402.
5. Y. Negishi, K. Nobusada and T. Tsukuda, *J. Am. Chem. Soc.*, 2005, **127**, 5261-5270.
6. N. Toshima and T. Yonezawa, *New J. Chem.*, 1998, **22**, 1179-1201.
7. D. Talapin, J. Lee, M. Kovalenko and E. Shevchenko, *Chem. Rev.* 2010, **110**, 389-458.
8. E. Dreaden, A. Alkilany, X. Huang, C. Murphy and M. El-Sayed, *Chem. Soc. Rev.*, 2012, **41**, 2740-2779.
9. K. Saha, S. Agasti, C. Kim, X. Li, and V. Rotello, *Chem. Rev.*, 2012, **112**, 2739-2779.
10. J. Edel, A. Kornyshev, A. Kucernak and M. Urbakh, *Chem. Soc. Rev.*, 2016, **45**, 1581-1596.
11. Y. Yu, X. Chen, Q. Yao, Y. Yu, N. Yan and J. Xie, *Chem. Mater.*, 2013, **25**, 946-952.
12. J. Zheng, C. Zhou, M. Yu, and J. Liu, *Nanoscale*, 2012, **4**, 4073.
13. S. Sculfort and P. Braunstein, *Chem. Soc. Rev.*, 2011, **40**, 2741-2760.
14. M. Ganguly, J. Jana, A. Pal and T. Pal, *RSC Adv.*, 2016, **6**, 17683-17703.
15. K. Dimuthu, M. Weerawardene and C. M. Aikens, *J. Am. Chem. Soc.* 2016, **138**, 11202-11210.
16. H. Chang, Y. Tseng, Z. Yuan, H. Chou, C. Chen, B. Hwang, M. Tsai, H. Chang and C. Huang, *Phys. Chem. Chem. Phys.*, 2017, **19**, 12085-12093.

17. F. Bertorelle, I. Antoine, N. Calin, C. Zerbino, A. Ledoux, S. Guy, P. Dugourd, P. Brevet, Z. Sander, M. Krstic, V. Koutecky, and R. Antoine, *J. Phys. Chem. Lett.* 2017, **8**, 1979-1985.
18. F. Miranda, M. Menziani, and A. Pedone, *J. Phys. Chem. C*, 2015, **119**, 10766–10775.
19. R. Senanayake, A. Akimov, and C. Aikens, *J. Phys. Chem. C*, 2017, **121**, 10653–10662.
20. P. Day, R. Pachter, and K. Nguyen, *J. Phys. Chem. A*, 2017, **121**, 326-333.
21. R. D. Corpuz, Y. Ishida and T. Yonezawa, *Phys. Chem. Chem. Phys.*, 2016, **18**, 8773-8776.
22. Y. Ishida, K. Narita, T. Yonezawa and R. Whetten, *J. Phys. Chem. Lett.*, 2016, **7**, 3718-3722.
23. Y. Ishida, Y.-L. Huang, T. Yonezawa, K. Narita, *Chem Nano Mat* **2017**, *3*, 298-302.
24. Y. Zheng, L. Lai, W. Liu, H. Jiang, X. Wang, *Advances in Colloid and Interface Science*, 2017, **242**, 1-16.
25. L. Zhang and E. Wang, *Nano Today*, 2014, **9**, 132-157.
26. J. Sun and Y. Jin, *J. Mater. Chem. C*, 2014, **2**, 8000-8011.
27. X. Yuan, Z. Luo, Q. Zhang, X. Zhang, Y. Zheng, J. Lee and J. Xie, *ACS Nano*, **2011**, *5*, 8800-8808.
28. X. Dou, X. Yuan, Y. Yu , Z. Luo , Q. Yao , D. Leong and J. Xie, *Nanoscale*, 2014, **6**, 157-161.
29. T. Schaaff, G. Knight, M. Shafiqullin, R. Borkman, and R. Whetten, *J. Phys. Chem. B*, 1998, **102**, 10643-10646.
30. Y. Lu and W. Chen, *Anal. Chem.* 2015, **87**, 10659-10667.

31. D. Lee, R. Donkers, G. Wang, A. Harper, and R. Murray, *J. Am. Chem. Soc.* 2004, **126**, 6193-6199.
32. X. Zhang, Z. Luo, J. Chen, X. Shen, S. Song, Y. Sun, S. Fan, F. Fan, D. Leong and J. Xie, *Adv. Mater.* 2014, **26**, 4565-4568.
33. D. Zhang, B. Gökce and S. Barcikowski, *Chem. Rev.* 2017, **117**, 3990-4103.
34. H. Wender, M. Andreatza, R. Correia, S. Teixeira, J. Dupont, *Synthesis of Gold Nanoscale*, 2011, **3**, 1240-1246.
35. M. Gelesky, A. Umpierre, G. Machado, R. Correia, W. Magno, J. Morais, G. Ebeling, and J. Dupont, *J. Am. Chem. Soc.* 2005, **127**, 4588-4589.
36. H. Wender, P. Migowski, A. Feil, S. Teixeira, J. Dupont, *Coordination Chemistry Reviews*, 2013, **257**, 2468-2483.
37. J. Dupont, *Acc. Chem. Res.* 2011, **44**, 1223-1231.
38. S. Kuwabata, T. Tsuda and T. Torimoto, *J. Phys. Chem. Lett.* 2010, **1**, 3177-3188.
39. T. Torimoto, T. Tsuda, K. Okazaki and S. Kuwabata, *Adv. Mater.* 2010, **22**, 1196-1221.
40. Y. Ishida, I. Akita, T. Sumi, M. Matsubara, T. Yonezawa, *Sci. Rep.* 2016, **29928**, 1-14.
41. Y. Shishino, T. Yonezawa, K. Kawai and H. Nishihara, *Chem. Commun.* 2010, **46**, 7211-7213.
42. Y. Shishino, T. Yonezawa, S. Udagawa, K. Hase, H. Nishihara, *Angew. Chem. Int. Ed.* 2011, **50**, 703-705.
43. T. Sumi, S. Motono, Y. Ishida, N. Shirahata and T. Yonezawa, *Langmuir*, 2015, **31**, 4323-4329.
44. Y. Ishida, T. Sumi, and T. Yonezawa, *New J. Chem.* 2015, **39**, 5895-5897.
45. I. Akita, Y. Ishida and T. Yonezawa, *Bull. Chem. Soc. Jpn.*, 2016, **89**, 1054-1056.

46. Y. Ishida, C. Lee, and T. Yonezawa, *Sci. Rep.* 2015, **5**, 15372–15377.
47. Y. Ishida, R. Nakabayashi, M. Matsubara and T. Yonezawa, *New J. Chem.* 2015, **39**, 4227-4230.
48. Y. Ishida, S. Udagawa and T. Yonezawa, *Colloids and Surfaces A: Physicochemical and Engineering Aspects*, 2016, **504**, 437-441.
49. M. Porta, M. Nguyen, T. Tokunaga, Y. Ishida, W. Liu and T. Yonezawa, *Langmuir*, 2016, **32**, 12159-12165.
50. M. Porta, M. Nguyen, Y. Ishida and T. Yonezawa, *RSC Adv.*, 2016, **6**, 105030–105034.
51. T. Iimori, Y. Hatakeyama, K. Nishikawa, M. Kato and N. Ohta, *Chemical Physics Letters* 2013, **586**, 100-103.
52. W. Grove, *Philosophical Magazine Series 4* **1852**.
53. G. Ye, T. Michely, V. Weidenhof, I. Friedrich and M. Wuttig, *Phys. Rev. Lett.* 1998.
54. C. Feng, H. Ge, M. Tong, G. Ye and Z. Jiao, *Thin Solid Films*, 1999, **342**, 30–34.
55. G. Ye, Q. Zhang, C. Feng, H. Ge, and Z. Jiao, *Phys. Rev., B Condens. Matter*, 1996, **54**, 14754–14757.
56. M. Wagener and B. Günther, *Journal of Magnetism and Magnetic Materials*, 1999, **201**, 41-44.
57. E. Borra, O. Seddiki, R. Angel, D. Eisenstein, P. Hickson, K. Seddon, S. Worden, *Nature*, 2007, **447**, 979-981.
58. T. Torimoto, K. Okazaki, T. Kiyama, K. Hirahara, N. Tanaka and S. Kuwabata, *Appl. Phys. Lett.*, 2006, **89**, 243117.
59. V. Raghuwanshi, M. Ochmann, A. Hoell, F. Polzer and K. Rademann, *Langmuir*, 2014, **30**, 6038-6046.

60. Y. Yasukawa, X. Liu, S. Shirsath, H. Suematsu, Y. Kotaki, Y. Nemoto, M. Takeguchi and A. Morisako, *Nanotechnology*, 2016, **27**, 385605-385613.
61. K. Richter, A. Birkner and AMudring, *Phys. Chem. Chem. Phys.* 2011, **13**, 7136-7136.
62. P. Slepíčka, R. Elashnikov, P. Ulbrich, M. Staszek, Z. Kolská and V. Švorčík, *J Nanopart Res*, 2015, **17**, 58-15.
63. V. Raghuwanshi, M. Ochmann, F. Polzer, A. Hoell and K. Rademann, *Chem. Commun.* 2014, **50**, 8693-8694.
64. J. Siegel, K. Kolářová, V. Vosmanská, S. Rimpelová, J. Leitner and V. Švorčík, *Materials Letters*, 2013, **113**, 59-62.
65. K. Okazaki, J. Sakuma, J. Yasui, S. Kuwabata, K. Hirahara, N. Tanaka and T. Torimoto, *Chem. Lett.*, 2011, **40**, 84–86.
66. O. Khatri, K. Adachi, K. Murase, K. Okazaki, T. Torimoto, N. Tanaka, S. Kuwabata and H. Sugimura, *Langmuir*, 2008, **24**, 7785-7792.
67. H. Wender, P. Migowski, A. Feil, L. de Oliveira, M. Prechtel, R. Leal, G. Machado, S. Teixeira and J. Dupont, *Phys. Chem. Chem. Phys.* 2011, **13**, 13552-13556.
68. E. Vanecht, K. Binnemans, S. Patskovsky, M. Meunier, J. Seo, L. Stappers and J. Fransaer, *Phys. Chem. Chem. Phys.*, 2012, **14**, 5662-10.
69. M. Staszek, J. Siegel, S. Rimpelová, O. Lyutakov and V. Švorčík, *Materials Letters* 2015, **158**, 351-354.
70. H. Yoshida, K. Kawamoto, H. Kubo, T. Tsuda, A. Fujii, S. Kuwabata and M. Ozaki, *Adv. Mater.*, 2010, **22**, 622–626.
71. T. Kameyama, Y. Ohno, T. Kurimoto, K. Okazaki, T. Uematsu, S. Kuwabata, and T. Torimoto, *Phys. Chem. Chem. Phys.* 2010, **12**, 1804-1811.

72. H. Castro, H. Wender, M. Alencar, S. Teixeira, J. Dupont and J. Hickmann, *J. Appl. Phys.* 2013, **114**, 183104.
73. Y. Hatakeyama, M. Okamoto, T. Torimoto, S. Kuwabata and K. Nishikawa, *J. Phys. Chem. C*, 2009, **113**, 3917-3922.
74. C. Zhang and Y. Feng, *J. Phys. Soc. Jpn.*, 2016, **85**, 094606-5.
75. S. Hamm, R. Shankaran, V. Korampally, S. Bok, S. Praharaj, G. Baker, J. Robertson, B. Lee, S. Sengupta and K. Gangopadhyay, *ACS Appl Mater Interfaces* 2012, **4**, 178-184.
76. Y. Ishida, S. Udagawa and T. Yonezawa, *Colloids and Surfaces A: Physicochemical and Engineering Aspects*, 2016, **498**, 106-111.
77. M. Verma, I. Tyagi, R. Chandra and V. Gupta, *Journal of Molecular Liquids*, 2017, **225**, 936-944.
78. K. Nakagawa, T. Narushima, S. Udagawa and T. Yonezawa, *J. Phys.: Conf. Ser.*, 2013, **417**, 012038-6.
79. M. Porta, M. Nguyen, T. Yonezawa, T. Tokunaga, Y. Ishida, H. Tsukamoto, Y. Shishino and Y. Hatakeyama, *New J. Chem.* 2016, **40**, 9337-9343.
80. M. Verma, R. Chandra and V. Gupta, *Biochemical Pharmacology*, 2016, **4**, 219-229.
81. A. Kusior, K. Kollbek, K. Kowalski, M. Borysiewicz, T. Wojciechowski, A. Adamczyk, A. Trenczek-Zajac, M. Radecka and K. Zakrzewska, *Applied Surface Science*, 2016, **380**, 193-202.
82. L. Luza, C. Rambor, A. Gual, F. Bernardi, J. Domingos, T. Grehl, P. Brünner and J. Dupont, *ACS Catal*, 2016, **6**, 6478-6486.
83. V. Souza, J. Scholten, D. Weibel, D. Eberhardt, D. Baptista, S. Teixeira and J. Dupont, *J. Mater. Chem. A*, 2016, **4**, 7469-7475.

84. T. Suzuki, K. Okazaki, S. Suzuki, T. Shibayama, S. Kuwabata, and T. Torimoto, *Chem. Mater.* 2010, **22**, 5209-5215.
85. T. Suzuki, S. Suzuki, Y. Tomita, K. Okazaki, T. Shibayama, S. Kuwabata and T. Torimoto, *Chem. Lett.*, 2010, **39**, 1072-1074.
86. Y. Oda, K. Hirano, K. Yoshii, S. Kuwabata, T. Torimoto and M. Miura, *Chem. Lett.* 2010, **39**, 1069-1071.
87. L. Foppa, L. Luza, A. Gual, D. Weibel, D. Eberhardt, S. Teixeira and J. Dupont, *Dalton Trans.* 2015, **44**, 2827-2834.
88. T. Tsuda, K. Yoshii, T. Torimoto and S. Kuwabata, *Journal of Power Sources*, 2010, **195**, 5980-5985.
89. T. Tsuda, T. Kurihara, Y. Hoshino, T. Kiyama, K. Okazaki, T. Torimoto and S. Kuwabata, *Electrochemistry*, 2009, **77**, 693-695.
90. C. Liu, R. Liu, Q. Sun, J. Chang, X. Gao, Y. Liu, S. Lee, Z. Kang and S. Wang, *Nanoscale*, 2015, **7**, 6356-6362.
91. J. Chang, C. Liu, J. Liu, Y. Zhou, X. Gao and S. Wang, *Nano-Micro Letters*, 2015, **7**, 307-315.
92. D. Sugioka, T. Kameyama, S. Kuwabata, T. Yamamoto and T. Torimoto, *ACS Appl Mater Interfaces*, 2016, **8**, 10874-10883.
93. T. Torimoto, Y. Ohta, K. Enokida, D. Sugioka, T. Kameyama, T. Yamamoto, T. Shibayama, K. Yoshii, T. Tsuda and S. Kuwabata, *J. Mater. Chem. A*, 2015, **3**, 6177-6186.
94. M. Hirano, K. Enokida, K. Okazaki, S. Kuwabata, H. Yoshida and T. Torimoto, *Phys. Chem. Chem. Phys.*, 2013, **15**, 7286-7289.

95. C. Liu, X. Cai, J. Wang, J. Liu, A. Riese, Z. Chen, X. Sun and S. Wang, *International Journal of Hydrogen Energy*, 2016, **41**, 13476-13484.
96. C. Liu, J. Liu, Y. Zhou, X. Cai, Y. Lu, X. Gao and S. Wang, *Carbon*, 2015, **94**, 295-300.
97. I. Cha, M. Ahn, S. Yoo and Y. Sung, *RSC Adv.*, 2014, **4**, 38575-38580.
98. S. Suzuki, Y. Tomita, S. Kuwabata and T. Torimoto, *Dalton Trans.* 2015, **44**, 4186-4194.
99. K. Okazaki, T. Kiyama, K. Hirahara, N. Tanaka, S. Kuwabata and T. Torimoto, *Chem. Commun.*, 2008, **6**, 691.
100. S. Suzuki, T. Suzuki, Y. Tomita, M. Hirano, K. Okazaki, S. Kuwabata and T. Torimoto, *Cryst Eng Comm*, 2012, **14**, 4922.
101. M. Nguyen, T. Yonezawa, Y. Wang and T. Tokunaga, *Materials Letters*, 2016, **171**, 75-78.
102. D. König, K. Richter, A. Siegel, A. Mudring and A. Ludwig, *Adv. Funct. Mater.*, 2013, **24**, 2049-2056.
103. Z. Zhao, J. Sun, S. Xing, D. Liu, G. Zhang, L. Bai and B. Jiang, *Journal of Alloys and Compounds*, 2016, **679**, 88-93.
104. P. Grammatikopoulos, J. Kioseoglou, A. Galea, J. Vernieres, M. Benelmekki, R. Diaz and M. Sowwan, *Nanoscale*, 2016, **8**, 9780-9790.
105. Y. Hatakeyama, T. Morita, S. Takahashi, K. Onishi and K. Nishikawa, *J. Phys. Chem. C*, 2011, **115**, 3279-3285.
106. Y. Hatakeyama, J. Kato, T. Mukai, K. Judai and K. Nishikawa, *Bull. Chem. Soc. Jpn.* 2014, **87**, 773-779.
107. H. Wender, L. de Oliveira, P. Migowski, A. Feil, E. Lissner, M. Prechtel, S. Teixeira and J. Dupont, *J. Phys. Chem. C*, 2010, **114**, 11764-11768.

108. D. Sugioka, T. Kameyama, S. Kuwabata and T. Torimoto, *Phys. Chem. Chem. Phys.* 2015, **17**, 13150–13159.
109. Y. Hatakeyama, K. Judai, K. Onishi, S. Takahashi, S. Kimura and K. Nishikawa, *Phys. Chem. Chem. Phys.* 2016, **18**, 2339-2349.
110. Y. Ishida, R. Nakabayashi, R. D. Corpuz and T. Yonezawa, *Colloids and Surfaces A: Physicochemical and Engineering Aspects*, 2017, **518**, 25-29.
111. R. D. Corpuz, Y. Ishida and T. Yonezawa, *New J. Chem.*, 2017, **41**, 6828-6833.

2 PHOTOLUMINESCENT GOLD NANOCUSTER BY CHEMICAL REDUCTION

Abstract

This chapter describes the synthesis of a novel positively charged photoluminescent gold nanocluster which shows blue emission by controlling the electrostatic repulsion of thiol ligand in the early stage of cluster formation. This was made possible by using thiocholine, a short quaternary ammonium cation as ligand and dodecylsulfate, an anionic surfactant which works in tandem to suppress the electrostatic repulsion. The clusters were characterized with UV-Vis, PL measurement, TEM and HAADF-STEM imaging techniques.

2.1 Introduction

Nanocluster synthesis is an interesting field of study, and various researchers are aiming at manipulating individual atoms, molecules, or groups of molecules to produce novel hybrid materials with unprecedented structures and properties¹⁻⁴. A typical example is the synthesis of gold nanoclusters with a non-metallic structure, whose distinctive optical properties are derived from the constituent gold nanoparticles, which generally show surface plasmon resonance at relatively larger diameters ($> 3\text{nm}$). The optical properties of gold nanoclusters are hypothesized to originate from the metallic cluster core, and they can be altered depending on the attached ligands. Unlike the collective oscillation of conduction electrons in the gold nanoparticle, a single electron transition results in molecule-like absorption and emission from the UV to NIR region in a gold nanocluster.⁵⁻⁷ Experimentally, it has been determined that the sharp contrast

between the optical properties of the gold nanocluster and gold nanoparticles become observable when the particle size is below 2.4 nm and the gold particles no longer exhibit metallic properties.⁸

Among the tunable properties of gold nanoclusters, we focused on their optical properties, particularly photoluminescence. Photoluminescence is an important property because of its potential application in biomedical fields, especially for imaging, sensing, and therapy.⁹ The nanomaterials commonly used for these applications are quantum dots,¹⁰ which contain toxic components such as Cd, Pd, Se, and Te, and are highly discouraged. Hence, many researchers have proposed that gold could be one of the most viable alternatives because of its chemical inertness, photostability, and biocompatibility. Unfortunately, gold in its nanoparticle form shows size-related toxicity,¹¹ and thus, a synthetic scheme for fluorescent gold nanoclusters is an urgent demand.

There are several reported synthetic routes to fluorescent gold nanoclusters using polymers,¹² dendrimers,¹³ DNA,¹⁴ or phosphine¹⁵ as the stabilizing compounds. We focus on gold nanoclusters with thiol stabilizers,¹⁶ pioneered by Murray and Whetten. In this regard, there are two commonly exploited methods involving the use of neutral and anionic thiol ligands including alkylthiols,¹⁷ tiopronin,¹⁸ phenylethylthiolate,¹⁹ and thiolate cyclodextrin.²⁰ However, there is no established method for the synthesis of fluorescent gold nanoclusters by means of conventional chemical reduction using cationic thiols. Such nanoclusters are expected to play a significant role in bioimaging²¹ and sensing as cellular proteins show high affinity for positively charged nanocomposites than for neutral and anionic nanocomposites. In particular, quaternary ammonium-terminated thiols have rarely been used for the preparation of gold nanoparticles.²² Quaternary ammonium groups are always positively charged under any pH conditions. Thus, we

hypothesized that a positively charged gold nanocluster could easily be absorbed inside the cell and potentially be used to study intercellular activities that are imperative in cancer research.⁹ The main limitation of cationic thiolate-protected gold nanoclusters is that the electrostatic repulsion between the cationic ligands on the surface of the nanoparticles hinders the formation of small clusters (<ca. 2 nm) during nucleation in solvents. Our previous research showed the formation of a red dispersion of thiocholine bromide-stabilized gold nanoparticles even at a high molar ratio of the thiocholine ligand as compared with the gold ions.²² Thiocholine is the smallest quaternary ammonium terminated mercapto ligand. Moreover, silver,²³ palladium,²⁴ and platinum²⁵ nanoparticles can be obtained by chemical reduction using thiocholine as the stabilizing reagent, but these nanoparticles, too, are large. Our objective is the utilization of the smallest cationic thiolate ligand, thiocholine (HS-(CH₂)₂-N(CH₃)₃⁺), to synthesize fluorescent gold nanoclusters by chemical reduction. Cationic thiolate-protected fluorescent gold nanoparticles or nanoclusters have been obtained only by a physical synthesis method by our group.²³ This paper reports the first successful synthesis of positively charged nanoclusters by the conventional chemical reduction method.

2.2 Experimental Section

2.2.1 Materials

HAuCl₄, sodium hydroxide (NaOH) (Junsei Chemicals Co., Ltd.), sodium borohydride (NaBH₄) (Kanto Chemicals Co., Inc), methanol (Junsei Chemicals Co., Ltd.), sodium dodecylsulfate (SDS) (Kishida Chemical Co. Ltd.),

2.2.2 Synthesis of photoluminescent Au nanocluster

Thiocholine chloride (TC), was synthesized as described in a previous paper (see SI).²⁴ Counter-ion exchange was carried out in order to eliminate the heavy metal effect of I^- . The purity of TC was verified by 1H -NMR and FT-IR analyses. First, we attempted to synthesize gold nanoclusters by the simple reduction of $HAuCl_4$ (Au) with excess $NaBH_4$ in the presence of TC. The Au-to-TC mol ratio was 1:3, 1:5, or 1:7. For our typical synthesis (1:7 mole ratio of $HAuCl_4$:TC), we dissolved 0.0218 g of thiocholine chloride in 1 mL of methanol followed by the addition of (1 mL, 20 mM) $HAuCl_4$ stock aqueous solution. It was then diluted with 8 ml distilled water-methanol solvent with 1:1 volume ratio and sonicated for 30 minutes prior to the addition of (50 μ L, 2M) $NaBH_4$. After the addition of $NaBH_4$, the resulting solution was then sonicated for another 90 minutes to ensure complete reduction of gold chloride.

2.2.3 Characterization

UV Vis extinction measurement (Jasco V-630 spectrometer), fluorescence measurement (Jasco FP-6600), particle size analysis: TEM (JEOL FX 2000, acceleration voltage of 200 kV) and STEM-HAADF (FEI TITAN III G2-Cubed, acceleration voltage of 300 kV).

2.3 Results and Discussion

The black line in Figure 2.1 shows the extinction spectrum immediately after the synthesis at the Au:TC mol ratio of 1:5. From this result, it could be seen that the samples exhibited plasmon absorption at around 540 nm. Transmission electron microscopy (TEM) images of the representative samples are shown in Figure S1, where the particle sizes are seen to exceed 4 nm, indicating that gold nanoclusters were not produced. As mentioned above, the strong repulsion between the TC ligands in the “nucleation stage” clusters hinder the formation of nanoclusters; the clusters coalesce spontaneously to form rather large nanoparticles. The use of a higher ligand ratio did not solve this problem

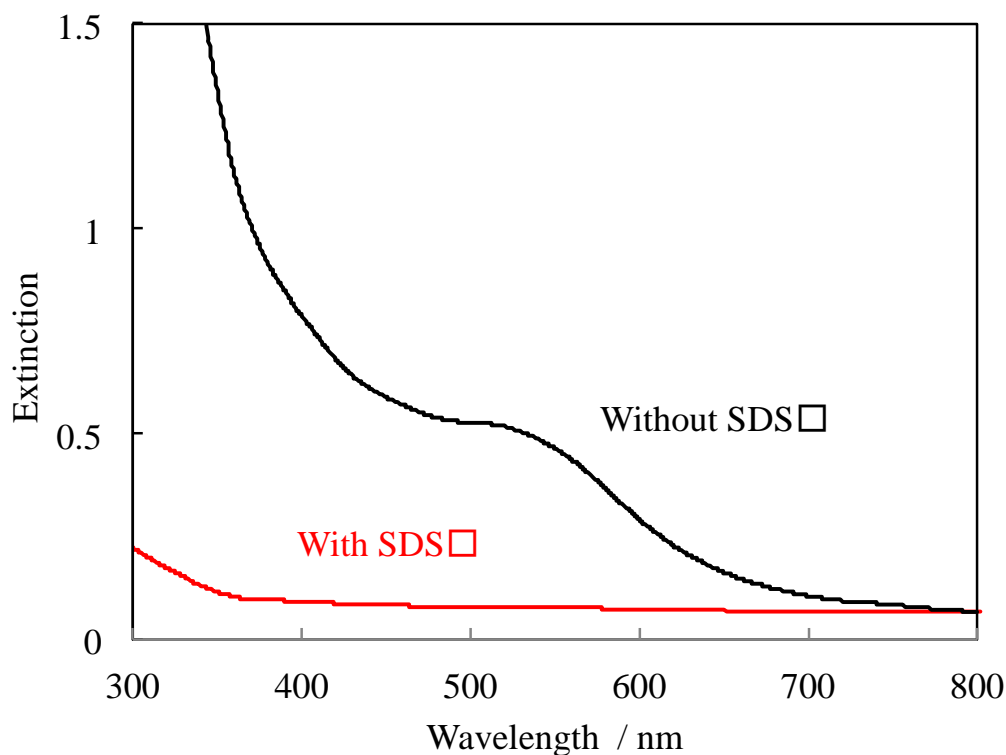


Figure 2.1 UV-Vis extinction spectra of Au nanoparticles and nanoclusters synthesized in the absence or presence of SDS (Au:TC:SDS = 1:5:0 and 1:5:5 (mol/mol/mol) for black and red spectra).

In order to suppress the electrostatic repulsion between TC ligands on the surface of gold nanoclusters during the nucleation, we added a negatively charged surfactant, sodium dodecylsulfate (SDS), to form a Au(I)-TC-SDS complex before the reduction, which may neutralize the cation on TC and minimize the repulsion between the TC molecules. Synthesizing the particles with SDS alone without thiocholine, only large aggregate (~20nm) were obtained (See Figure S4). To verify this concept, we synthesized gold nanoclusters at Au:TC:SDS molar ratios of 1:3:3, 1:5:5, and 1:7:7. In our typical experiment (1:7:7 mol ratio of H₂AuCl₄: TC:SDS), we dissolved 0.0218 g of TC and 0.0404 g of SDS in 5 mL methanol followed with the addition of (1 mL, 20 mM) H₂AuCl₄ stock aqueous solution. The resulting solution was diluted with 3 mL distilled water and sonicated for 60 minutes until the solution becomes white indicating the formation of Au-thiolate complexes. NaBH₄ (1 mL, 20 mM) was then added and the resulting solution was sonicated for another 60 minutes. The colour change from yellow to pale yellow/white indicated the reduction of Au(III) to Au(I) by the excess thiol compounds (Figure S5). The red line in Figure 1 shows the UV-Vis extinction spectra of the gold nanoclusters synthesized at the Au:TC:SDS molar ratio of 1:5:5. This result suggested that in the presence of SDS, non-plasmonic particles were formed. We then observed the TEM images to determine the particle sizes (Figure 2.2). The sample showing plasmon absorption (Au:TC:SDS = 1:3:3, see Figure S2 for the spectrum) had particles with diameters larger than 3 nm. The samples that did not exhibit plasmon absorption (Au:TC:SDS = 1:5:5 and 1:7:7), on the other hand, had particles with diameters well below 2 nm, indicating successful gold nanocluster formation. It is difficult to determine the exact diameter of such small clusters (~ 1 nm of diameter) by conventional TEM; however, we observed a clear decreasing trend in the particle size with an increase in the mol ratios of TC and SDS.

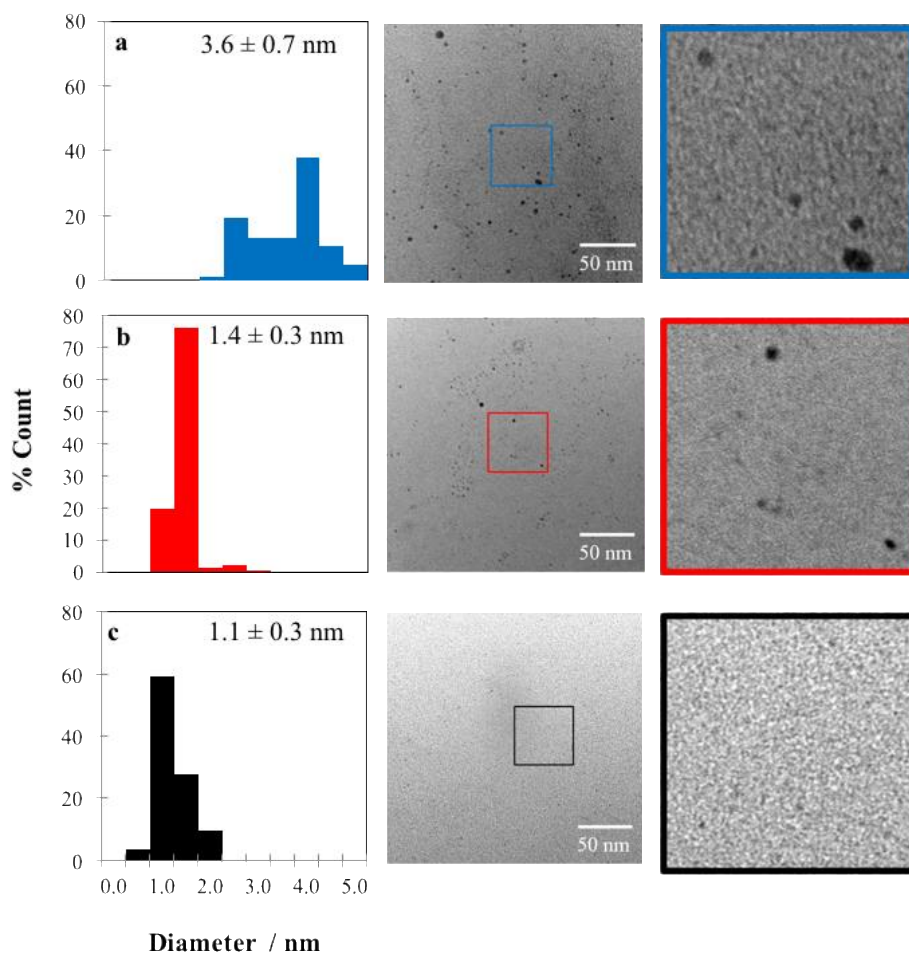


Figure 2.2 TEM images and particle size distributions of Au nanoparticles or nanoclusters synthesized at Au:TC:SDS mol ratios of (a) 1:3:3, (b) 1:5:5, and (c) 1:7:7 (mol/mol/mol). For the histograms, 200 particles were counted from several enlarged TEM images.

Judging from the TEM and extinction spectra as well as previous data,^{5,13,25–27} we expected our gold nanoclusters to show fluorescence in the visible region. In order to increase the solubility of obtained gold nanoclusters, we introduced NaOH so that SDS attached to the surface of the TC-stabilized clusters can be removed (i.e. de-neutralization, see the detailed procedure outlined in SI). As shown in Figure S3, after NaOH addition, an absorption shoulder appears at around 350 nm, which could be attributed to gold nanoclusters; a similar peak at this position was observed by other researchers, which was attributed to small gold nanoclusters consisting of 11 gold atoms or fewer⁵ (will be discussed later with fluorescence spectrum).

Under irradiation at 300 nm, we observed blue fluorescence, as shown in Figure 2.3 (see images of samples under UV irradiation in the inset). The maximum excitation wavelength was around 357 nm, which was in good agreement with that for gold nanoclusters comprising 11 gold atoms and fewer, particularly those reported by Tran¹³ and Scherer²⁶ for Au₄ (~313 nm) and Au₃ (~303 nm), respectively, and Dickson²⁷ for Au₅ (330 nm) and Au₈ (~384 nm). Moreover, the maximum fluorescence wavelength (~448 nm) agreed well with that of the Au₈ cluster (455 nm).²⁷ Hence, we hypothesized that the observed emission wavelength mainly originates from the Au₈ nanocluster or a gold nanocluster with a similar size. Other smaller or larger nanoclusters (e.g. Au₁₂, Au₁₀, Au₅, or Au₄ which fluoresce at ~ 630 nm,²⁸ ~523 nm,²⁹ ~385 nm,²⁷ or ~371 nm,¹³ respectively) could be minor contributors to the observed emission, and consequently, our gold nanoclusters showed relatively broad fluorescence.

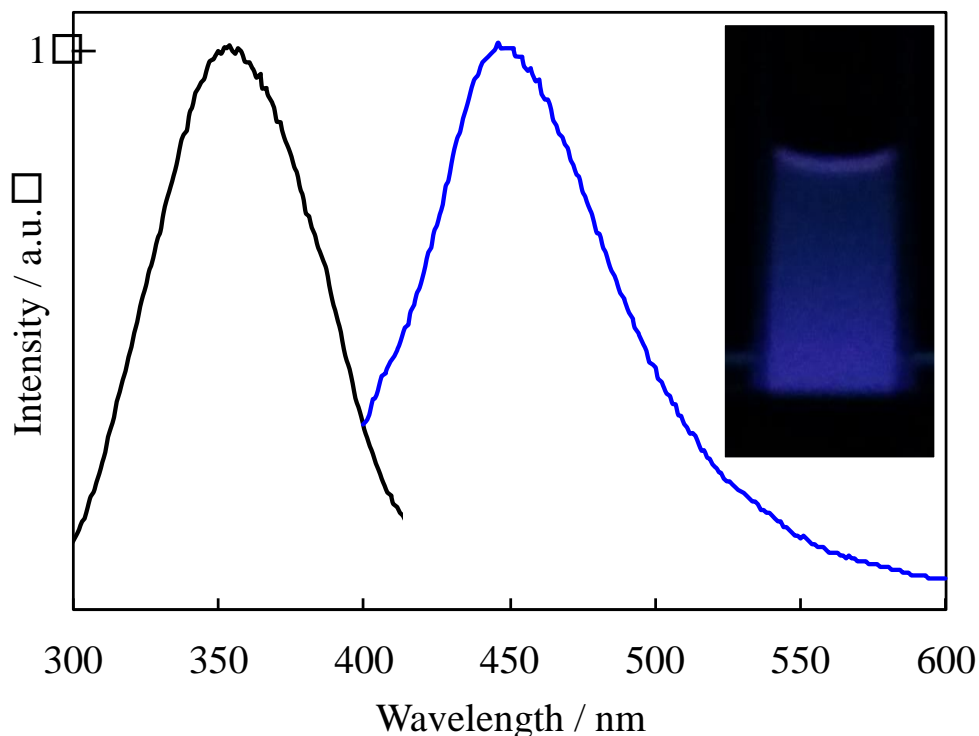


Figure 2.3 Fluorescence emission (blue) and excitation (black) spectra of synthesised gold nanoclusters (excitation wavelength = 300 nm, Au:TC:SDS = 1:7:7 (mol/mol/mol)).

High-angle annular dark-field (HAADF) images of scanning transmission electron microscopy (STEM) were recorded in order to confirm the existence of very small nanocluster components. Small gold nanoclusters are unstable and easily coalesce under strong electron beam irradiation; however, very small clusters composed only of Au atoms were observed in our experiments, consistent with our speculation based on fluorescence measurements.

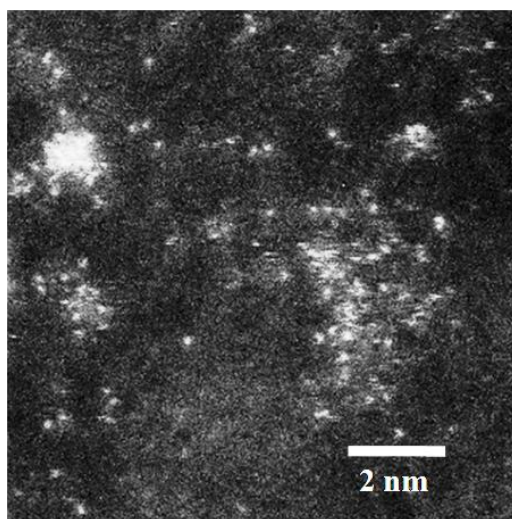


Figure 2.4 STEM-HAADF image of obtained Au nanoclusters.

2.4 Conclusions

In summary, fluorescent gold nanoclusters were successfully prepared for the first time using the shortest cationic thiol, TC. By introducing SDS to minimize electrostatic repulsion between the TC ligands on the surface of the gold nanoclusters during nucleation, we could obtain non-plasmonic particles, which showed blue emission at around 448 nm. Without SDS, on the other hand, only large non-fluorescent gold nanoparticles were obtained. The

method developed in this study is expected to be beneficial to the field of bioimaging and biosensing and be of interest to scientists pursuing research on nanoclusters.

2.5 References

1. V. Malgras, Q. Ji, Y. Kamachi, T. Mori, F. Shieh, K. Wu, K. Ariga and Y. Yamauchi, *Bull. Chem. Soc. Jpn.*, 2015, **88**, 1171-1200.
2. K. Ariga, A. Vinu, Y. Yamauchi, Q. Ji and J. Hill, *Bull. Chem. Soc. Jpn.*, 2012, **85**, 1-32.
3. K. Ariga, Y. Yamauchi, G. Rydzek, Q. Ji, Y. Yonamine, K. Wu and J. Hill, *Chem. Lett.*, 2014, **43**, 36-68.
4. L. Wang, C. Liu, Y. Nemoto, N. Fukata, K. Wu and Y. Yamauchi, *RSC Adv.*, 2012, **2**, 4608-4611.
5. J. Zheng, C. W. Zhang and R. M. Dickson, *Phys. Rev. Lett.*, 2004, **93**, 0077402.
6. S. K. Ghosha and T. Pal, *Phys. Chem. Chem. Phys.*, 2009, **11**, 3831–3844.
7. R. P. Gotor and E. Grueso, *Phys. Chem. Chem. Phys.*, 2011, **13**, 1479–1489.
8. A. Das, T. Li, K. Nobusada, Q. Zeng, N. L. Rosi and R. Jin, *J. Am. Chem. Soc.*, 2012, **134**, 20286–20289.
9. Y. Tao, M. Li, J. Rena and X. Qu, *Chem. Soc. Rev.*, 2015, **44**, 8636.
10. M. Bottrill and M. Green, *Chem. Commun.*, 2011, **47**, 7039–7050.
11. N. Khlebtsov and L. Dykmana, *Chem. Soc. Rev.*, 2011, **40**, 1647–1671.
12. S. Kanaoka, N. Yagi, Y. Fukuyama, S. Aoshima, H. Tsunoyama, T. Tsukuda and H. Sakurai, *J. Am. Chem. Soc.*, 2007, **129**, 12060-12061.
13. M. L. Tran, A. V. Zvyagin and T. Plakhotnik, *Chem. Commun.*, 2006, 2400–2401.
14. G. Liu, Y. Shao, K. Ma, Q. Cui, F. Wu and S. Xu, *Gold Bull.*, 2012, **45**, 69–74.

15. J. M. Pettibonea and J. W. Hudgens, *Phys. Chem. Chem. Phys.*, 2012, **14**, 4142–4154.
16. R.S Ingram, M.J. Hostetler, R.W. Murray, T.G. Schaff, J. Khoury, R. L. Whetten, T. P Bigioni, D. K. Guthrie and P. N. First, *J. Am. Chem. Soc.*, 1997, **119**, 9279-9280.
17. A. Kyrychenko, G. V. Karpushina, D. Svechkarev, D. Kolodezny, S. I. Bogatyrenko, A. P. Kryshstal, and A. O. Doroshenko, *J. Phys. Chem. C*, 2012, **116**, 21059–21068.
18. A. P. Gies, D. M. Hercules, A. E. Gerdon, and D. E. Cliffel, *J. Am. Chem. Soc.*, 2007, **129**, 1095-1104.
19. R. Jin, *Nanoscale*, 2010, **2**, 343–362.
20. T. Das, P. Ghosh, M. S. Shanavas, A. Maity, S. Mondala and P. Purkayastha, *RSC Adv.*, 2012, **2**, 12210–12215.
21. K. Kobayashi, J. Wei, R. Iida, K. Ijiro and K. Niikura, *Polymer J.*, 2014, **46**, 460–468.
22. T. Yonezawa, S. Onoue, and N. Kimizuka, *Chem. Lett.*, 2002, **31**, 1172–1173.
23. Y. Ishida, C. Lee and T. Yonezawa, *Sci. Rep.*, 2015, **5**, 15372.
24. Y. Ishida, T. Jirasupangkul and T. Yonezawa, *New J. Chem.*, 2015, **39**, 4214–4217.
25. Z. Luo, X. Yuan, Y. Yu, Q. Zhang, D. T. Leong, J. Y. Lee, and J. Xie, *J. Am. Chem. Soc.*, 2012, **134**, 16662–16670.
26. R. Jin, S. Egusa and N. F. Scherer, *J. Am. Chem. Soc.*, 2004, **126**, 9900-9901.
27. J. Zheng, P. R. Nicovich and R. M. Dickson, *Ann. Rev. Phys. Chem.*, 2007, **58**, 409-431.
28. Y. Negishi and T. Tsukuda, *Chem. Phys. Lett.*, 2004, **383**, 161–165.
29. P. Yu, X. Wen, Y. R. Toh, and J. Tang, *J. Phys. Chem. C*, 2012, **116**, 6567–6571.

3 PHOTOLUMINESCENT

COINAGE METAL NANOCCLUSERS BY SINGLE TARGET SPUTTERING

Abstract

This chapter demonstrates the synthesis of cationically charged photoluminescent noble metal nanoclusters of Au, Ag and Cu which are known plasmonic elements utilizing 11-mercaptoundecyl-N,N,N-trimethyl ammonium bromide as stabilizing and capping ligand via a sputtering deposition over liquid polymer matrix. TEM and HAADF-STEM analysis shows that the Au, Ag and Cu nanoclusters produced have particle size well below 2 nm and are quite monodispersed while XPS analysis on the other hand, reveals that these clusters are probably consist of positively charged atoms. Interestingly, the produced nanoclusters exhibit emission in both solution and solid states.

3.1 Introduction

Metal nanocluster is one of the hottest topics for both theoretical and experimental research today. It had gained increasing popularity due to its potential application in diverse fields of biomedicine,¹⁻³ nanoelectronics,^{4,5} optics,⁶⁻⁸ energy,^{9,10} chemical sensing¹¹⁻¹³ and catalysis.¹⁴⁻¹⁸ Considered as the transition from a single metal atom and metal nanoparticle, nanocluster is hypothesized to provide the missing information on how an individual metal atoms form to a more ordered plasmonic nanoparticles¹⁹⁻²². To understand its behavior, various synthetic strategies were developed which could be broadly classified into bottom-up and top-down approach. In either way, the essence of producing the metal nanocluster is the attachment of protecting or capping ligand, especially thiolate ligands, to stabilize and control the size of the particles.

Thiolate ligands can be broadly categorized as neutral, anionic and cationic ones. However, most of the reported synthesis for metal nanoclusters usually used either neutral or anionic ligands.²³⁻²⁶ Experimentally, using cationic ligand, such as thiol molecules with quaternary ammonium group (which shows positive charge in all pH conditions), is quite challenging due to the strong steric and electrostatic repulsion once the number of coordinating ligand increased per particle. In our previous paper which deals with chemical synthesis of metal nanoclusters, we came up with the idea of controlling the repulsion by introducing an anionic surfactant and successfully synthesized a blue fluorescent gold nanocluster.²⁷ We also successfully obtained Au₂₅(cationic thiol)₁₈ clusters (but not fluorescent) by chemical reduction in the presence of soft anions.^{28,29} Herein, we investigated the idea of synthesizing nanocluster of various coinage metals (Au, Ag and Cu) using a cationic ligand with longer carbon chain (11-mercaptoundecyl-*N,N,N*-trimethyl-ammonium bromide, MUTAB) but this time instead of simple chemical reduction we resort to physical approach, that is by sputtering²⁹⁻³⁶ of ejected metal atoms or clusters in a viscous polymer solvent. Thiocholine-stabilized and mercaptohexyltrimethyl ammonium-stabilized gold NPs have been prepared using this method.^{31,32} The advantages of the present scheme compared with the common chemical reduction to produce the cationically charge photoluminescent clusters are that firstly, the clusters produced do not need tedious purification process, secondly, it is very fast and scalable thus the clusters could readily be mass produced, and lastly, it is eco and biologically friendly since there is no need for toxic chemical reducing reagents and thus clusters could be safely used for in vivo biomedical applications such as for bioimaging, biosensing and biotherapy.

3.2 Experimental Section

3.2.1 Materials.

In this study we used 11-mercaptoundecyl-*N,N,N*-trimethyl-ammonium bromide (MUTAB, Aldrich) as capping and stabilizing ligand and Polyethylene Glycol 600 (Junsei, Japan) as liquid polymer matrix. Chemical structure of both ligand and polymer matrix is shown in Figure 3.1. Metal targets used in this experiment are Au with 99.9% purity, Ag with 99.99% purity (Tanaka Precious Metals, Japan) and Cu (Nilaco, Japan) with 99.5% purity.

3.2.2 Synthesis of Photoluminescent Au, Ag and Cu nanoclusters by sputtering in polymer liquid.

Preparation procedure (Fig. 3.1) was similar to the previous study using mercaptoundecanoic acid wherein the working distance between the metal target and the capturing medium was set at 5 cm.³⁰ In a typical synthesis, 0.02 g of MUTAB was mixed with 3.384 g PEG (initially degassed and dried at 100 °C under vacuum for 2 hrs) in a petri dish with 30 mm inner diameter and a height of 15 mm. The resulting solution was then further degassed for another 15 minutes at 100 °C to ensure removal of volatile components. After degassing, sputtering was then started by setting the stirring speed at 100 rpm and then evacuating the sputtering chamber for about 40 min until the pressure reached the 10^{-4} Pa value done at ambient temperature. Afterwards, Argon gas was then introduced in the chamber and gas exchange was performed by repeatedly evacuating the chamber for about 20 min before setting up the final chamber pressure at 2.0 Pa. Sputtering current was then set at 10 mA and pre-sputtering was conducted for 10 min on an aluminium foil prior to 10 min actual sputtering on a liquid polymer matrix.

3.2.3 Characterization.

UV-Vis Extinction measurement was done using a 10 mm×10 mm transparent quartz cuvette cell mounted in Shimadzu UV-1800 spectrophotometer operated within the wavelength range: 200-800 nm. The same cuvette cell and solution was mounted in a Jasco FP-6600 spectrofluorometer to investigate the photoluminescence spectra. STEM-HAADF (FEI TITAN III G2-Cubed, acceleration voltage 300 kV) and Transmission Electron Microscopy (JEOL JEM-2000FX, acceleration voltage 200 kV) images were obtained determine the particle size and distribution of the synthesized clusters.

The obtained suspension was further purified by the re-precipitation using acetonitrile as a poor solvent to remove PEG and excess MUTAB for further characterization. XPS spectra was obtained using JEOL JPS-9200 X-ray photoelectron spectroscopy (XPS) device equipped with a monochromatic Al K α source operating at 100 W under ultrahigh vacuum ($\sim 1.0 \times 10^{-7}$ Pa) conditions. Binding energies were referenced to the C_{1s} binding energy of the adventitious carbon contamination.

3.3 Results and Discussion

Figure 3.1 shows the schematic diagram of the experimental sputtering set up used in this study. In our modified sputtering technique, under high vacuum the argon is ionized leading to the generation of plasma which consequently etched the metal target as the ionized gases collide with it. In the process, the surface atoms that have binding energy less than the kinetic energy of the colliding gas are detached and ejected from the bulk, leading to the generation of unstable group of atoms or clusters in the gas phase under vacuum. The clusters are then captured using a petri dish filled with stabilizing

ligand (cationic thiolate: MUTAB) dissolved in a liquid polymer solvent (PEG) and constantly stirred to homogenize the solution.

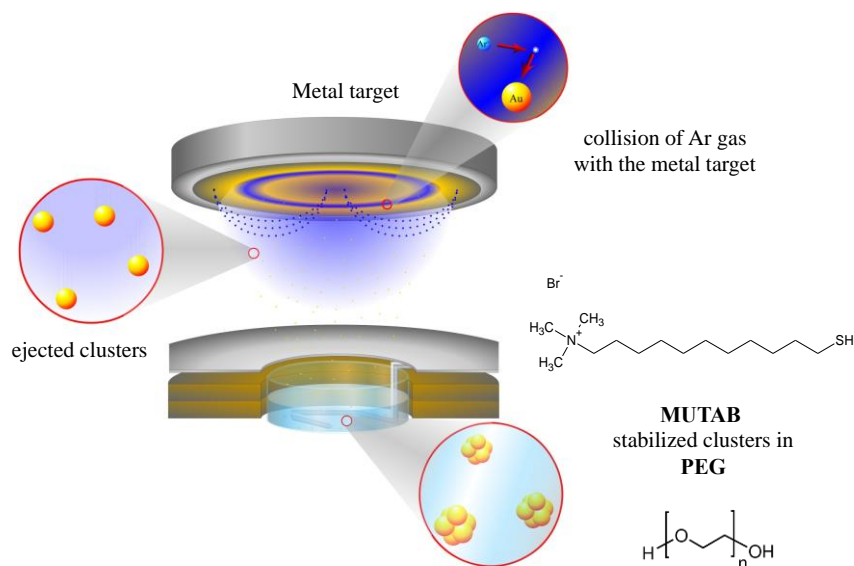


Figure 3.1 Schematic diagram of experimental sputtering set-up.

Figure 3.2 shows the extinction spectra of the synthesized samples. It can be observed that the obtained Au, Ag and Cu particles did not show plasmon absorbance in the visible region. Usually Au, Ag and Cu nanoparticles with particle sizes well above 2-3 nm have plasmon absorption in the visible region when the frequency of electromagnetic wave is coherent with the natural frequency of the conduction electron of the said particles.³⁷ This could indicate that nanoclusters were possibly produced instead of nanoparticles as can be inferred from the absence of plasmon absorption around 520 nm for Au nanoparticles, around 420 nm for Ag nanoparticles and around 570 nm for Cu nanoparticles. For instance, when we tried to synthesize without the MUTAB ligand (Figure S1) under the same sputtering current and time, we are able to detect the plasmon absorption profile of the said nanoparticles (Figure S2) indicating that the ligand indeed had a significant influence in producing the photoluminescent clusters.

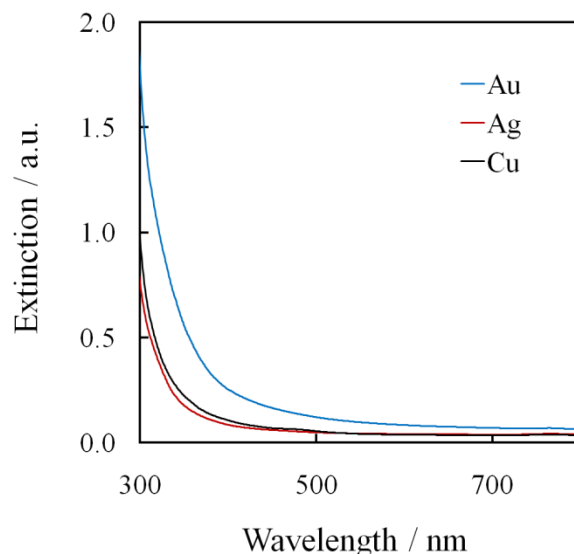


Figure 3.2 UV-Vis Extinction spectra of Au, Ag and Cu nanoclusters in PEG dispersions with MUTAB.

Absences of plasmon absorption for very small nanoclusters are well documented. In fact, group of Jin *et al.*,³⁸ Ammar *et al.*,³⁹ and Goswami *et al.*⁴⁰ showed similar behavior in the case of photoluminescent Au nanoclusters synthesized by means of chemical reduction. In case of sputtering to synthesize a photoluminescent Au nanocluster, Iimori *et al.*⁴¹ and our group^{30,31,32,36} also reported similar absence of plasmon absorption. In case of Ag and Cu nanoclusters, the phenomena were also observed for clusters synthesized by means of chemical reduction.⁴²⁻⁴⁴ Our group is the first to report the phenomena by means of sputtering for both Ag⁴⁵ and Cu⁴⁶ nanoclusters, respectively. Thus, these absorption features suggest the formation of very small nanoclusters by the current sputtering system.

Figure 3.3 shows the photoluminescence spectra of obtained nanoclusters in the PEG dispersion. It can be deduced that Au nanocluster showed photoluminescence in the NIR region as can be inferred from the broad emission curve which spans from 500 nm to

850 nm. The maximum emission wavelength for this synthesized Au nanoclusters is at 629 nm once excited at 304 nm. On the other hand, the synthesized Ag and Cu nanoclusters both showed photoluminescence in the blue region at 432 nm (Ag) and 428 nm (Cu).

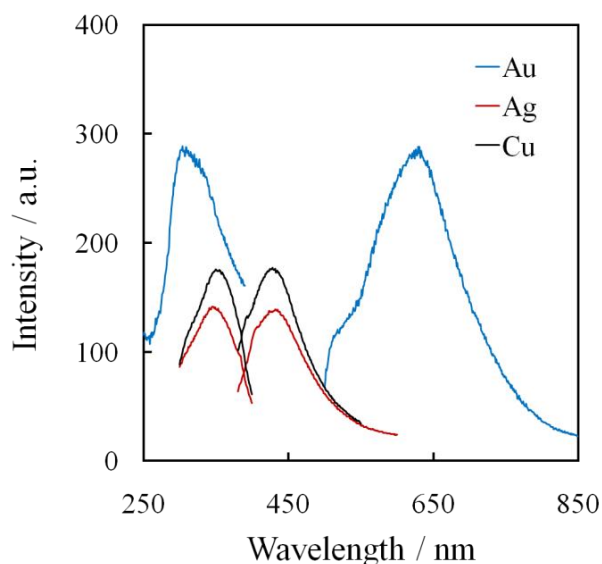


Figure 3.3 Photoluminescence spectra of Au, Ag and Cu nanoclusters in PEG dispersions with MUTAB.

Photoluminescence phenomenon in the case of metal nanoclusters is commonly attributed firstly, with the particle size or the number of atoms comprising the cluster due to quantum size effect wherein the particle started to behave somewhat like a molecule when its particle size is well below 2 nm.^{5, 47-49} However, in the case of Au nanocluster synthesized by means of sputtering, the cluster only showed photoluminescence in the NIR region and the stoke shift is quite large (~ 325 nm) as already discussed in our previous paper.³² This is contrary to our Au nanocluster produced by means of chemical reduction which mostly have small stoke shift (~100 nm) and the emission maxima is found in the blue region.²⁷

With regard to the photoluminescence of Ag nanocluster, we found that it has emission in the blue region. This is a new finding in this study; our previous report about the photoluminescence of Ag nanocluster using a thiolate ligand showed emission in the NIR region.⁴⁵ The size of obtained Ag clusters was significantly different from the previous NIR photoluminescent ones⁴⁵ as described later with TEM images and this may be attributed to the difference of their photoluminescence energies. For Cu nanocluster, we found the emission in the blue region as well similar with our previous report using 11-mercaptoundecanoic acid as the ligand.⁴⁶ Figure S3 shows the colour of these nanocluster dispersions under sunlight and under UV-light. In all cases the clusters of Au, Ag and Cu have pale yellow colour under sunlight, however, under UV light irradiation, Au nanocluster solution showed orange emission whereas both Ag and Cu nanocluster solution showed blue emission. When we tried to purify and collect the powder by re-precipitating the cluster using a poor dispersing solvent, acetonitrile, we found out that even in the solid state, these clusters show similar emission colour (Figure S4) and were homogeneously soluble in water. To understand the origin of these photoluminescence, we analyzed the TEM images of our synthesized nanoclusters by measuring the diameter of at least 300 particles from several TEM images.

Figure 3.4 shows the TEM images of Au, Ag and Cu nanoclusters and their corresponding particle size distributions. It can be observed that in all cases the average particle sizes are well below 2 nm. The average particle sizes were ca. 1.2, 1.3 and 1.0 nm for Au, Ag and Cu nanoclusters, respectively. These very small particle diameters could be the origin of photoluminescence of obtained nanoclusters wherein the particle started to behave somewhat like a molecule.^{5,47-49} Relatively broad histograms obtained are

attributed to the small concentration of MUTAB ligand (20 mM) in PEG where the stabilization of sputtered nanoclusters was insufficient to achieve homogeneous nanoclusters as reported elsewhere.³⁰

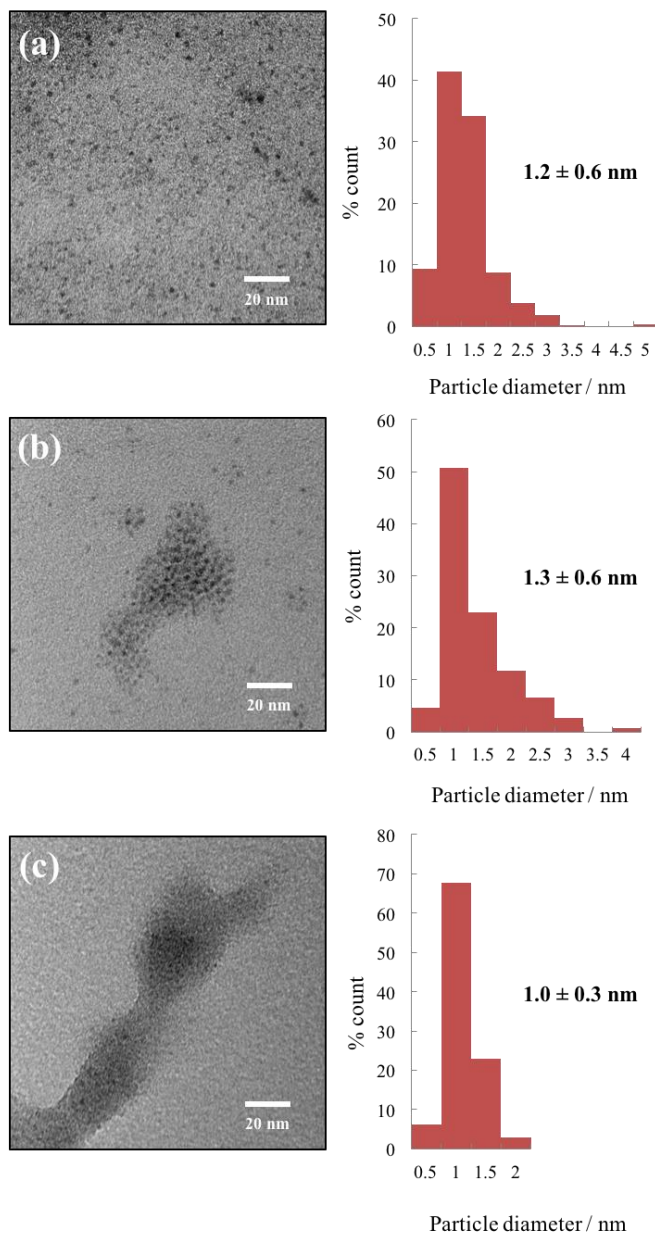


Figure 3.4 Transmission Electron Microscopy (TEM) images and size distribution histograms of (a) Au, (b) Ag and (c) Cu nanoclusters.

It is interesting to note that all particle diameter histogram include relatively larger sizes over 2 nm, however, plasmon absorption were not observable in the current experiments. We recently reported a similar phenomenon of absence of plasmonic absorption for larger sputtered Ag NPs.⁴⁵ The average TEM diameter varied from 2.5 to 13.7 nm however NIR emission still remained and plasmonic absorption was not observable in such very large nanoparticles due to the secondary aggregation of photoluminescent nanocluster species.

To understand the bonding and charge states of the synthesized photoluminescent nanoclusters, XPS analysis was conducted. Figure 3.5 shows the narrow scan spectra at Au 4f and Ag 3d regions. It is evident in Au 4f region that the spectra is significantly shifted in higher binding energy in comparison to the binding energy of neutral bulk Au at Au 4f_{7/2} and Au 4f_{5/2} (located at 84 eV and 88 eV respectively) and slightly shifted in the lower binding energy compared to the binding energy of Au(I)-thiolate complexes at Au 4f_{7/2} and Au 4f_{5/2} (~86 eV and ~90 eV respectively).⁵⁰ Thus, it can be deduced that the Au atoms comprising the photoluminescent Au nanocluster are mainly in its Au(I) charge states as can be seen from the peaks in the Au 4f_{7/2} and Au 4f_{5/2} located at 85.5 eV and 89.1 eV which corresponds to the ring type cluster Au₁₀(SR)₁₀ and Au₁₅(SR)₁₃, the smallest known cluster which has Au₄ core theoretically predicted by Whetten et al.⁵⁰ and was isolated by Tsukuda et al.⁵¹ way back in 2004 by chemical synthesis and recently verified by our group in physical synthesis.³⁰ With respect to Ag 3d region on the other hand, we found prominent peaks at around 367.7 eV and 373.7 eV in Ag 3d_{5/2} and Ag 3d_{3/2} respectively which is slightly shifted to lower binding energy in comparison to the neutral bulk Ag at 368.2 eV and 374.2 eV respectively and significantly shifted to higher

binding energy with respect to Ag(I) complexes which has binding energy at 366.8 eV and 372.8 eV in Ag 3d_{5/2} and Ag 3d_{3/2} respectively.⁵²

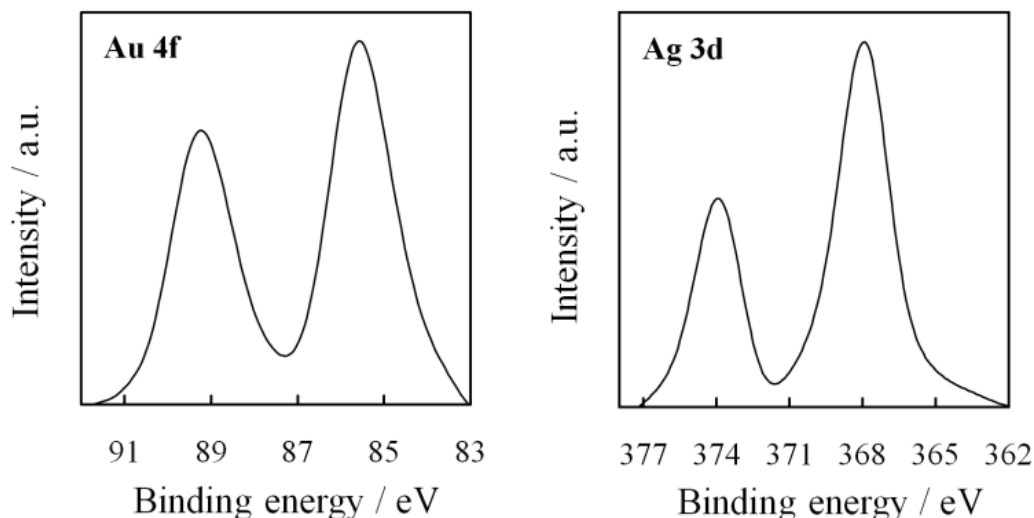


Figure 3.5 XPS spectra at Au 4f and Ag 3d for photoluminescent Au and Ag nanoclusters respectively.

This result indicate that the atoms comprising the photoluminescent Ag nanoclusters are dominantly consists of Ag(I) species as reported by other reaserchers.⁵²⁻⁵⁷ Cu 2p region on the other hand (Figure S5), shows prominent peaks at 933 eV and 953 eV at Cu 2p_{3/2} and Cu 2p_{1/2} respectively. Although there is a probability that the species are dominantly consist of Cu(I), we find it difficult to verify since Cu(0) and Cu(I) have similar binding energies in the said region.⁵⁴ Cu₂S nanoclusters might possibly be present as shown by our previous report³⁴ but we believed that the quantity of these clusters is negligible in the present case since Cu₂S have emission maximum in the red region which is contrary to what we found as emission maximum for our newly synthesized blue photoluminescent nanoclusters using MUTAB as ligand.

Hence, from these results it could be deduced that the photoluminescent Au, Ag and Cu nanoclusters were emissive primarily due to quantum size effects⁵ and secondly, via aggregation induced emission due to possible presence of Au(I)-thiolates, Ag(I)-thiolates and Cu(I)-thiolates as isolated polynuclear complexes or metal(I)-thiolates bonded to a core like in the case of Au₁₅(SR)₁₃ which are known to exhibit metallophilic attraction due to relativistic effects⁵⁹ leading to aggregation and its consequent photoluminescent emission. Figure 3.6 is the STEM-HAADF images of the synthesized Au, Ag and Cu nanoclusters showing the existence of particles with dimensions well below ~1 nm.

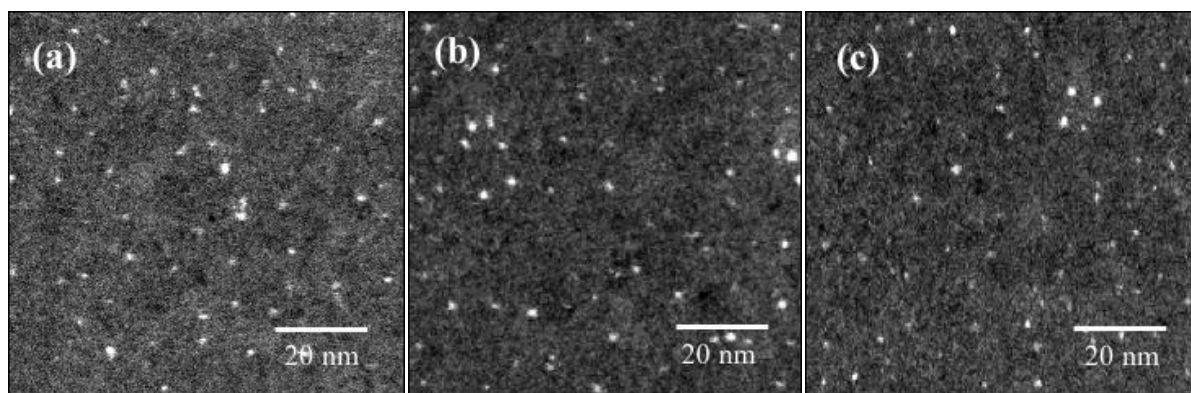


Figure 3.6 STEM-HAADF images of photoluminescent (a) Au, (b) Ag and (c) Cu nanoclusters.

As for the formation mechanism of photoluminescent nanoclusters, in PEG alone what can be formed in our sputtering system are plasmonic Au, Ag and Cu nanoparticles due to possible aggregation and coalescence of naked metal atoms / metal clusters on the vacuum-liquid interface and further growth in the liquid polymer matrix which has no effective coordinating group to stabilize the sputtered particles. On the other hand, in the PEG-MUTAB system, as the

naked atoms / clusters reached the vacuum-liquid interface, the coalescence and spontaneous growth were effectively prevented due to presence of thiol molecules which has high bonding affinity for metal atoms. However, these stabilized nanoclusters have the tendency to aggregate in the liquid polymer matrix.³⁰

3.4 Conclusions

In this study we have demonstrated the versatility of our modified sputtering approach in synthesizing cationically charged photoluminescent nanoclusters of known plasmonic metal elements Au, Ag and Cu using 11-mercaptoundecyl-*N,N,N*-trimethylammonium bromide as stabilizing and capping ligand. Our report shows photoluminescence of Au nanocluster in the NIR region with maximum emission wavelength located at 629 nm. In addition, we found blue emission for both Ag and Cu nanoclusters with emission maxima positioned at 432 nm and 428 nm, respectively. TEM and STEM-HAADF analyses on the other hand, showed that the nanoclusters produced have particle diameters well below 2 nm confirming the existence of photoluminescent nanoclusters and XPS analysis of these photoluminescent nanoclusters show that the clusters are most probably consists of positively charged atoms. The method presented therefore would be beneficial for the widely-applicable material synthesis for positively-charged photoluminescent nanoclusters.

3.5 References

1. X. Song, N. Goswami, H. Yang and J. Xie, *Analyst*, 2016, **141**, 3126-3140.
2. X. Tan and R. Jin, *Nanomed. Nanobiotechnol.*, 2013, **5** 569-581.
3. C. J. Lin, C. Lee, J. Hsieh, H. Wang, J. K. Li, J. Shen, W. Chan, H. Yeh and W. Chang, *J. Med. Biol. Eng.*, 2009, **29**, 276-283.
4. M. Homberger and U. Simon, *Phil. Trans. R. Soc. A*, 2010, **368**, 1405-1453.
5. G. Schmid, *Adv. Eng. Mater.*, 2001, **10**, 737-743.
6. X. Yuan, Z. Luo, Y. Yu, Q. Yao and J. Xie, *Chem. Asian J.*, 2013, **8**, 858-871.
7. L. Shang and G. U. Nienhaus, *Biophys Rev.*, 2012, **4**, 313-322.
8. D. M. Chevrier, A. Chatt and P. Zhang, *J. Nanophotonics*, 2012, **6**, 064504 1-16.
9. A. Mathew and T. Pradeep, *Part. Part. Syst. Charact.*, 2014, **31**, 1017-1053.
10. Y. Chen, H. Choi and P. V. Kamat, *J. Am. Chem. Soc.*, 2013, **135**, 8822-8825.
11. L. Chen, C. Wang, Z. Yuan and H. Chang, *Anal. Chem.*, 2015, **87**, 216-229.
12. J. Sun and Y. Jin, *J. Mater. Chem. C*, 2014, **2**, 8000-8011.
13. X. Luo, A. Morrin, A. J. Killard and M. R. Smyth, *Electroanal.*, 2006, **18**, 319-326.
14. J. D. Aiken III and R. G. Finke, *J. Mol. Catal. A*, 1991, **145**, 1-44.
15. G. Che, B. B. Lakshmi, C. R. Martin and E. R. Fisher, *Langmuir*, 1999, **15**, 750-758.
16. J. Wang and H. Gu, *Molecules*, 2015, **20**, 17070-17092.
17. B. Liu, H. Yao, W. Song, L. Jin, I. M. Mosa, J. F. Rusling, S. L. Suib and J. He, *J. Am. Chem. Soc.*, 2016, **138**, 4718-4721.
18. E. C. Tyo and S. Vajda, *Nature Nanotechnol.*, 2015, **10**, 577-588.
19. M. Kumar, G. Reddy, *Physica E*, 2010, **42**, 1940-1943.
20. M. Kumar, T. Kumar and D. Avasthi, *Scripta Materialia*, 2015, **105**, 46-49.

21. M. Kumar and G. Reddy, *Plasmonics*, 2016, **11**, 261-267.
22. A. Javid, M. Kumar, S. Yoon, J. Lee and J. Han, 2017, **19**, 237-244.
23. A. Kyrychenko, G. V. Kapurshina, D. Svechkarev, D. Kolodezny, S. I. Bogatyrenko, A. P. Kryshstal and A. O. Doroshenko, *J. Phys. Chem. C*, 2012, **116**, 21059-21068.
24. A. P. Gies, D. M. Hercules, A. E. Gerdon and D. E. Cliffler, *J. Am. Chem. Soc.*, 2007, **129**, 1095-1104.
25. R. Jin, *Nanoscale*, 2010, **2**, 343-362.
26. T. Das, P. Ghosh, M.S. Shanavaras, A. Maity, S. Mondala and P. Purkayastha, *RSC Adv.*, 2012, **2**, 12210-12215.
27. R. D. Corpuz, Y. Ishida and T. Yonezawa, *Phys. Chem. Chem. Phys.*, 2016, **18**, 8773-8776.
28. Y. Ishida, K. Narita, T. Yonezawa and R. Whetten, *J. Phys. Chem. Lett.*, 2016, **7**, 3718-3722.
29. Y. Ishida, Y.-L. Huang, T. Yonezawa and K. Narita, *ChemNanoMat*, in press (2017).
DOI: 10.1002/cnma.201700012
30. Y. Ishida, I. Akita, T. Sumi, M. Matsubara and T. Yonezawa, *Sci. Rep.*, 2016, **6**, 29928, 1-14.
31. Y. Ishida, C. Lee and T. Yonezawa, *Sci. Rep.*, 2015, **5**, 15372, 1-6.
32. Y. Shishino, T. Yonezawa, K. Kawai and H. Nishihara, *Chem. Comm.*, 2010, **46**, 7211-7213.
33. Y. Shishino, T. Yonezawa, S. Udagawa, K. Hase and H. Nishihara, *Angew. Chem. Int. Ed.*, 2011, **50**, 703-705.

34. M. Porta, M. T. Nguyen, T. Tokunaga, Y. Ishida, W. Liu and T. Yonezawa, *Langmuir*, 2016, **32**, 12159-12165.
35. Y. Ishida, R. Nakabayashi, M. Matsubara and T. Yonezawa, *New J. Chem.*, 2015, **39**, 4227-4230.
36. T. Sumi, S. Motono, Y. Ishida, N. Shirahata and T. Yonezawa, *Langmuir*, 2015, **31**, 4323-4329.
37. C. Kumara, X. Zuo, D. A. Cullen and A. Dass, *ACS Nano*, 2014, **8**, 6431-6439.
38. R. Jin, S. Egusa and N. F. Scherer, *J. Am. Chem. Soc.*, 2014, **126**, 9900-9901.
39. A. Ammar, D. Sierra, F. Merola, N. Hildebrandt and X. L. Guevel, *ACS Nano*, 2016, **10**, 2591-2599.
40. N. Goswami, F. Lin, Y. Liu, D. T. Leong and J. Xie, *Chem. Mater.*, 2016, **28**, 4009-4016.
41. T. Iimori, Y. Hatakeyama, K. Nishikawa, M. Kato and N. Ohta, *Chem. Phys. Lett.*, 2013, **586**, 100-103.
42. B. Li, J. Li and J. Zhao, *Spectrochim. Acta A*, 2015, **134**, 40-47.
43. U. Anand, S. Ghosh and S. Mukherjee, *J. Phys. Chem. Lett.*, 2012, **3**, 3605-3609.
44. H. Huang, H. Li, J. J. Feng, H. Feng, A. J. Wang and Z. Qian, *Sensors Actuators B*, 2017, **241**, 292-297.
45. Y. Ishida, S. Udagawa and T. Yonezawa, *Colloids Surf. A*, 2016, **504**, 437-441.
46. M. Porta, M. T. Nguyen, Y. Ishida and T. Yonezawa, *RSC Adv.*, 2016, **6**, 105030-105034.
47. J. Zheng, C. W. Zhang and R. M. Dickson, *Phys. Rev. Lett.*, 2004, **93**, 0077402.
48. S. K. Ghosha and T. Pal, *Phys. Chem. Chem. Phys.*, 2009, **11**, 3831-3844.

49. R. P. Gotor and E. Grueso, *Phys. Chem. Chem. Phys.*, 2011, **13**, 1479-1489.
50. A. Flores, M. Yacaman and R. Whetten, *Phys. Chem. Chem. Phys.*, 2013, **15**, 19557-19560.
51. Y. Negishi, K. Nobusada and T. Tsukuda, *J. Am. Chem. Soc.*, 2005, **127**, 5261-5270.
52. Y. Mao, Y. Yang, H. Yang, J. Han, Y. Zeng, J. Wei, X. Meng and C. Wang, *RSC Adv.*, 2016, **6**, 12311-12314.
53. Z. Q. Tian, Y. Z. Lian, J. Q. Wang, S. J. Wang and W. H. Li, *J. Electroanal. Chem.*, 1991, **308**, 357-363.
54. X. Yuan, T. J. Yeow, Q. Zhang, J. Y. Lee and J. Xie, *Nanoscale*, 2012, **4**, 1968-1971.
55. S. Gao, D. Chen, Q. Li, J. Ye, H. Jiang, C. Amatore and X. Wang, *Sci. Rep.*, 2014, **4**, 4384 1-6.
56. A. Ferraria, A. Carapeto and A. Rego, *Vacuum*, 2012, **86**, 1988-1991.
57. A. Shahzad, T. Yu, and W. S. Kim, *RSC Adv.*, 2016, **6**, 54709-54717.
58. C. Vericat, M. E. Vela, G. Corthey, E. Pensa, E. Cortes, M. H. Forticelli, F. Ibanez, G. E. Benitez, P. Carro and R. C. Salvarezza, *RSC Adv.*, 2014, **4**, 27730-27754.
59. S. Sculfort and P. Braunstein, *Chem. Soc. Rev.*, 2011, **40**, 2741-2760.

4

PHOTOLUMINESCENT

BIMETALLIC GOLD-SILVER
NANOCLUSTERS BY DOUBLE TARGET
SPUTTERING ON A BIOCOMPATIBLE
LIQUID POLYMER MATRIX

Abstract

This chapter illustrates the synthesis of a novel positively charged photoluminescent Au-Ag bimetallic nanocluster synthesized using 11-mercaptoundecyl-*N,N,N*-trimethylammonium bromide as capping ligand by means of “green” double target sputtering method on a biocompatible polymer matrix. The photoluminescent Au-Ag bimetallic cluster showed emission tunability from the blue to Near Infrared (NIR) regions with respect to change in composition and could have potential benefit in biomedical fields particularly for biosensing, bioimaging, biotherapy and targeted drug delivery owing to the inherent purity of the present synthetic method.

4.1 Introduction

Bimetallic nanocluster is a hot topic in research community due to its improved optical and catalytic properties typically attributed to synergistic effects¹ when two types of atoms having distinct properties mixed and combined with each other to form electronically and geometrically stable nanoclusters. Among of the bimetallic clusters, Au-Ag bimetallic system is the most intensively investigated due to the noble characteristics of Au and Ag and the fact that these two elements with comparable sizes form homogeneous solution in wide range of composition.²⁻⁴

Bimetallic Au-Ag photoluminescent nanoclusters are typically produced by utilizing capping and protecting ligand such as protein⁵, DNA⁶, and gelatin⁷ to control the number of

atoms and its growth. To date these photoluminescent bimetallic clusters were only successfully synthesized by means of chemical reduction via galvanic exchange reaction⁸, co-reduction⁹, and anti-galvanic reaction methods¹⁰ and typically utilized toxic reducing reagents thus its utilization for biomedical applications is still subject for intensive researches and clinical trials due to purity and toxicity related issues.

In this study, we introduced a novel green physical method in producing a bimetallic Au-Ag photoluminescent nanocluster utilizing a positively charged long thiol molecule, 11-mercaptoundecyl-*N,N,N*-trimethylammonium bromide (MUTAB) as capping ligand by means of double target sputtering on a biocompatible liquid polymer matrix, polyethylene glycol (PEG). Unlike the chemical synthesis, this novel method requires neither reducing agent nor tedious purification processes to produce Near Infrared (NIR) emissive bimetallic nanoclusters. NIR emissive nanoclusters has the advantage for its deep tissue penetrating photons¹¹, making it positively charge will make these photoluminescent nanoclusters adhere to cell selectively and thus it could potentially be used for targeted drug delivery and as selective photoluminescent probe to investigate cell activities owing to high affinity of proteins inside the cell for positively charged particles¹².

4.2 Experimental Section

4.2.1 Materials

Au and Ag targets with 99.99% purity were obtained from Tanaka Precious Metals, Tokyo. PEG (Wako) and MUTAB (Aldrich) were used as received.

Shown in Figure 4.1 is the schematic diagram of experimental double target sputtering set-up used in this study. Metal targets Au and Ag were utilized to produce the photoluminescent

bimetallic nanocluster. In a usual sputtering process, under high vacuum the metal targets were simultaneously etched by ionized Ar gas which consequently generates unstable mixtures of Au and Ag particles. In this novel set up, the targets are oriented at an angle slightly facing each other which increase the probability of collision among etched particles to form bimetallic nanoclusters in the gas phase and on the surface of the polymer matrix initially mixed with MUTAB.

4.2.2 Synthesis of monometallic and bimetallic nanocluster

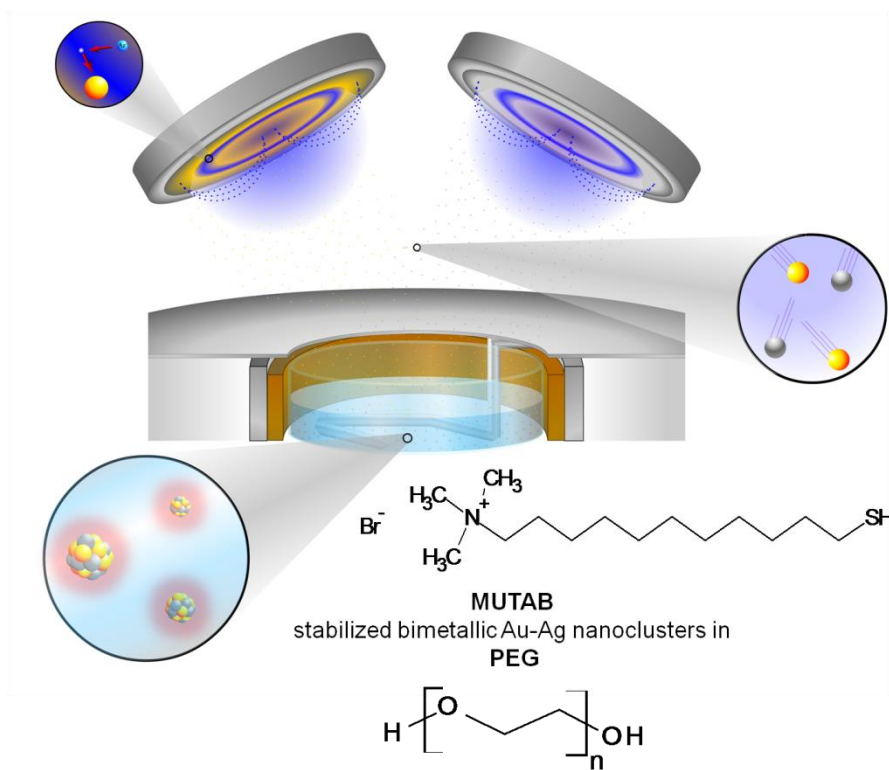


Figure 4.1 Schematic diagram of experimental double target sputtering set up to produce bimetallic Au-Ag photoluminescent nanoclusters.

In a typical synthesis, the liquid polymer solvent used (polyethylene glycol (PEG) 600) was initially degassed at 100 °C for 2 hrs to ensure removal of volatile components. 10.152 g of

PEG was then mixed with 0.04 g 11-mercaptoundecyl-*N,N,N*-trimethylammonium bromide (MUTAB) ligand followed with 15 min degassing prior to sputtering process. Before sputtering, the chamber was evacuated until the pressure reaches the 10^{-4} Pa value done at ambient temperature. Ar gas was then introduced in the chamber and gas exchange was done multiple times for 20 minutes. After which the current for each metal target was then set and pre-sputtering on aluminum foil was done for 10 min before the actual 15 min sputtering. Shown in Table 4.1 are the sputtering conditions used in this study. Plasmonic Au, Ag and bimetallic Au-Ag nanoparticles synthesized without MUTAB were designated as samples **1**, **2** and **3** respectively. Monometallic nanoclusters Au and Ag synthesized with MUTAB on the other hand, were designated as samples **4** and **5** respectively, and the bimetallic nanoclusters synthesized with MUTAB under varied applied sputtering current are designated as samples **6–11**.

Table 4.1 Sputtering conditions for the synthesis of Au-Ag bimetallic nanoclusters.

Sample	Applied current (mA)		MUTAB
	Au	Ag	
1	20	0	Absence
2	0	34	
3	20	34	
4	20	0	Presence
5	0	34	
6	10	50	
7	14	46	
8	18	38	
9	20	34	
10	24	20	
11	26	14	

4.2.3 Characterization

Right after sputtering, UV-Vis extinction measurement was conducted using a 10 mm x 10 mm quartz cuvette cell mounted in a Shimadzu UV-1800 spectrophotometer. The same sample was then subjected for photoluminescent measurement using JASCO FP-6600 spectrofluorometer. TEM images of the sample were taken to determine the particle size and size distribution using JEOL JEM-2000FX operated at 200kV. TEM samples were prepared by dropping gold dispersion of PEG onto collodion-coated copper grids. The grids were then soaked into methanol for 30 min in order to remove the excess PEG and dried under vacuum.

The obtained PEG suspension was purified by the re-precipitation using acetonitrile as a poor solvent to remove PEG and excess MUTAB for further characterization. XPS was detected by JEOL JPS-9200 X-ray photoelectron spectroscopy device equipped with a monochromatic Al K α source operating at 100 W under ultrahigh vacuum ($\sim 1.0 \times 10^{-7}$ Pa) conditions. Binding energies were referenced to the C_{1s} binding energy of the adventitious carbon contamination. XPS elemental quantification and ICP-AES (ICPE-9000 Shimadzu Corporation) elemental analyses were obtained to determine the elemental composition of bimetallic Au-Ag nanocluster. For ICP-AES measurements, standard gold and silver aqueous solutions were prepared with the following concentrations: 0 ppb (blank), 500 ppb, 1 250 ppb, 2 500 ppb, 5 000 ppb and 10 000 ppb, 6 ml of each solution was then mixed with 2 ml aqua regia (3 wt %) to generate a calibration curve. The samples with unknown concentrations initially re-precipitated using acetonitrile, purified by centrifugation (15 000 rpm, 10 min, 2 times repetition) and vacuum dried were then diluted with 6 ml water and mixed with 2 ml aqua regia (3 wt %) and concentrations were then automatically analyzed using the plotted standard calibration curve. The concentrations obtained were then converted to atomic % composition. STEM-HAADF (FEI TITAN III G2- Cubed, acceleration

voltage 300 kV) and EDS elemental mapping were conducted to verify the existence of bimetallic Au-Ag nanocluster.

4.3 Results and Discussion

In our previous report¹³ using the double target sputtering, we tried to tune the plasmon absorbance of Ag-Au alloy nanoparticles by manipulating the current of the metal targets. Consequently, we were able to correlate the observed absorbance of the resulting alloy to its corresponding composition. Inspired by this result, in this study we extended the double target sputtering method to synthesize photoluminescent Au-Ag bimetallic nanoclusters. Most of our studies regarding photoluminescent nanoclusters were limited only to monometallic ones such as the monometallic photoluminescent Au, Ag and Cu nanoclusters using various types of neutral, anionic and cationic thiol molecule ligands.¹⁴⁻¹⁷ Herein, we investigated the effect of varying the composition ratio of Ag/Au in synthesizing a photoluminescent Au-Ag bimetallic nanoclusters.

Figure 4.2 shows the UV-Vis spectra of as synthesized samples with and without the addition of MUTAB (the corresponding color of these samples under sunlight are shown in Figure S1). **1** and **2** showed the typical plasmon absorbance of Au and Ag nanoparticles with extinction maximum around 535 nm and 435 nm respectively. These plasmonic absorbances are attributed to the collective oscillation of the conduction electrons as it interacts with the electromagnetic wave. With the addition of MUTAB, this plasmonic absorbance in the case of monometallic nanoclusters **4** and **5** were no longer observable as can be seen in the featureless extinction profile in the visible region for these particular samples. This phenomenon suggests the formation of photoluminescent nanoclusters which has particle sizes well below 2 nm wherein the particles started to behave somewhat like a molecule due to quantum size effects.^{18,19}

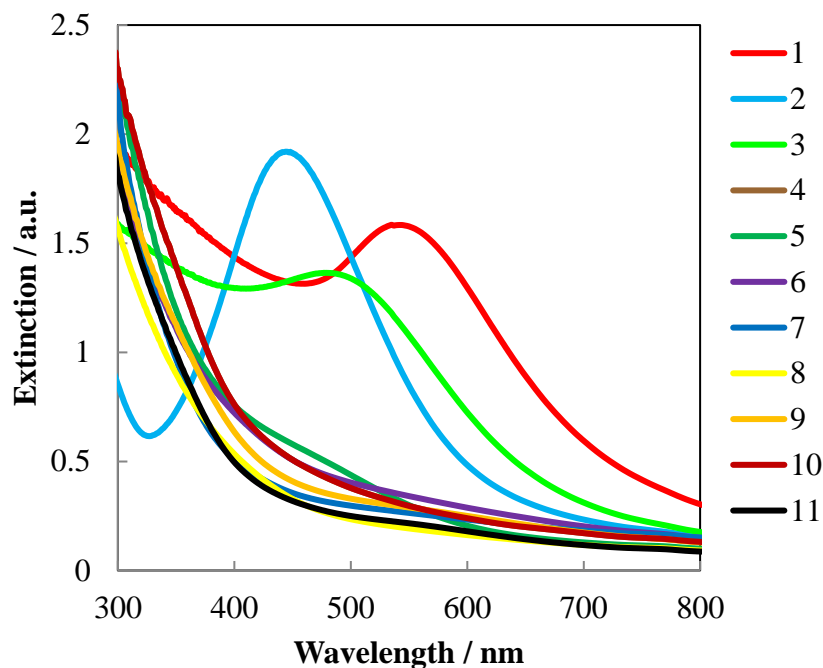
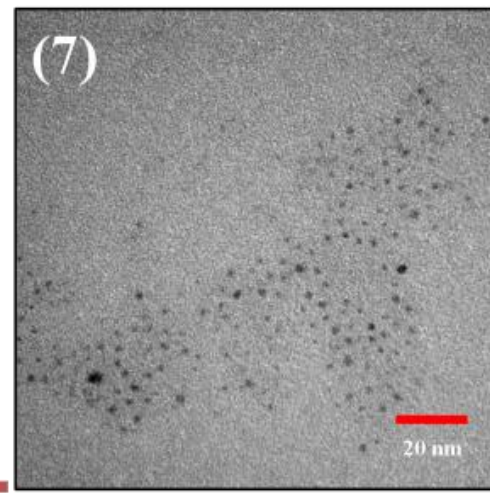
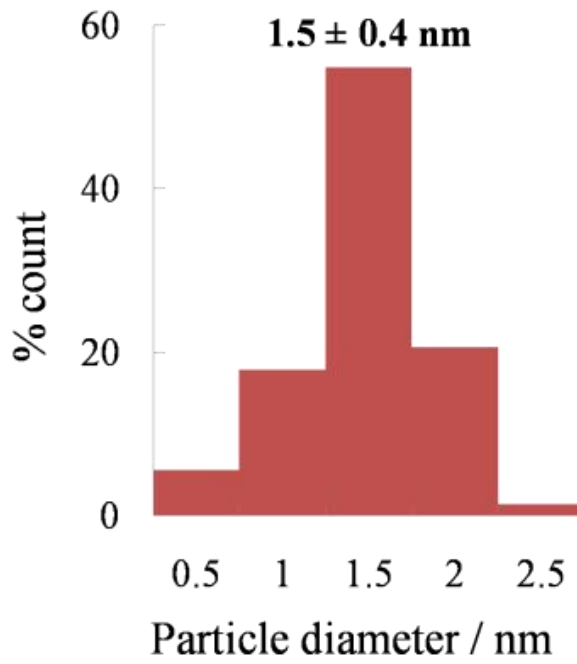
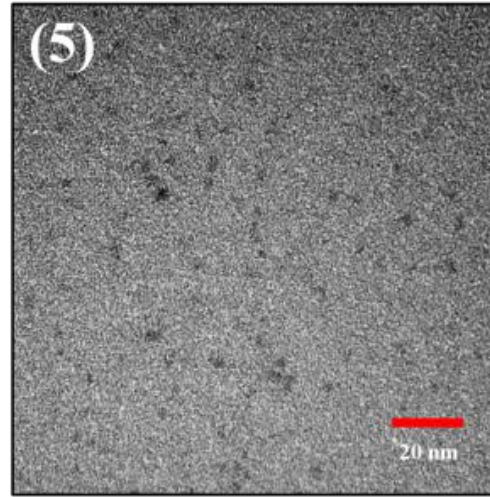
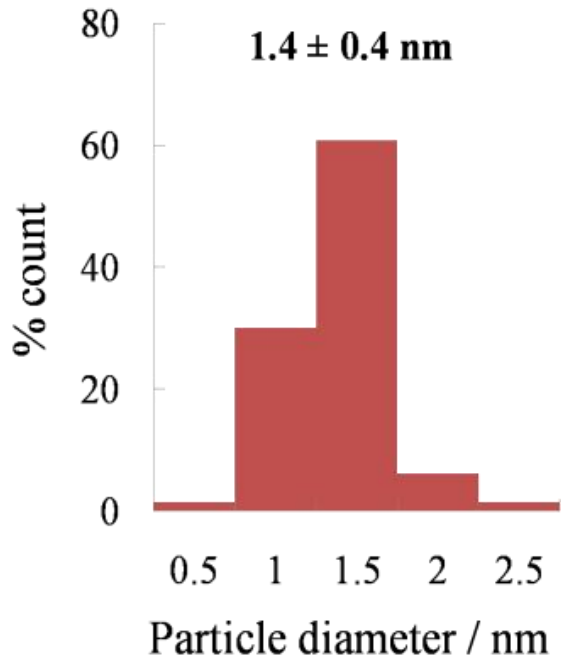


Figure 4.2 UV-Vis Extinction spectra of as synthesized samples without and with MUTAB.

3 shows the typical plasmon absorbance when Au-Ag bimetallic alloy nanoparticle is formed.^{13,20,21} It can be observed that the new extinction maximum around 480 nm blue shifted with respect to the maximum plasmon extinction of gold nanoparticle and red shifted with respect to the maximum extinction of silver nanoparticle. With the addition of MUTAB however, the plasmon absorbance of the Au-Ag alloy nanoparticle is no longer observable as can be seen in the extinction profile of **9**. Similarly, **6**, **7**, **8**, **10** and **11**, synthesized at different Ag/Au current ratios with MUTAB ligand also showed featureless extinction profile. This phenomenon is similar to the ones reported by Mohanty et al.²², Pramanik et al.²³ and Paramanik et al.²⁴ for the formation of photoluminescent bimetallic Au-Ag nanocluster synthesized by means of chemical reduction. To understand these phenomena, we conducted particle size analysis for each sample using TEM.



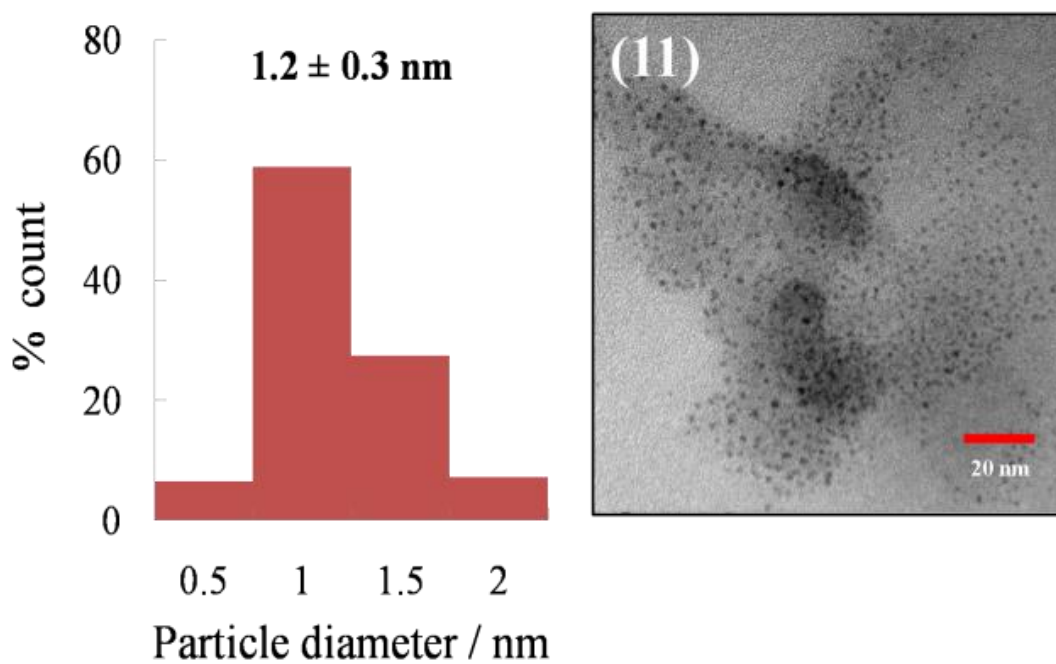
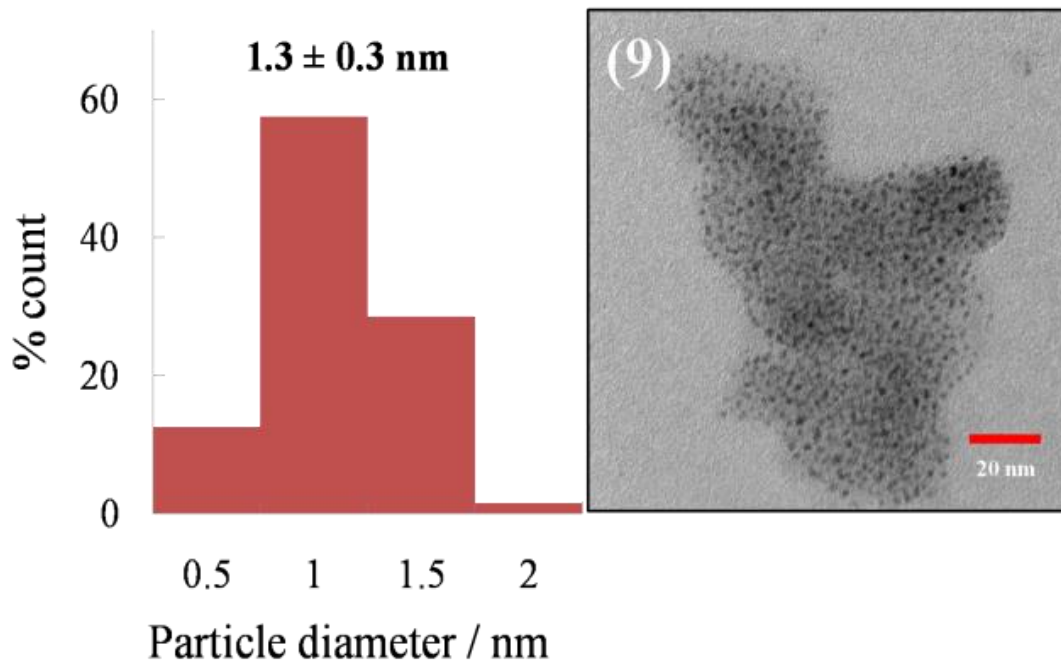


Figure 4.3 TEM images and particle size distribution histogram of samples with MUTAB. (5) Ag@34mA, (7) Au@14mA-Ag@46mA, (9) Au@20mA-Ag@34mA, and (11) Au@26mA-Ag@14mA.

Upon checking the particle sizes and size distributions of the samples we found out that the average sizes of all samples are well below 2 nm as shown in Figure 4.3 and Figure S2. For the monometallic clusters **4** and **5** the average diameters were 1.1 ± 0.3 nm and 1.4 ± 0.4 nm, respectively. On the other hand, the average diameters for bimetallic nanoclusters **6**, **7**, **8**, **9**, **10** and **11** are 1.5 ± 0.5 nm, 1.5 ± 0.4 nm, 1.3 ± 0.4 nm, 1.3 ± 0.3 nm, 1.2 ± 0.5 nm and 1.2 ± 0.3 nm, respectively. Thus it can be inferred that the featureless extinction profiles exhibited by the samples are an indication also of the formation of emissive bimetallic Au-Ag nanoclusters as can be deduced from its corresponding particle sizes. To verify if this observation is correct we irradiated the samples with UV light. Shown in Figure S3 and S4 are the images under UV light irradiation. It can be observed that **1**, **2** and **3** did not emit as expected for plasmonic nanoparticle whereas the emission color for nanoclusters synthesized with MUTAB is red for **4**, **10** and **11**, blue for **5**, **6** and **7**, and yellow-orange for **8** and **9**. We then measured the photoluminescence spectra of each sample.

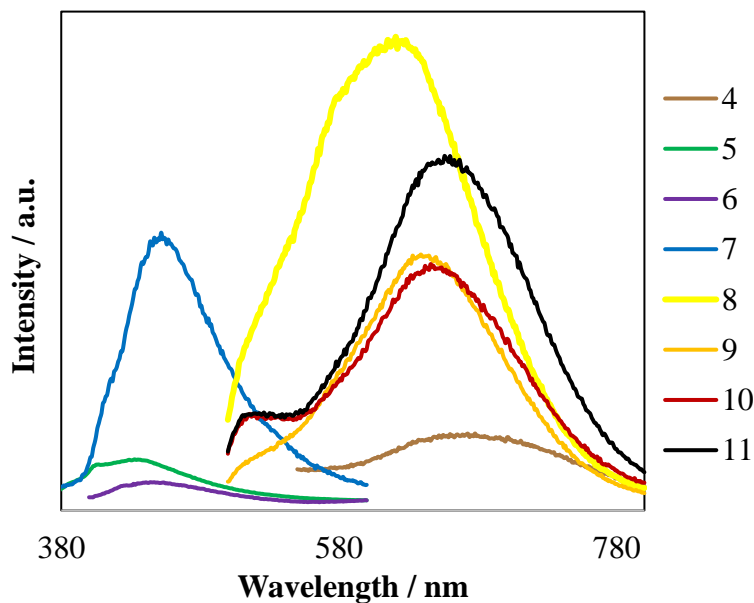


Figure 4.4 Emission spectra of obtained photoluminescent monometallic nanoclusters (**4** and **5**), and bimetallic nanoclusters (**6–11**).

Figure 4.4 shows the emission spectra of samples **4–11** (corresponding excitation spectra of these samples are shown in Figure S5). Monometallic Au nanocluster **4** has emission in the red region with maximum peak located at 678 nm whereas monometallic Ag nanocluster **5** showed blue emission with maximum peak located at 431 nm. It could be observed that with respect to monometallic gold nanocluster, the bimetallic clusters **6, 7, 8, 9, 10** and **11** are blue shifted with emission peaks located at 444 nm, 452 nm, 621 nm 639 nm, 656 nm and 661 nm, respectively. Theoretically using the spherical Jellium model, it has been predicted in the case of monometallic cluster that as the number of atoms decrease, a blue shift in emission is usually to be expected.²⁵ In the present case however wherein we are already considering two distinct metal atoms such theoretical prediction is not observed, in fact, with slight decrease in average particle size, we found that the emission peak shifted towards the red region which led us to hypothesized that there are other factors contributing to this behavior other than the particle size of the nanoclusters produced. Similar result was reported by Andolina et al.²⁶ in the case of emissive bimetallic Au-Cu nanocluster wherein there is no correlation between the decrease in particle size and the shift in emission peaks. In Au-Ag photoluminescent bimetallic nanoclusters synthesized by chemical reduction, there are reports²⁷⁻²⁹ wherein the blue shift in emission peak position correlates with the increase in Ag composition, thus to verify if this is also the case in our present study, we attempted to determine the composition of **4–11** using XPS and ICP-AES analyses.

Table 4.2 Bimetallic composition measured by XPS and ICP-AES with respect to average diameter and emission peak energy.

Sample	Current ratio (mA : mA) Au : Ag	XPS		ICP-AES		Average diameter (nm)	Emission energy (eV)
		(atomic %)		(atomic %)			
		Au	Ag	Au	Ag		
4	20:0	100	0	100	0	1.1 ± 0.3	1.82
5	0:34	0	100	0	100	1.4 ± 0.4	2.88
6	10:50	15	85	16	84	1.5 ± 0.5	2.79
7	14:46	31	69	31	69	1.5 ± 0.4	2.74
8	18:38	41	59	39	61	1.3 ± 0.4	1.99
9	20:34	56	44	52	48	1.3 ± 0.3	1.94
10	24:20	72	28	72	28	1.2 ± 0.5	1.92
11	26:14	79	21	83	17	1.2 ± 0.3	1.89

Table 4.2 tabulates the summary of the atomic compositions obtained using XPS and ICP-AES. As can be seen from Table 4.2 both measurements were in good agreement with each other. It can also be observed that with increasing Ag/Au current ratio, there is a corresponding increase in Ag composition and increase in the position of emission peak energy which may suggest that this blue shift in emission peak is probably related with the increase in Ag/Au composition ratio in these bimetallic nanoclusters.

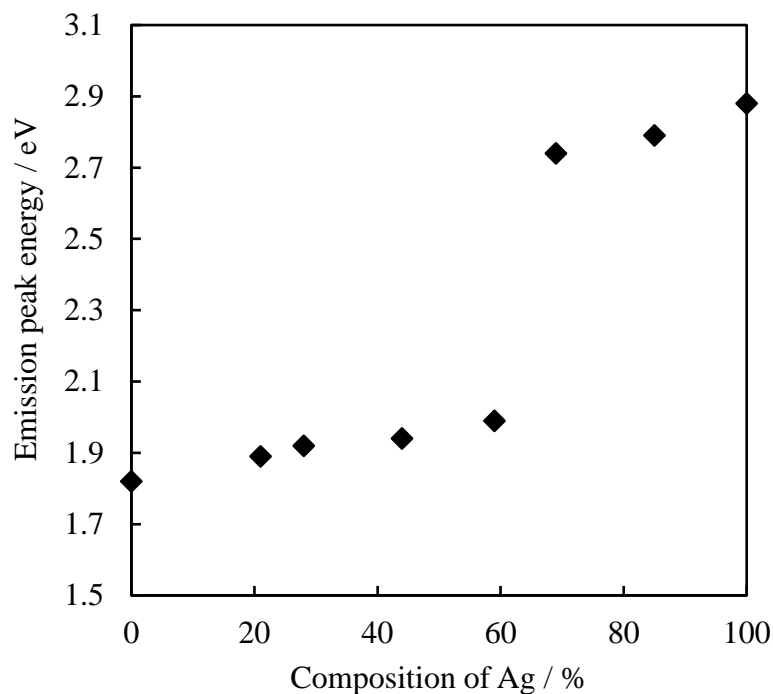


Figure 4.5 Correlation between the emission energies and the atomic percent of Ag determined by XPS.

Figure 4.5 shows the relationship between the composition and the position of maximum emission peaks. It can be observed that with increasing atomic (%) of Ag, the emission maxima shifted towards high energy which is in good agreement with the results obtained by Negishi et al.²⁷ due to continuous modulation in electronic structure upon addition of Ag atoms. In the present case, we found a linear relationship between Ag atomic composition and peak energy in low energy region when the Ag atomic composition is below 59% and another linear relationship between emission peak energy and Ag atomic composition in the high energy region when Ag atomic composition is above 59% (Figure 5). To understand the bonding and formation of Au-Ag bimetallic nanoclusters, XPS analysis at Au 4f and Ag 3d regions was conducted to determine the charge states.

Table 4.3 Summary of Binding energies at Au 4f and Ag 3d regions.

Sample	Binding Energy (eV)			
	Au 4f		Ag 3d	
	7/2	5/2	5/2	3/2
4	84.8	88.8		
5			366.8	372.8
6	83.9	87.6	367.6	373.6
7	83.8	87.4	367.5	373.5
8	83.7	87.3	367.4	373.4
9	83.6	87.2	367.2	373.2
10	83.4	87.0	366.8	372.5
11	83.1	86.7	366.6	372.3

Table 4.3 shows the summary of the position of binding energies at Au 4f and Ag 3d regions of the photoluminescent monometallic nanoclusters (**4** and **5**) and bimetallic Au-Ag nanoclusters (**6–11**) (corresponding XPS spectra and plot of binding energy with respect to composition ratio are shown in Figure S6). With respect to the Au 4f region, the position of the peak of **4** (84.8 eV and 88.8 eV for Au 4f_{7/2} and Au 4f_{5/2} respectively) lie between the binding energies of neutral bulk Au (84.0 eV and 88 eV at Au 4f_{7/2} and Au 4f_{5/2} respectively) and Au(I) complexes (~86 eV and ~90 eV at Au 4f_{7/2} and Au 4f_{5/2} respectively)²⁸ suggesting that **4** is mainly consist of positively charge Au atoms. The peak positions of bimetallic nanoclusters **6–11** on the other hand, are in the lower binding energies with respect to the bulk gold which could suggests that the Au atoms for these samples are negatively charged. With regard to the Ag 3d region on the other hand, the peak position of monometallic Ag nanocluster **5** (366.8 eV and 372.8 eV for Ag 3d_{5/2} and Ag 3d_{3/2} respectively) is in a much lower binding energy in comparison with that of bulk Ag (368.2 eV and 374.2 eV at Ag 3d_{5/2} and Ag 3d_{3/2} respectively) and closely match with the binding energy of Ag(I) complexes (366.8 eV and 372.8 eV at Ag 3d_{5/2} and Ag 3d_{3/2}

respectively)²⁹ suggesting that the nanocluster most probably contains positively charge Ag atoms. Correspondingly, the bimetallic nanoclusters **6–11** have binding energies located at lower energies with respect to the bulk Ag, suggesting that the Ag atoms of these nanoclusters are mostly positively charge also. In our previous report³⁰ using single target sputtering for the synthesis of monometallic Au nanocluster, the peaks of the binding energy at Au 4f_{7/2} and Au 4f_{5/2} are located at 85.5 eV and 89.2 eV respectively which suggest the existence of Au(I) species. In the present case, although **4** has main peaks at 84.8 eV and 88.8 eV at Au 4f_{7/2} and Au 4f_{5/2} respectively which are typical binding energy reported for Au₂₅(SR)₁₈ nanoclusters with a core-shell structure³¹, close examination of the spectra reveals that other secondary peaks in Au 4f_{7/2} and Au 4f_{5/2} regions with almost similar peak location with that of our previous report³⁰ were observable, suggesting that the nanocluster might be mixtures of various sizes as expected from TEM images. The peak position of **5** on the other hand (366.8 eV and 372.8 eV at Ag 3d_{5/2} and Ag 3d_{3/2} respectively), suggests the dominance of Ag(I) species^{27,32-36} for this sample. In the case of bimetallic nanoclusters **6–11**, Negishi et al.²⁷ reported similar scenario wherein Au and Ag atoms are in its negative and positive charge states respectively for photoluminescent bimetallic (Au_{25-x}Ag_x)(SR)₁₈ nanoclusters. Thus this clearly indicates that samples **6–11** are bimetallic nanoclusters wherein the Au atoms which is more electronegative than Ag atoms assume negative charge and the Ag atoms assume positive charge and were covalently bonded to form a stable Au-Ag bimetallic nanoclusters.²⁷ To confirm the formation and existence of Au-Ag bimetallic nanoclusters we investigated the samples using STEM-HAADF and conducted EDS elemental mapping and quantification.

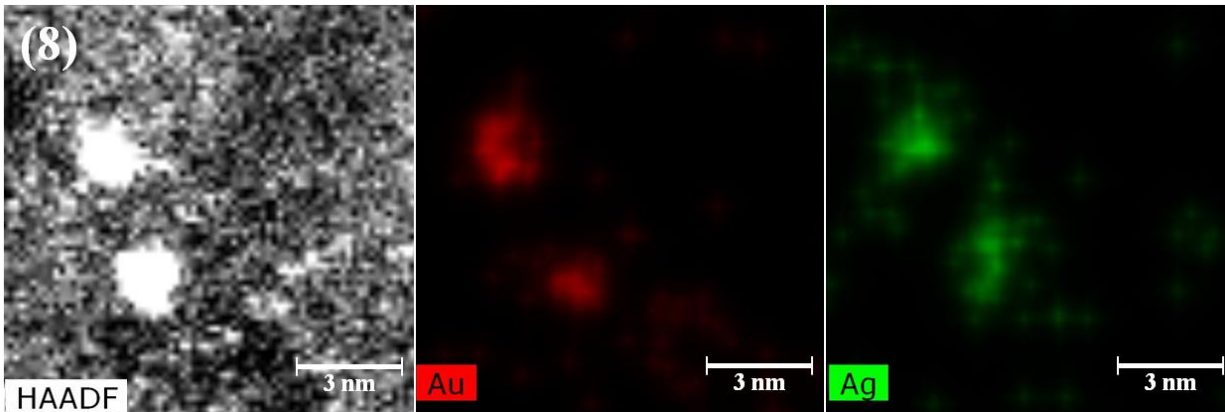


Figure 4.6 Representative STEM-HAADF image and EDS mapping of sample **8** (Au@18mA-Ag@38mA).

Figure 4.6 and Figure S7 show the STEM-HAADF images and the corresponding elemental mapping of samples **6-11**. It is evident from these figures that the bimetallic nanoclusters were formed as can be deduced from its corresponding elemental distributions. Quantification of the elements (Table S1) showed that the compositions of the bimetallic nanoclusters 6-11 obtained by STEM-EDS were in good agreement with the results acquired in XPS and ICP-AES analyses shown in Table 2.

4.4 Conclusions

In conclusion, we successfully synthesized an NIR emitting positively charged photoluminescent bimetallic Au-Ag nanoclusters using 11-mercaptoundecyl-*N,N,N*-trimethylammonium bromide as capping ligand by means of novel double target sputtering set-up which could have potential applications in biomedical fields. Results showed tunability of emission from blue to NIR region with respect to change in nanocluster composition. High resolution HAADF-STEM and elemental mapping in tandem with XPS analysis evidently showed the formation of bimetallic nanoclusters. This finding is the first physical synthesis showing an obvious correlation of nanocluster composition to the observed emission. The results

presented here is therefore important for the synthesis of high purity photoluminescent bimetallic nanoclusters.

4.5 References

1. M. Ganguly, J. Jana, A. Pal and T. Pal, *RSC Adv.*, 2016, **6**, 17683-17703.
2. S. Link, Z. L. Wang and M. A. El-Sayed, *J. Phys. Chem. B*, 1999, **103**, 3529-3533.
3. S. Ristig, D. Kozlova, W. M. Zaika and M. Epple, *J. Mater. Chem. B*, 2014, **2**, 7887–7895.
4. D. Tiedemann, U. Taylor, C. Rehbock, J. Jakobi, S. Klein, W. A. Kues, S. Barcikowski and D. Rath, *Analyst*, 2014, **139**, 931-942.
5. X. Guevel, B. Hotzer, G. Jung, K. Hollemeyer, V. Trouillet, and M. Schneider, *J. Phys. Chem. C*, 2011, **115**, 10955–10963.
6. T. Zhang, H. Xu, S. Xu, B. Dong, Z. Wu, X. Zhang, L. Zhang and H. Song, *RSC Adv.*, 2016, **6**, 51609–51618.
7. N. A. Alarfaja and M. F. El-Tohamy, *Luminescence*, 2016, **31**, 1194–1200.
8. C. Wang, L. Xu, X. Xu, H. Cheng, H. Sun, Q. Lin and C. Zhang, *J. Colloid Interface Sci.*, 2014, **416**, 274–279.
9. H. Huang, H. Li, J. Feng and A. Wang, *Sensors and Actuators B*, 2016, **223**, 550-556.
10. Z. Wu, *Angew. Chem. Int. Ed.*, 2012, **51**, 2934 –2938.
11. G. Hong, S. M. Tabakman, K. Welsher. Z. Chen, J. T. Robinson, H. Wang, B. Zhang and H. Dai, *Angew. Chem. Int. Ed.*, 2011, **50**, 4644-4648.
12. P. Wang, X. Wang, L. Wang, X. Hou, W. Liu and C. Chen, *Sci. Technol. Adv. Mater.*, 2015, **16**, 1-15.

13. M. T. Nguyen, T. Yonezawa, Y. Wang, T. Tokunaga, *Mater. Lett.*, 2016, **171**, 75-78.
14. Y. Ishida, C. Lee and T. Yonezawa, *Scientific Reports*, 2015, **5**, 15372:1-6.
15. T. Sumi, S. Motono, Y. Ishida, N. Shirahata and T. Yonezawa, *Langmuir*, 2015, **31**, 4323-4329.
16. M. Porta, M. T. Nguyen, Y. Ishida and T. Yonezawa, *RSC Adv.*, 2016, **6**, 105030-105034.
17. Y. Ishida, R. Nakabayashi, R. D. Corpuz, T. Yonezawa, *Coll. Surf. A: Physicochem. Eng. Aspects*, 2017, **518**, 25–29.
18. G. Schmid, *Adv. Eng. Mater.*, 2001, **3**, 737-743.
19. C. Kumara, X. Zuo, D. A. Cullen and A. Dass, *ACS Nano*, 2014, **8**, 6431-6439.
20. L. Feng, G. Gao, P. Huang, K. Wang, X. Wang, T. Luo, C. Zhang, *Nano Biomed. Eng.*, 2010, **2**, 258-267.
21. D. Mott, N. T. B. Thuy, Y. Aoki and Y. Maenosono, *Phil. Trans. R. Soc. A*, 2010, **368**, 4275-4292.
22. J. S. Mohanty, P. L. Xavier, K. Chaudhari, M. S. Bootharaju, N. Goswami, S. K. Pal and T. Pradeep, *Nanoscale*, 2012, **4**, 4255-4262.
23. S. Pramanik, A. Saha and P. S. Devi, *RSC Adv.*, 2015, **5**, 33946-33954.
24. B. Paramanik and A. Patra, *J. Mater. Chem. C*, 2014, **2**, 3005–3012.
25. J. Zheng, C. Zheng, C. Zhang and R. M. Dickson, *Phys. Rev. Lett.*, 2004, **93**, 077402.
26. C. M. Andolina, A. C. Dewar, A. M. Smith, L. E. Marbella, M. J. Hartmann, and J. E. Millstone, *J. Am. Chem. Soc.*, 2013, **135**, 5266–5269.
27. Y. Negishi, T. Iwai, M. Ide, *Chem. Commun.*, 2010, **46**, 4713-4715.
28. Y. Negishi, K. Nobusada and T. Tsukuda, *J. Am. Chem. Soc.*, 2005, **127**, 5261-5270.

29. Y. Mao, Y. Yang, H. Yang, J. Han, Y. Zeng, J. Wei, X. Meng and C. Wang, *RSC Adv.*, 2016, **6**, 12311-12314.
30. Y. Ishida, I. Akita, T. Sumi, M. Matsubara and T. Yonezawa, *Scientific Reports*, 2016, **6**, 29928:1-14.
31. T. Ohta, M. Shibuta, H. Tsunoyama, Y. Negishi, T. Eguchi, and A. Nakajima, *J. Phys. Chem. C*, 2013, **117**, 3674-3679.
32. X. Yuan, T. J. Yeow, Q. Zhang, J. Y. Lee and J. Xie, *Nanoscale*, 2012, **4**, 1968-1971.
33. Z. Q. Tian, Y. Z. Lian, J. Q. Wang, S. J. Wang and W. H. Li, *J. Electroanal. Chem.*, 1991, **308**, 357-363.
34. S. Gao, D. Chen, Q. Li, J. Ye, H. Jiang, C. Amatore and X. Wang, *Scientific Reports*, 2014, **4**, 4384:1-6.
35. A. Ferraria, A. Carapeto, and A. Rego, *Vacuum*, 2012, **86**, 1988-1991.
36. A. Shahzad, T. Yu, and W. S. Kim, *RSC Adv.*, 2016, **6**, 54709-54717.

5 GENERAL CONCLUSIONS

This study demonstrates the possibility of producing photoluminescent metal nanoclusters using short and long carbon chain cationic thiol molecule ligand in both chemical and physical method. In the second chapter, thiocholine chloride a short quaternary ammonium cation was utilized as ligand to synthesize the first known cationic thiolate protected photoluminescent Au nanocluster. However, even at high concentration of this thiol molecule, it was found that what can be produced are just plasmonic nanoparticles of Au as can be seen from its UV-Vis extinction spectra due to existence of strong electrostatic repulsion which hinders the effective stabilization and protection of the nanocluster at the early stage of cluster formation. To address this problem, Sodium dodecylsulfate, an ionic surfactant was introduced to control the existing electrostatic repulsion. At higher concentration of both thiocholine and SDS we found that the particle size became small as verified by both TEM and STEM-HAADF images and the particles produced started to exhibit blue photoluminescence emission once irradiated with UV-light. However, the difficulty of producing pure product in this particular chemical reduction method prompted us to find an eco and biofriendly scheme to make these photoluminescent nanoclusters useful in biomedical fields which usually require high purity materials thus we resort to physical synthesis by means of sputtering technique which is a greener alternative.

In chapter 3 we found a general scheme to produce photoluminescent monometallic Au, Ag and Cu nanocluster for the first time using 11-mercaptoundecyl-*N,N,N*-trimethylammonium bromide (MUTAB) as stabilizing ligand in a single target sputtering on Liquid Polymer Matrix, Polyethylene Glycol (PEG). These produced nanoclusters are photoluminescent in both solution and solid states. Au nanoclusters have orange emission color with emission maximum wavelength at 629 nm. Ag nanoclusters on the other hand had blue emission with emission maximum wavelength at 432 nm and Cu nanoclusters had blue emission as well with maximum

emission wavelength located at 428 nm. Measurement of its average particle sizes using TEM and STEM-HAADF imaging technique showed that all nanoclusters produced have particle diameter well below 2 nm which could be the reason as to why are these nanoclusters showed photoluminescence. XPS analyses of the samples showed that the nanoclusters most probably contain positively charged metal atoms.

The fourth chapter aimed to produce NIR emitting bimetallic Au-Ag nanoclusters by controlling the Au/Ag composition through manipulation of the sputtering current of the metal targets simultaneously in double target sputtering system. Likewise, we used MUTAB as ligand to stabilize the bimetallic nanoclusters produced. The composition of the bimetallic nanoclusters was determined by XPS and ICP-AES measurement wherein we found that below 59 Ag atomic %, the bimetallic nanoclusters show tunable NIR emission which red shifted as the Ag atomic % decreases. Above 59 Ag atomic % on the other hand, the emission is tunable in the blue region and blue shifted as the Ag atomic composition increased. TEM and HAADF-STEM of the samples verified the existence and formation of bimetallic Au-Ag nanocluster with diameter less than 2 nm and the composition as measured by XPS and ICP-AES was further confirmed by EDS-STEM elemental mapping of the clusters even in this very small dimensions. This result is the first experimental evidence showing an obvious correlation between atomic percent composition and emission energy in sputtering system and could have significant contribution to the science of this very promising field.

Appendix I. Supplementary information for Chapter 2

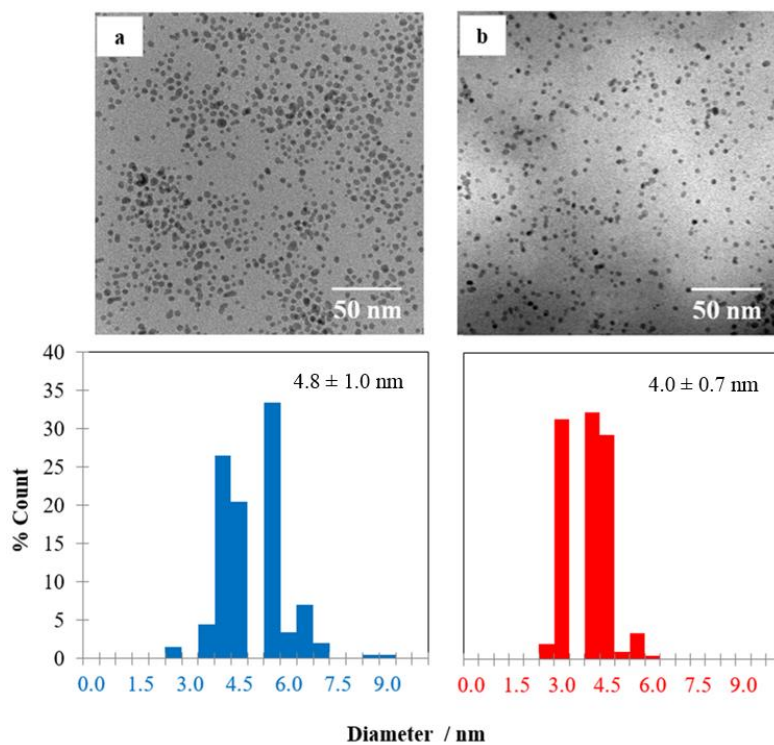


Figure S1. TEM images and particle size distributions of obtained Au nanoparticles synthesized under the mol ratio of Au:TC = 1:3 (a) and 1:5 (b).

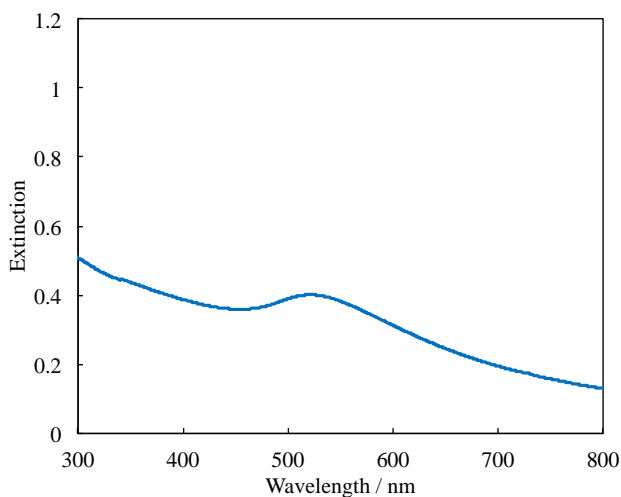


Figure S2. Extinction spectra of obtained Au nanoparticles synthesized at Au:TC:SDS = 1:3:3.

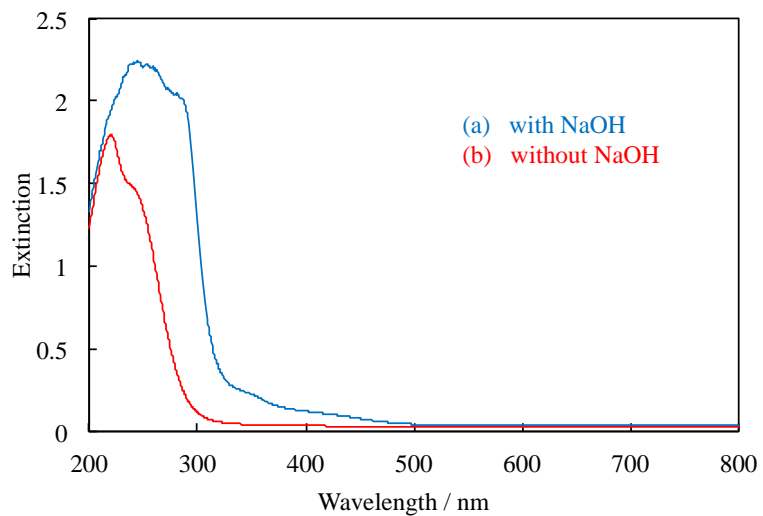


Figure S3. Extinction spectra of obtained Au nanoclusters with and without NaOH.

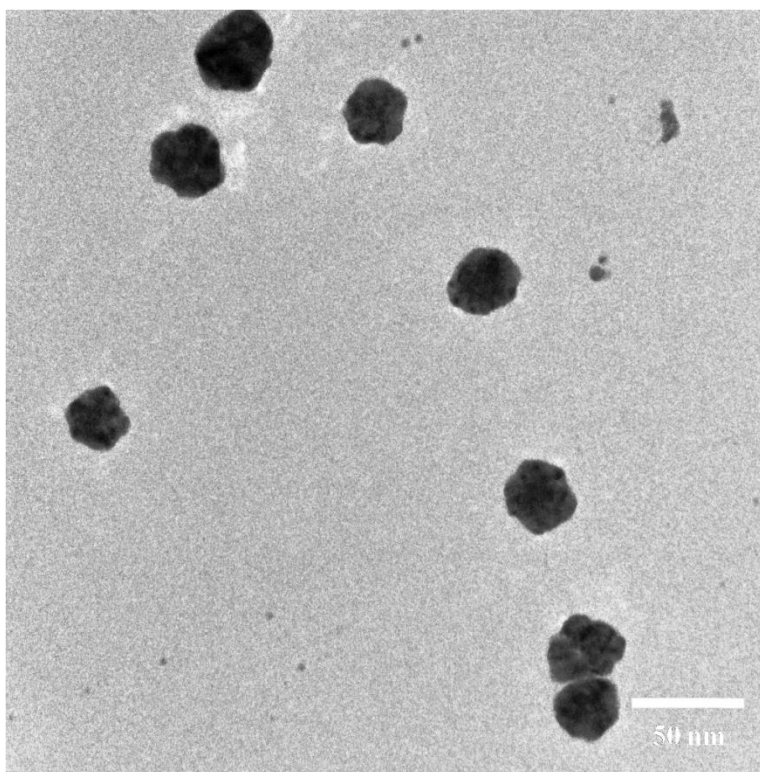


Figure S4. Large aggregates of particles (~20 nm) were obtained after synthesizing gold nanoparticles using SDS alone without thiocholine.

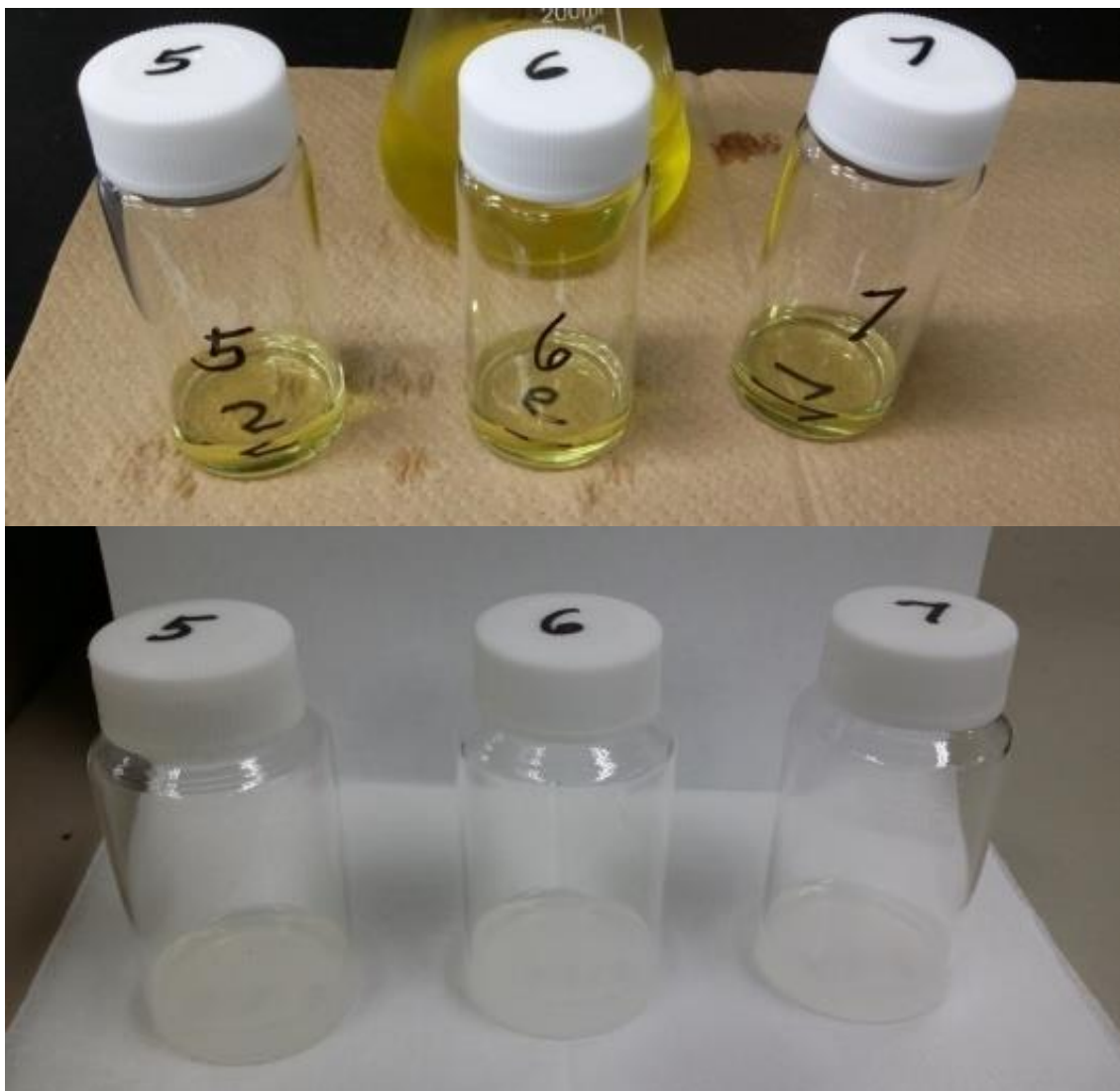


Figure S5. Changes in color before (top) and after (bottom) addition of TC on HAuCl_4 .

Appendix II. Supplementary Information for Chapter 3

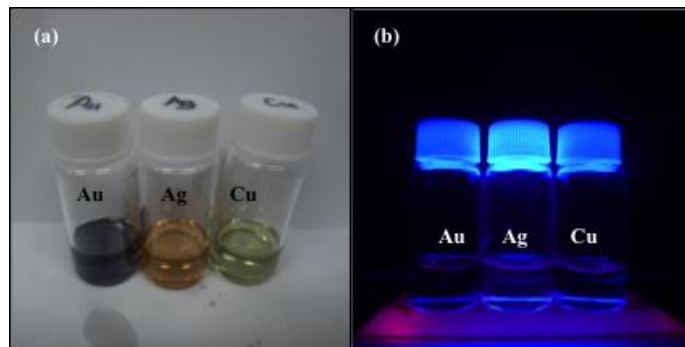


Figure S1. Colour of the solution of Au, Ag and Cu plasmonic nanoparticles under (a) sunlight and (b) UV-light irradiation. These plasmonic particles were surely non-photoluminescence.

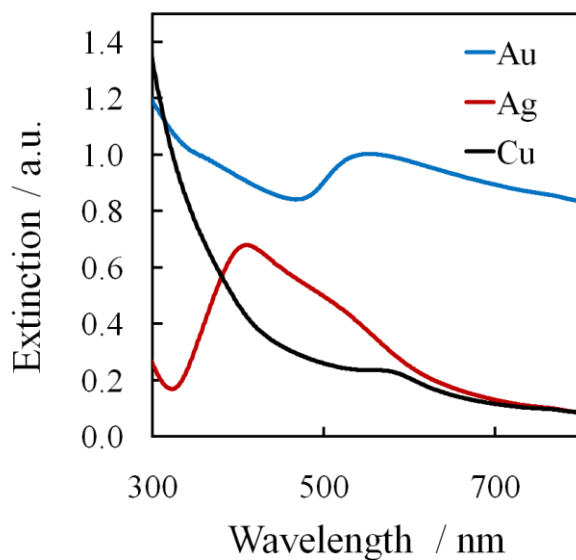


Figure S2. UV-Vis extinction spectra of the synthesized plasmonic Au, Ag and Cu nanoparticles in PEG in the absence of MUTAB ligand.

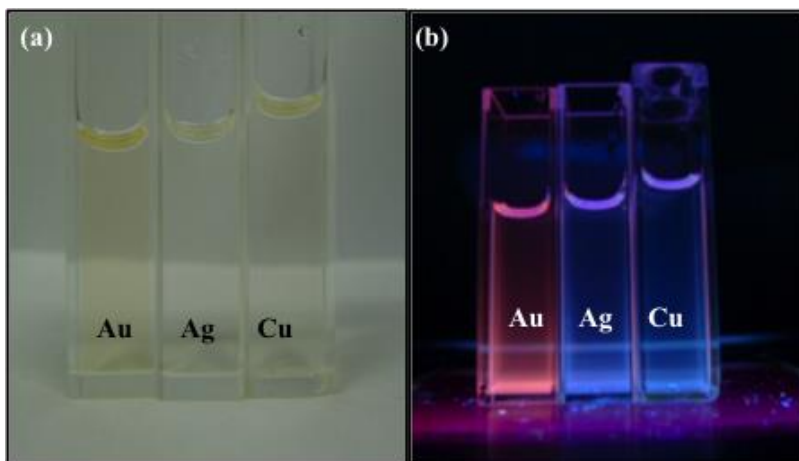


Figure S3. Colour of Au, Ag and Cu nanoclusters in PEG with MUTAB: (a) under sunlight and (b) under UV light irradiation.

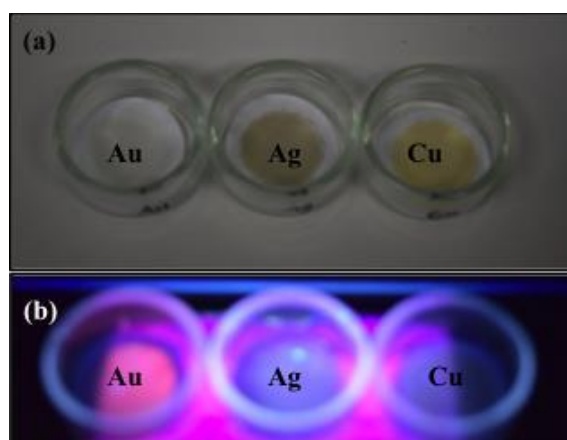


Figure S4. Colour of filtrate after filtration using 0.2 μm hydrophobic PTFE filter: (a) under sunlight and (b) under UV light irradiation.

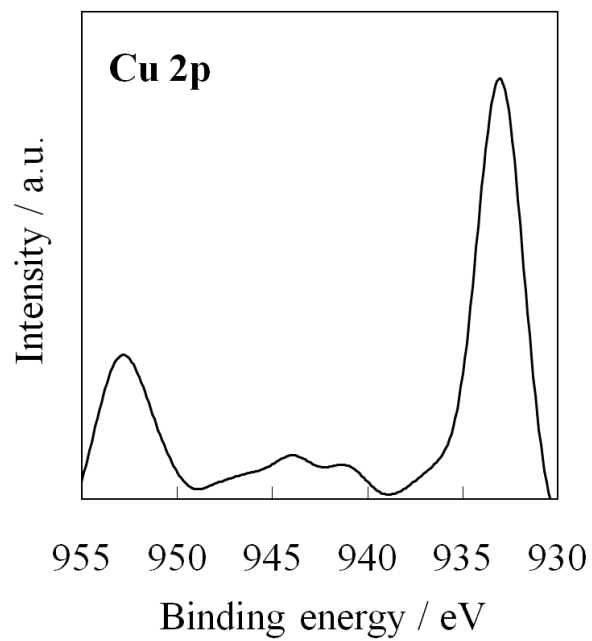


Figure S5. XPS spectra of photoluminescent Cu nanocluster at Cu 2p region.

Appendix III. Supplementary Information for Chapter 4

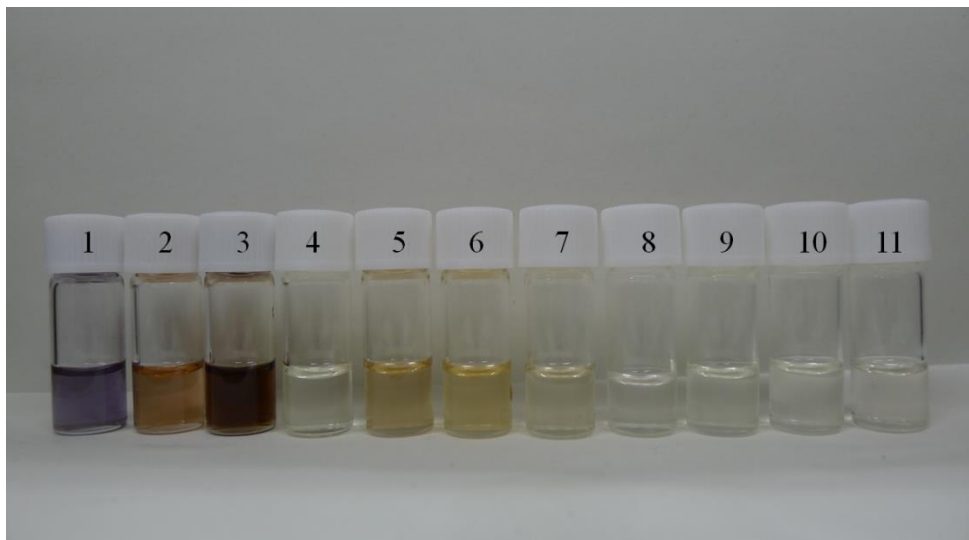


Figure S1. Color of the solution without MUTAB: (1) Au@20mA, (2) Ag@34mA and (3) Au@20mA-Ag@34mA, and with MUTAB: (4) Au@20mA, (5) Ag@34mA, (6) Au@10mA-Ag@50mA, (7) Au@14mA-Ag@46mA, (8) Au@18mA-Ag@38mA, (9) Au@20mA-Ag@34mA, (10) Au@24mA-Ag@20mA and (11) Au@26mA-Ag@14mA under sunlight.

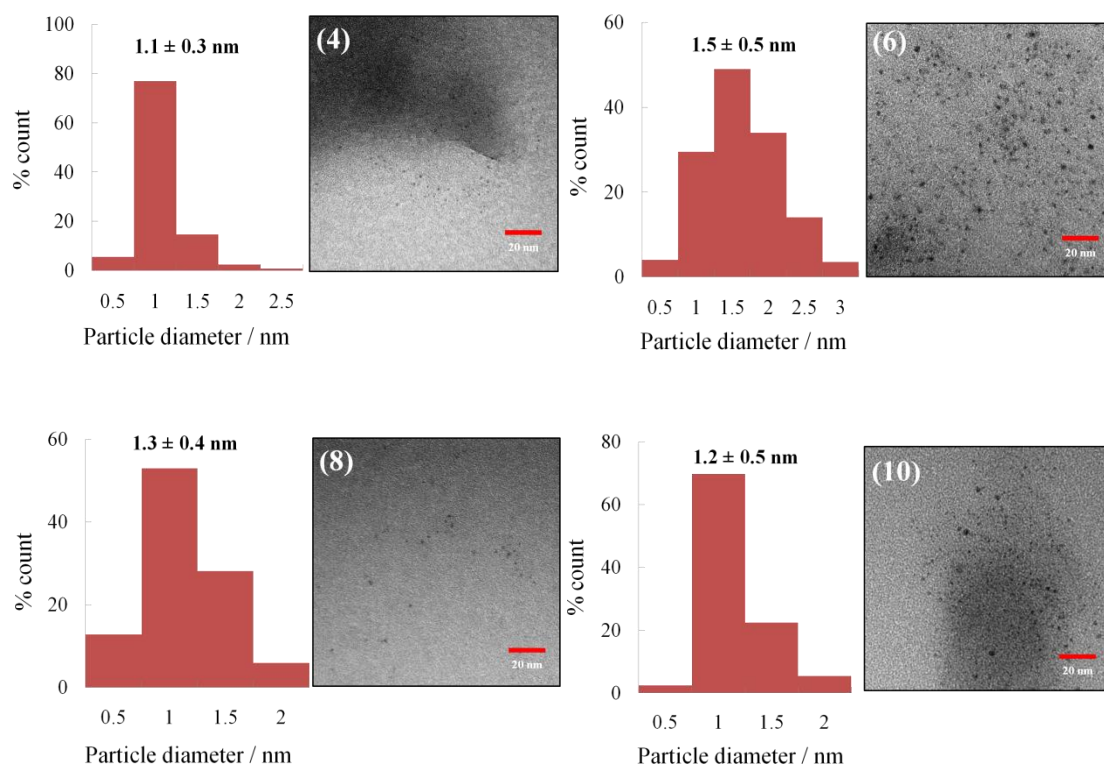


Figure S2. TEM images and particle size distribution histogram of samples with MUTAB. **(4)** Au@20mA, **(6)** Au@10mA-Ag@50mA **(8)** Au@18mA-Ag@38mA, and **(10)** Au@24mA-Ag@20mA.



Figure S3. Color of the solution of monometallic plasmonic nanoparticles: (1) Au@20mA, (2) Ag@34mA and its corresponding plasmonic alloy nanoparticle (3) Au@20mA-Ag@34mA and monometallic photoluminescent nanoclusters synthesized with MUTAB: (4) Au@20mA and (5) Ag@34mA under UV-light irradiation.

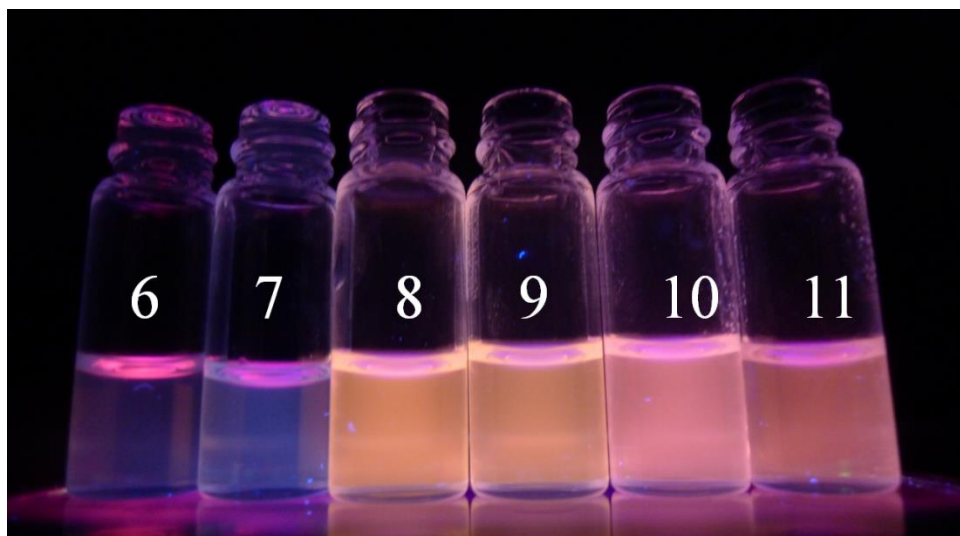


Figure S4. Color of the solution of bimetallic photoluminescent nanoclusters: (6) Au@10mA-Ag@50mA, (7) Au@14mA-Ag@46mA, (8) Au@18mA-Ag@38mA, (9) Au@20mA-Ag@34mA, (10) Au@24mA-Ag@20mA and (11) Au@26mA-Ag@14mA under UV-light irradiation.

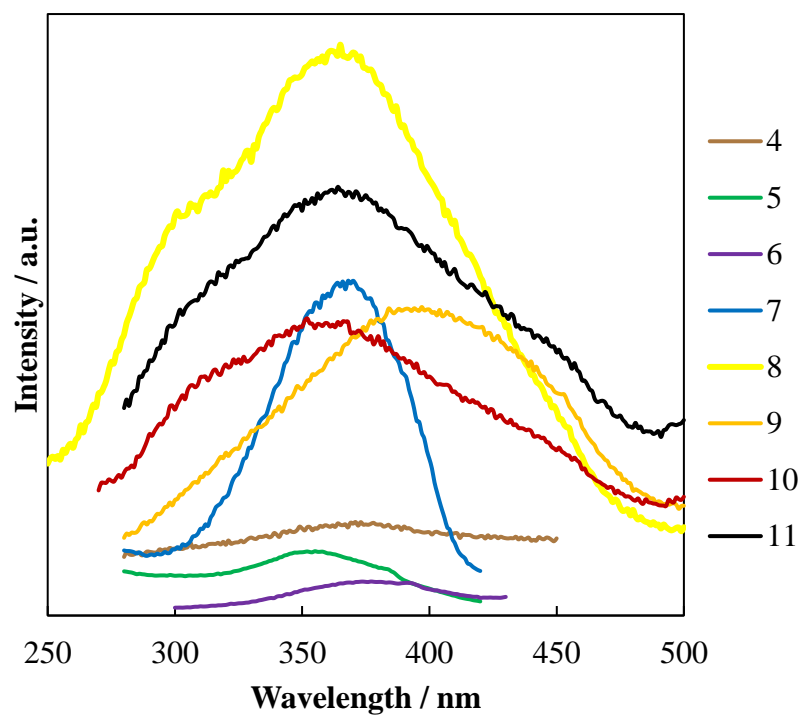
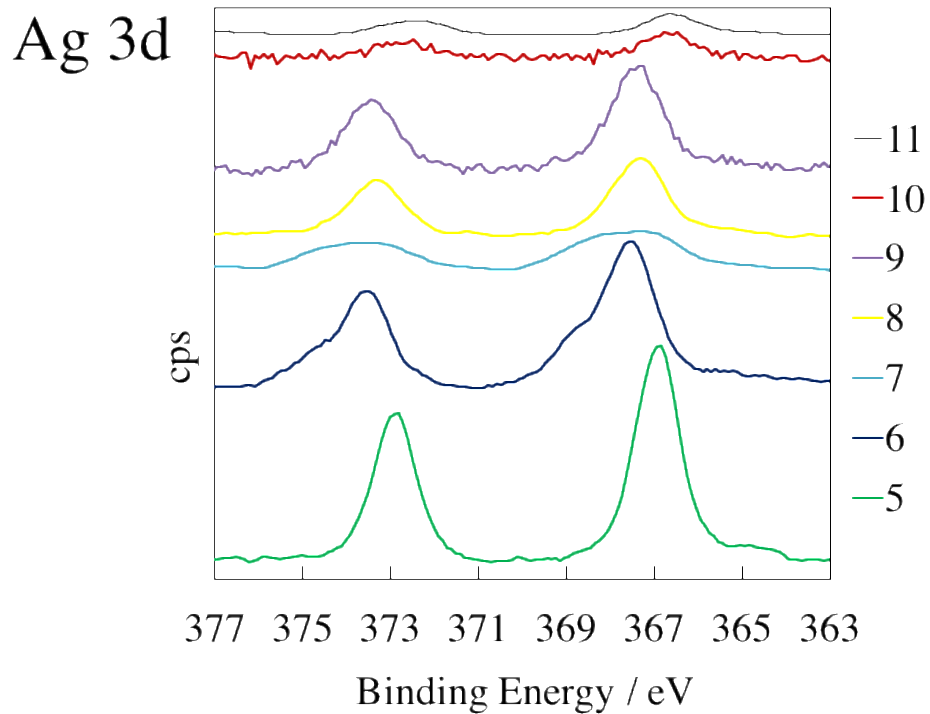
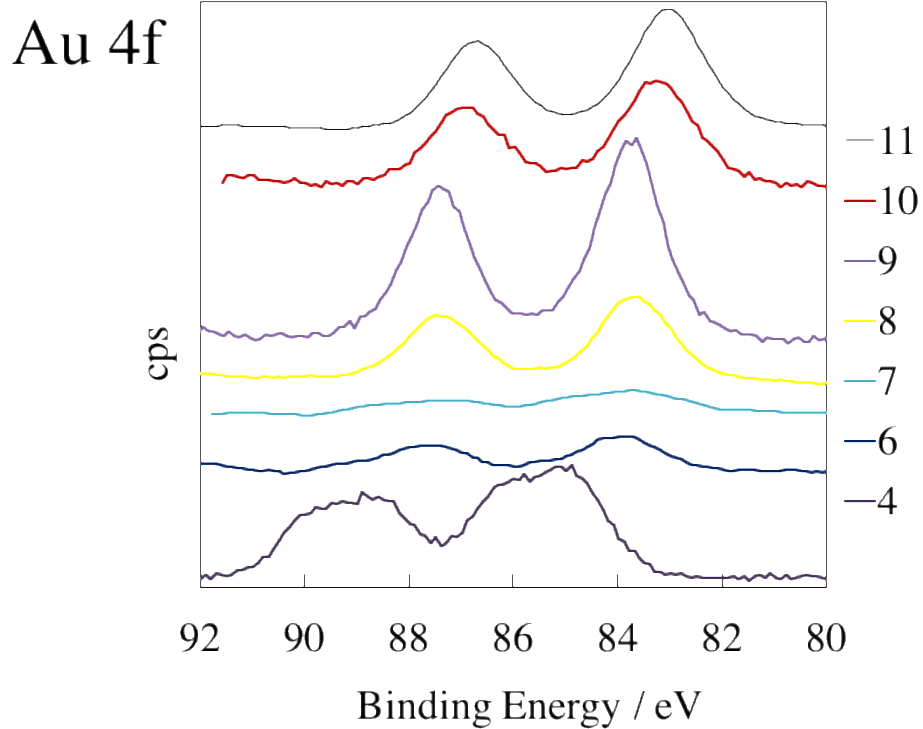


Figure S5. Excitation spectra of samples synthesized with MUTAB. Monometallic nanoclusters: **(4)** Au@20mA and **(5)** Ag@34mA, and bimetallic nanoclusters: **(6)** Au@10mA-Ag@50mA, **(7)** Au@14mA-Ag@46mA, **(8)** Au@18mA-Ag@38mA, **(9)** Au@20mA-Ag@34mA, **(10)** Au@24mA-Ag@20mA and **(11)** Au@26mA-Ag@14mA.



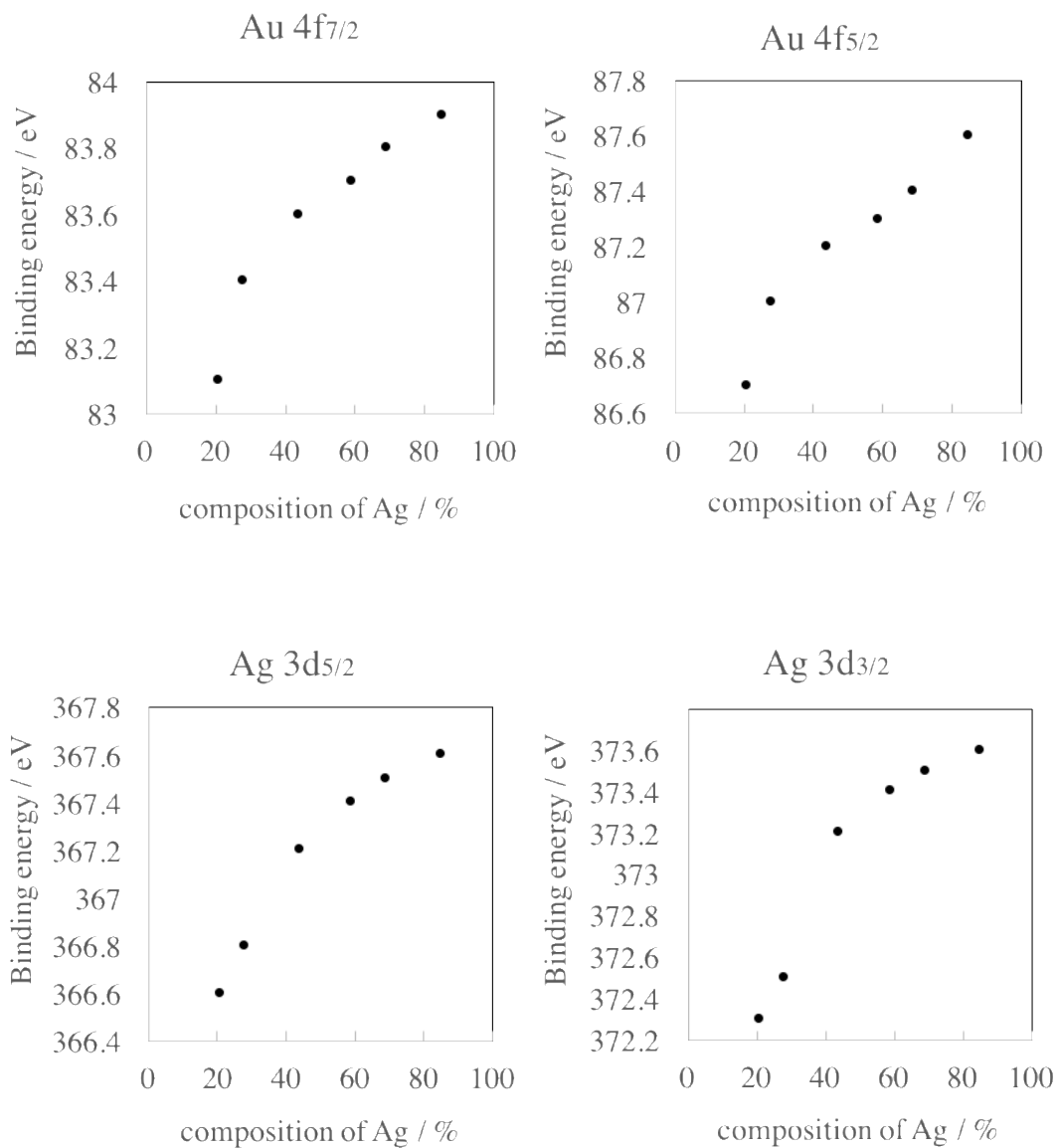
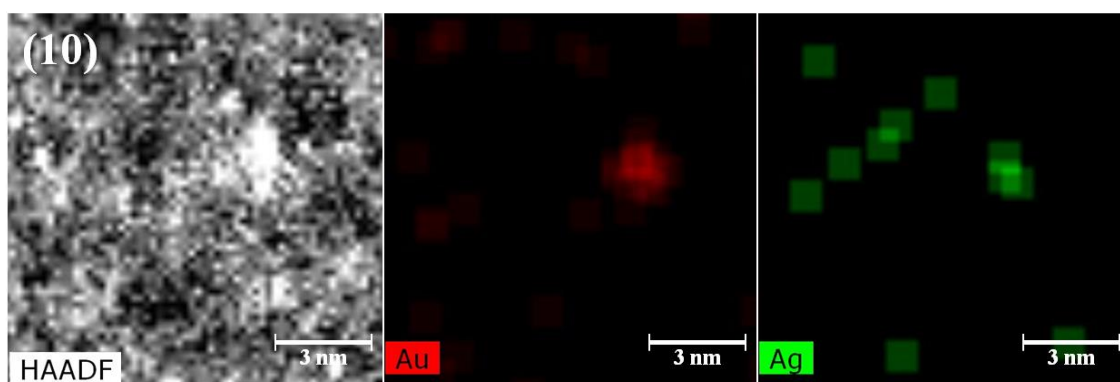
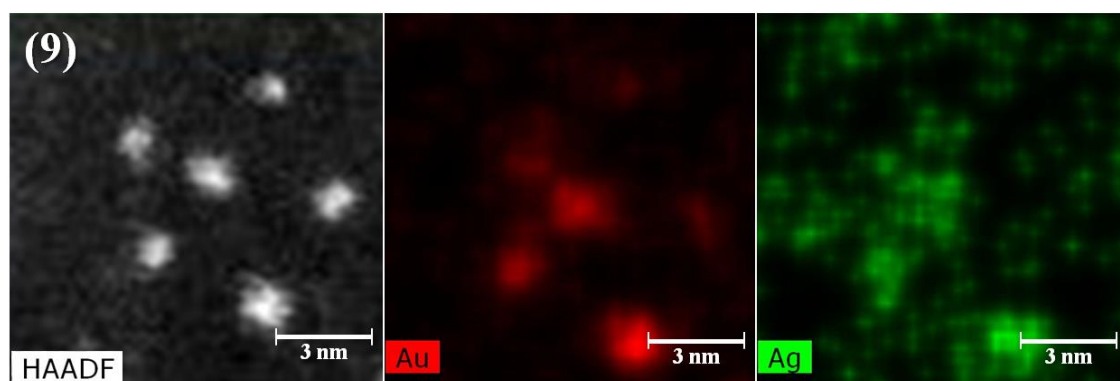
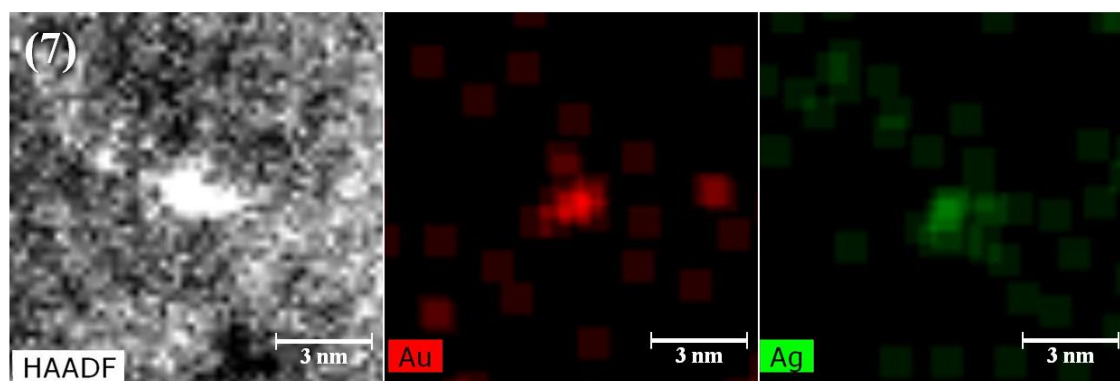
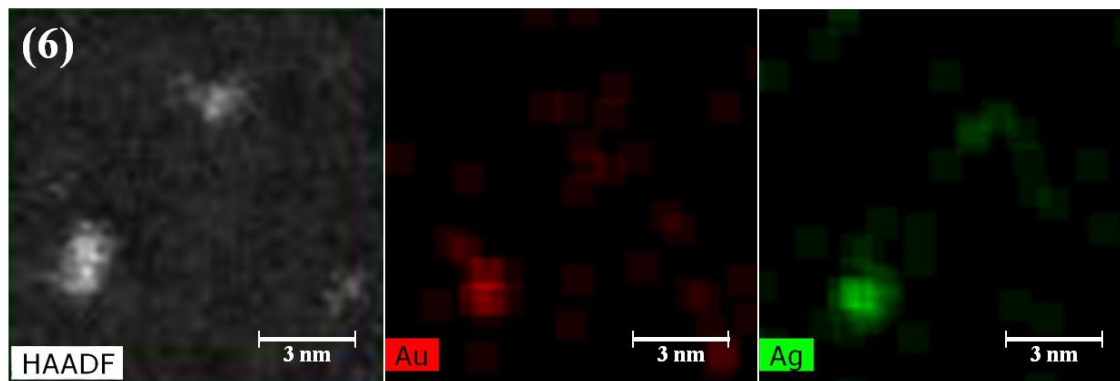


Figure S6. XPS spectra of photoluminescent bimetallic Au-Ag nanocluster and graph of binding energy with respect to Ag composition at Au 4f and Ag 3d regions.



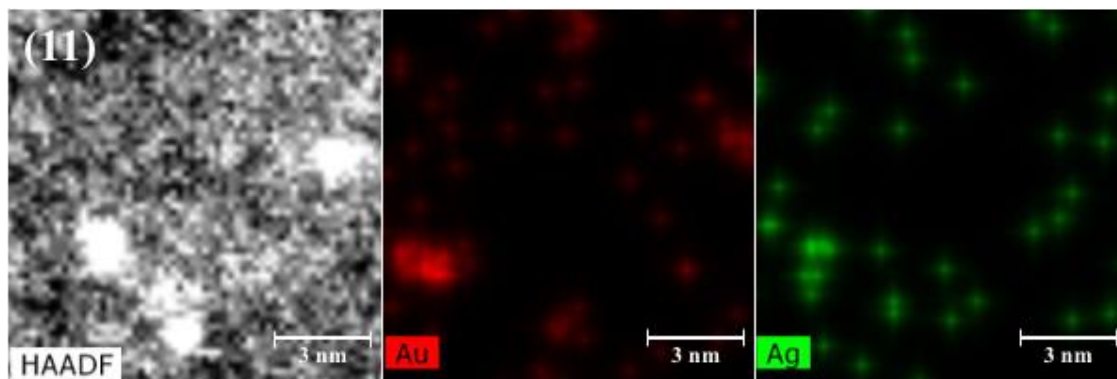


Figure S7. STEM-HAADF images and elemental mapping of photoluminescent bimetallic Au-Ag nanoclusters: (6) Au@10mA-Ag@50mA, (7) Au@14mA-Ag@46mA, (9) Au@20mA-Ag@34mA, (10) Au@24mA-Ag@20mA and (11) Au@26mA-Ag@14mA

Table S1. Elemental composition of bimetallic Au-Ag nanoclusters obtained by STEM-EDS Analysis.

sample	STEM-EDS	
	Atomic percent (%)	
	Au	Ag
6	15	85
7	32	68
8	42	58
9	58	42
10	75	25
11	79	21

RESUME

Nationality: Filipino

Current address: JICA International Center Hokkaido, Minami 4-25 Hondori 16 Chome Shiroishi
Ku 003-9926 Sapporo, Japan

Name: Ryan Dula Corpuz

Date of birth: July 23, 1985

Educational background

< /06/1998> Diploma in High School, Integrated Developmental School,
<30/03/2002> Mindanao State University-Iligan Institute of Technology (MSU-IIT)
< /06/2002> BS in Ceramics Engineering, Department of Chemical, Metallurgical and
<30/04/2007> Ceramics Engineering, College of Engineering, MSU-IIT
<06/06/2010> MS in Materials Science and Engineering, DMMME,
<04/11/2012> College of Engineering, University of the Philippines-Diliman
<28/09/2014> PhD in Materials Science and Engineering, Division of Materials Science and
< present > Engineering, Faculty of Engineering, Hokkaido University

Professional background

<06/06/2009> Instructor I, Mindanao State University-Iligan Institute of Technology
<26/02/2014>
<26/02/2014> Assistant Professor IV (permanent), Mindanao State University
<Present> Iligan Institute of Technology (MSU-IIT)

Research background

< /06/2002> Department of Chemical, Metallurgical and Ceramics
<30/04/2007> Engineering, College of Engineering, MSU-IIT
<06/06/2010> Department of Metallurgical, Mining and Materials
<04/11/2012> Engineering, College of Engineering, University of the Philippines-Diliman
<28/09/2014> Division of Materials Science and Engineering,
<28/09/2017> Faculty of Engineering, Hokkaido

I certify that the above are true records.

Date:

Ryan Dula Corpuz
Signature

LIST OF PUBLICATIONS

Dissertation submitted for the degree title: PhD in Materials Science and Engineering

1st Author

- i. Controlling an electrostatic repulsion by oppositely charged surfactants towards positively charged fluorescent gold nanoclusters
R.D. Corpuz, Y. Ishida and T. Yonezawa, *Phys. Chem. Chem. Phys.*, 2016, **18**, 8773-8776.
- ii. Synthesis of cationically charged photoluminescent coinage metal nanoclusters by sputtering over liquid polymer matrix
R. D. Corpuz, Y. Ishida, and T. Yonezawa, *New J. Chem.*, 2017, **41**, 6828-6833.
- iii. Synthesis of positively charged photoluminescent bimetallic Au-Ag nanoclusters by double target sputtering method on a biocompatible polymer matrix
R. D. Corpuz, Y. Ishida, M. T. Nguyen and T. Yonezawa
(under review)

Co-Authored

- i. Water-Dispersible fluorescent silver nanoparticles via sputtering deposition over liquid polymer using a very short thiol ligand
Y. Ishida, R. Nakabayashi, R. D. Corpuz and T. Yonezawa, *Colloids and Surf A*, 2017, **518**, 25-29.

Date:

Signature

LIST OF RESEARCH ACCOMPLISHMENTS

Conference attended

- i. The 64th SPSJ (The Society of Polymer Science, Japan) Annual Meeting
(oral presentation)
Effect of Cationic Thiol Ligand and Anionic Surfactant on the Synthesis of Fluorescent Gold Nanocluster
(2015.5.27)
- ii. The 15th Annual meeting of Society of Nano Science and Technology
(oral presentation)
Synthesis of Cationically Charged Photoluminescent Noble Metal Nanoclusters by sputtering over liquid polymer matrix
(2017.5.12)
- iii. The Chemical Society of Japan Hokkaido Section 2017 Summer Study Presentation
(oral presentation)
Synthesis of cationically charged photoluminescent bimetallic Au-Ag nanocluster with tunable emission by double target sputtering method
(2017.7.22)

Date:

Signature